DYNAMIC PHENOMENA IN TRANSPORT THROUGH SUB-MICRON DEVICES

A Dissertation

Presented to the Faculty of the Graduate School

of Cornell University

in Partial Fulfillment of the Requirements for the Degree of

Doctor of Philosophy

by

Mikhail Lvovich Polianski

January 2005

DYNAMIC PHENOMENA IN TRANSPORT THROUGH SUB-MICRON DEVICES

Mikhail Lvovich Polianski, Ph.D.

Cornell University 2005

This thesis considers dynamic phenomena in transport through electronic devices on sub-micron scale. It consists of two closely related parts, the first considering DC current through a quantum dot as a response to a periodic perturbation of its shape and the second, conversely, explores a finite-frequency spin wave in a ferromagnet due to a constant electric current. Both systems are very similar in their theoretical treatment by scattering matrix formalism.

The Chapters 2–4 consider a charge current induced by a periodic perturbation of an open quantum dot's shape. A dot being mesoscopic, its transport properties strongly fluctuate from sample to sample and therefore knowledge of full sample-to-sample distributions is essential. We consider a "quantum pumping" regime of reservoirs in equilibrium and periodic variation of the dot's shape by AC voltages applied at the gates. Experimentally measurable first several moments of mesoscopic distribution of charge pumped in one cycle are explored.

Chapter 2 considers distributions of adiabatically pumped current $\bar{I}$ and voltage $\bar{V}$ and finds that even in a slow weak pumping regime they are not simply related

via time-averaged conductance $\bar{G}$. Moreover, values of $\bar{I} - \bar{V}\bar{G}$ for few-channel dots exhibit strong mesoscopic fluctuations, comparable with those of $\bar{I}$.

Chapter 3 explores mesoscopic distributions of noise and current-to-noise ratio in a weak pumping regime in a wide region of temperatures and pumping frequencies. Fluctuations of noise in the multi-channel limit $N \to \infty$ are found to be small as $1/N$. For a multi-channel system the ensemble-averaged noise is analytically found and calculated for experimentally relevant temperatures, frequencies and pumping strengths.

The Chapter 4 concerns the formalism of time-dependent scattering matrix theory and finds correlators of matrix elements up to the fourth order. Our findings allow a systematic treatment of various transport properties, as well as their ensemble-averaged correlations. We also compare our results with results obtained in Hamiltonian approach of Random Matrix theory.

The second part, Chapter 5, considers magneto-transport through a single ferromagnetic layer. Electric current flowing perpendicular to the plane of a thin layer is shown to excite a finite frequency response in form of a spin wave. Unlike the previously known spin-torque due to a polarized current, another mechanism able to induce a destabilizing torque on a local magnetization is found. Spin-diffusion of reflected spins from one point on the normal-ferromagnet boundary to another might excite a spin wave at sufficiently strong currents. We analytically find the critical current value and discuss our results for experimentally relevant parameters.

Biographical Sketch

The author was born in Nizhniy Novgorod, Russia on February 27, 1975. In 1992 he graduated from the Physics and Mathematics oriented high school and entered Moscow Institute for Physics and Technology (MIPT). There he received a B.S. in 1996 and M.S. in 1998 with honors, in Theoretical Physics, specializing in Solid State Physics. From 1996 till 1999 he made a research under supervision of Prof. Kravtsov in Landau Institute for Theoretical Physics (ITP). After one year of graduate studies in ITP he entered the Graduate School at Cornell University in the fall of 1999, in Physics Department. In the summer 2000 he joined the research group of Prof. Piet Brouwer. He received the M.S. in January 2003 and expects to receive the Ph.D. in January 2005, both in Physics.

I dedicate this thesis to my family

Acknowledgements

First, I would like to thank my thesis advisor Piet Brouwer, who was guiding my research during my five years in Cornell University. Although very busy, he always found time to discuss with me any question I come up with, which was very stimulating for my research. It is not an overestimate to say that his contribution to this thesis is the most significant: Piet has always proposed very interesting problems and helped me with his physical intuition to remove my numerous errors.

I learned a lot from him, both in theoretical methods I applied in research and generally in physics from the courses he taught. In research, Piet guided me through formalism of Random Matrix Theory and subtleties of Fortran computations. In his courses I understood how important to have a qualitative understanding of physical phenomena. I have taken much from his courses in solid state physics and diagrammatic technique that I graded, because the problems he made up were invariably very instructive. Besides, Piet is also a very nice person and it was very exciting to have such a perfect chief during my four-year research. If I do understand something in physics it is completely due to Piet Brouwer, and I am very glad that I had a chance to work with him.

I would like to thank Prof. Vinay Ambegaokar, the most durable member of my thesis committee from my first year in Cornell. His exam questions were always

very stimulating, and the problem he gave me on the A-exam finally became a solid part of a paper. It was always very refreshing to talk to him in the kitchen of the fifth floor with a cup of tea, as a respite from sometimes tedious calculations.

I am also very grateful to Prof. Dan Ralph, who represents the experimental side of my committee. Various projects of his group helped me understand how important it is to keep in touch with experimenters, who have completely different point of view on the same phenomena. It is due to Dan's research that I had an opportunity to plunge into applied part of the solid state physics.

In addition, doing my research I have had numerous discussion and informal talks with many bright people on lower stages of academic hierarchy. Piet Brouwer's research group was always of much help to me, namely, Shaffique Adam, Stephan Braig, Denis Gorokhov, and Prashant Sharma. Their valuable comments on my practices of conference talks hopefully helped me improve my presentation style, which is essential in the Western science. Yaroslav Bazaliy from ANL and Maxim Vavilov were always very helpful explaining physics to me. People from other theoretical groups in Cornell helped me survive among fast Linux computer upgrades and subtleties of foreign languages: Connie Chang, Michael Crawford, my office-mate Uzi Hizi, Xavier Waintal, and Josh Waterfall. On the experimental side, discussions with guys from Dan Ralph's and Bob Buhrman's groups were very stimulating and helped me not to do a useless work (and hopefully do the useful one). These are Nathan Emley, Sergey Kiselev, Ilya Krivorotov, and Jack Sankey.

Small but united Russian community helped me survive in foreign country of United States. My best friends, Sergey Viktorovich Pankov and Roman "RRR" Rafikov have been invaluable friends with their wise advises and support. My other class-mate Sergey Ivanych Kiselev, the oldest cornellian I know, was always eager

to help me, as well as other Russians in Cornell: Alexey Kiselev, Sergey Kriminskiy and Dasha Kriminskaya, Maxim Vavilov, Robert Scherbakov, Vera Sazonova, Yuliya Epifantseva and Andrey Baliakin, Lena and Alexey Ershov, Yera Hakobyan and Valera Smirichinski, Lyuda Rovba, Ivan Lysyuk, Karen Mkhoyan, Zhenya Nazaretsky, Larisa Vygran, and Volodya Khmelenko. Outside Cornell, the hospitable house of Elya Valieva and RRR in New Jersey was a vitally important base on my trips home and back.

I would also thank my first-year American house-mates: Lincoln, Matt, and Steve – thanks to them I had a chance to know American life much better. A vast, but constantly changing, community of football players on Arts Quad gave me a lot of fun. These people rather prevented me from doing the research then helped me there, but nevertheless, my life without football games with them would have lost much. Among them are Sergey Korolev, Sasha Slivkins, Val Kaper, Matt van Adelsberg, Jason Marshall, and lots of other enthusiasts.

The last but not least is invaluable support of my family. Understanding and love of my parents, brother and sister helped me through these five years at Cornell. Although very far, they have always shared with me all my achievements and problems. I devote this thesis to my family as a sign of my gratitude and love.

Table of Contents

List of Tables

List of Figures

Table 1: Table of notations.

Notation	Meaning	Defined in
$\mathbf{a}(E), \mathbf{a}(t)$	Amplitudes of incoming scattering modes	(1.2, 3.3)
$\mathbf{b}(E), \mathbf{b}(t)$	Amplitudes of outgoing scattering modes	(1.2, 3.3)
B	External magnetic field	
C	Capacitance of a dot (reservoir)	
$C_{c(l)}$	Circular (linear) pumping parameter	(3.28)
$\mathcal{C}$	The Cooperon	(3.33)
d	Thickness of a ferromagnet	Chapter 5
$\mathcal{D}$	The Diffuson	(3.32)
E	Kinetic energy of electrons	
$f(E)(\tilde{f}(E))$	Equilibrium electron (hole) Fermi distribution	
$f(t)(\tilde{f}(t))$	Fourier transform of $f(E)(\tilde{f}(E))$	(3.25, 3.12)
$\mathcal{F}$	Kernel of the 4-element matrix correlator	(4.21, 4.32)
g, G	Dimensionless conductance, $N_L N_R/(N_L + N_R)$	Chapters 1–4
$G_{\alpha\beta}$	Spin-dependent conductance of NF layer	(5.2)
H	The Hamiltonian of a closed dot	Chapters 1–4
$I_\alpha, I_\alpha(t)$	Pumped current through the α-th contact	(3.6)
$\bar{I}$	Time-averaged current	(3.9)
J	Exchange constant in a ferromagnet	(5.3)
$j_e, \mathbf{j}$	Charge and spin currents in FNF system	(5.1)
$j_{\rm f}$	Ferromagnetic parameter, in units of current	(5.4)
$K_{1,2}$	Anisotropy constants	(5.3)
l	Mean free path of electrons	
L	Typical size of a dot	
$l_{\rm sf}$	Spin-diffusion length in Normal metal	(5.1)
$L_\pm$	Length of a normal metal	Chapter 5
L_ϕ	Dephasing length	
$\mathbf{m}, \mathbf{M}$	Magnetizations of magnetic layers	Chapters 1,5
M, N	Size of a matrix	Cahpters 1–4
M	Magnetization value of a ferromagnet	Chapter 5
$N_{L,R}, N_{1,2}$	Number of scattering channels	Chapters 1–4
$P(...)$	Distribution function of (...)	Chapters 1–4
q	Spin-wave wave-number	(5.6)
$q_{\rm f}$	Ferromagnetic paramater, units of length^{-1}	(5.4)
r, r'	Reflection (diagonal) blocks of $\mathcal{S}$	(1.3)

Table 2: Table of notations (contd.)

Notation	Meaning	Defined in
S	Scattering matrix	Chapter 1
$\mathcal{S}$	Scattering matrix	Chapters 2–4
S	Noise power	Chapters 3–4
$S^{N,P,S}$	Nyquist, Pumping and Shot noise	Chapters 3–4
T	Temperature	
T^*	Heating temperature	(3.36)
t, t'	Transmission (off-diagonal) blocks of $\mathcal{S}$	(1.3)
$v_{\rm F}$	Fermi velocity	
V	Applied voltage	
W	Width of a NFN contact	Chapter 5
W_i	Correlator of $2i$ scattering matrix elements	Chapter 4
$X(\delta X)$	Pumping strength	Chapters 2–4
$\mathcal{X}$	Vector of pumping parameters	Chapter 3
$\alpha, \tilde{\alpha}$	Gilbert damping parameter	(5.3, 5.8)
β	Dyson symmetry parameter	Chapters 2–4
γ	Escape rate from a dot, $\gamma = N\Delta/2\pi$	Chapters 1–4
$\gamma, \tilde{\gamma}$	Gyromagnetic ratio	(5.3, 5.7)
Δ	Mean level spacing in a dot	
ε	Kinetic energy of electrons	
η	Capacitive division between reservoirs	Chapter 2
$\lambda_{\rm F}$	Fermi wavelength	
$\Lambda_{\alpha\beta}$	Traceless diagonal matrix	(3.8)
$\mu_e, \boldsymbol{\mu}$	Charge and spin-dependent potentials	(5.1)
ν	Density of states near Fermi energy	
σ	Conductivity of a normal metal	Chapter 5
$\tau_{\rm erg}$	Ergodic time of a quantum dot	Chapters 2–4
$\tau_{\rm dwell}$	Dwell time inside a dot, $1/\gamma$	Chapters 2–4
τ_H	Heisenberg time $2\pi\hbar/\Delta$	
$\tau_{\rm sf}$	Spin-diffusion time	Chapter 5
τ_0	Observation time	Chapters 3–4
ϕ	Phase shift between pumps	Chapters 2–4
Φ	Magnetic field flux through a dot	Chapter 4
Φ_0	Flux quantum	
$\langle ... \rangle$	Ensemble averaging	Chapters 1–4
$\bar{...}$	Quantum-mechanical averaging	Chapters 3-4

Chapter 1

Introduction

This thesis considers dynamical phenomena in transport through electronic devices on sub-micron scale. Of wide variety of transport problems here we consider two important and interesting questions, namely, of quantum pumped charge current through an open quantum dot and of spin-wave excitation induced by electric current through a thin magnet. Sub-micron elements of electrical circuit are of great technological importance, with existing modern trend to miniaturize computers and enhance their computational power. Though quite different, these two questions have several important issues in common.

The first problem concerns charge transport at low temperatures through an island ("dot") of two-dimensional electron gas. A measurable direct electrical current is created by periodic manipulation of the dot's shape ("quantum pumping"). Absent in the classical limit, this dynamical response is essentially a quantum effect, because these periodic variations in finite frequency ω adjust electronic wave functions extended beyond the size of the dot; at small frequencies ("adiabatic pumping") pumped current is proportional to ω [1, 2]. Thus, a non-stationary external perturbation induces a stationary effect (DC current) and therefore probes

dynamical response properties of the dot.

In the second problem, a direct non-equilibrium electric current passes perpendicularly to a thin ferromagnet. Unexpectedly, a vector of mono-domain magnetization $\mathbf{m}$ (stable at zero current) undergoes a transition to a dynamically stable spin-wave, that is a periodic time-space modulation in $\mathbf{m}$. This effect occurs due to interaction between the conduction electron spins and the local magnetization of the layer. One can view such a spin-wave excitation effect at finite frequency as a probing of dynamical response properties of a ferromagnet to a stationary external current source.

Although performed in quite different experimental regimes of low temperatures and small perturbations in the first and room temperatures and strong current source in the second case, both questions are essentially related: dynamical property of a small scale device is measured, either in form of induced stationary or non-stationary measured effect. As demonstrated later, this is not just a coincidence. Without knowing microscopic details of the samples (a dot or a ferromagnet) one might expect that a limited set of measurable parameters is sufficient to explain these dynamic effects.

Indeed, in transport through a dot it is possible to find a pumped current and noise, related to the first and second moments of a Full Counting Statistics (FCS) of pumped charge. Without giving a full solution of FCS-problem, we can express these measurable quantities in terms of the scattering matrix $\mathcal{S}$ that characterizes probability amplitudes to scatter one state, *e.g.* a plane wave, into another. With varying parameters, to find a time-dependent scattering matrix $\mathcal{S}(t, t')$ is a more complicated problem, not yet fully addressed in the literature. However, one still can use this formalism and consider a sample-to-sample distribution of such dynamical

effects of the system as current, noise, and current-to-noise ratio, which are of much interest for both theorists and experimenters.

The $\mathcal{S}$-matrix approach is also efficient in the second case of transport through a magnet. Interested in spin-dependent effects, one introduces a time- and spin-dependent $\mathcal{S}$ matrix of the layer. With reasonable assumptions about the form of the matrix, one is not only able to connect spin-dependent currents and potentials on the ferromagnetic boundary, but also satisfactorily explain an experimentally measured enhancement of magnetization damping coefficient [3]. $\mathcal{S}$-matrix formalism allows one to simplify theoretical treatment of magneto-transport equations and predict new effects.

The last but not least is a industrial use of the effects considered. A mechanism similar to the charge quantum pump may be also applied for a spin quantum pump. Theoretical treatment presented in this thesis allows one to predict a time-dependent transport phenomena in a systematic $\mathcal{S}$-matrix approach. Spin-dependent transport in layered magnetic systems has already found its application in hard disk drives and is probably the best candidate for use in Random Access Memory (RAM), with memory elements not only read, but also switched by electric current. Whether spin waves are desirable in a device (GHz resonators) or not (RAM), the problem of current-induced spin wave is of vital importance for explanation of great variety of recent experiments.

In summary, both transport-related problems considered in this thesis concern dynamical response of devices on finite frequencies, utilize similar theoretical treatment of the scattering matrix approach and are of importance for potential industrial use. Below we review several topics to introduce a reader into the problems we present.

The Section 1.1 explains the problem of mesoscopic quantum transport through an open dot in general, both from experimental and theoretical point of view. Then the scattering matrix formalism for time-independent transport and the adiabatic approximation are introduced in Section 1.2, with generalization of the problem on the time-dependent case. In the Section 1.3 we describe current situation with the theory of spin-dependent transport through multilayered systems and qualitatively explain some recent experimental results. Section 1.4 we give an overview of this thesis.

1.1 Coherent transport through a quantum dot.

The problem of quantum transport through small devices has been extensively explored during last twenty years both theoretically and experimentally. Transport through a sample is coherent if its size is smaller then the decoherence length L_ϕ defined by the interaction strength. In this *mesoscopic* limit, sample-to-sample fluctuations of physical properties might become comparable with their values averaged over large number of samples. The term "mesoscopic physics" applies to macroscopically small systems, $L \ll L_\phi$, with large number of electrons. In experiments at low temperatures in clean systems the mesoscopic limit is attainable, so that a theoretical investigation of mesoscopic, or sample-to-sample, distributions is needed to characterize a system. This approach is in striking contrast with usual macroscopic treatment, when fluctuations around ensemble-averaged values are small. An example of physically interesting mesoscopic problem is coherent transport through a quantum dot.

A typical quantum dot is usually created on top of semiconducting heterostructures $GaAs/Al_xGa_{1-x}As$. Electronic motion perpendicular to the plane of het-

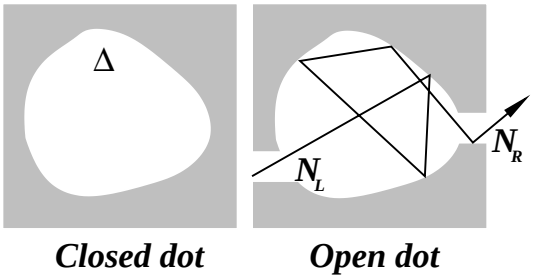

Figure 1.1: Left panel: Closed quantum dot disconnected from environment. Mean level spacing $\Delta \gg 1/\tau_{\rm erg}$ ensures universality. Right panel: Open dot. Two quantum point contacts with $N_{L,R}$ open channels connect the dot with reservoirs

erostructures is strongly quantized, so that electrons form a two-dimensional electron gas (2DEG). Metallic gates applied on the top form the shape of a small island in 2DEG and control the number of electrons within. If a special care is not taken to form a regularly shaped ballistic dot ("quantum billiard"), the dynamics of electrons inside is classically chaotic. For a closed dot of the size L and mean free path l an electron with velocity $v_{\rm F} = \partial E/\partial p$ at Fermi energy $E_{\rm F}$ explores the phase space of the dot during ergodic time $\tau_{\rm erg} \sim L^2/(lv_{\rm F})$ for diffusive dot with a large number of impurities, $l < L$, or $\tau_{\rm erg} \sim L/v_{\rm F}$ for irregularly shaped ballistic dot, $L < l$ [4]. Within the energy band $E_{\rm Th} = \hbar/\tau_{\rm erg}$, the spectral properties of a non-interacting closed quantum dot with mean level spacing $\Delta \ll E_{\rm Th}$ are well described in terms of Hamiltonian Random Matrix Theory (RMT) in the limit $N \to \infty$. In RMT one considers random Hermitian matrices. Such $N \times N$ random matrix H is statistically distributed according to the Gaussian Law:

$$P(H) \propto \exp(-\frac{\beta\pi^2}{N\Delta^2}{\rm tr}\, H^2). \tag{1.1}$$

The symmetry parameter $\beta = 1$ (2) corresponds to the presence (absence) of time-reversal symmetry. These pure ensembles are called Gaussian Orthogonal Ensemble

(GOE) and Gaussian Unitary Ensemble (GUE)[5]. In experiment one can make a crossover from GOE to GUE by applying magnetic field; the limit of GUE is reached if the flux through a dot exceeds flux quantum $\Phi_0 = \pi c\hbar/e$. A conjecture in good agreement with experiments, predictions of (1.1) for the spectral statistics are independent of microscopic details of impurity configuration and depends on symmetry only.

If a quantum dot is attached to electronic reservoirs by reflectionless ballistic quantum point contacts, it is called an *open dot*, see right panel in Fig. 1.1. Open samples do not have well-resolved energy levels, the density of states being rather a continuous then discrete function. Driving a charge current trough a dot one can measure various transport properties of the system, like conductance in the linear regime or shot noise power etc. There are two approaches in the random-matrix theory, namely Hamiltonian and Scattering Matrix approach, that describe open samples [4]. Both use a scattering matrix of a dot, $\mathcal{S}$.

In the first approach, the "random Hamiltonian approach", the scattering matrix is expressed via random Hermitian matrix H, which represents the Hamiltonian of closed sample, see Eq. (1.1). Transport properties and their fluctuations are then calculated in terms of the known statistical distribution of the random matrix H [6, 7]. Within the second method, the "random scattering matrix approach", the scattering matrix $\mathcal{S}$ itself is considered as a fundamental random quantity. Both approaches were shown to be equivalent [7, 8] and in the end it is a matter of taste, which method to use.

It was recently demonstrated by Brouwer [1] that if one periodically varies voltages on the metallic gates that form the dot, a DC charge current through the dot is created; later a related experiment was performed by Marcus' group [2]. A

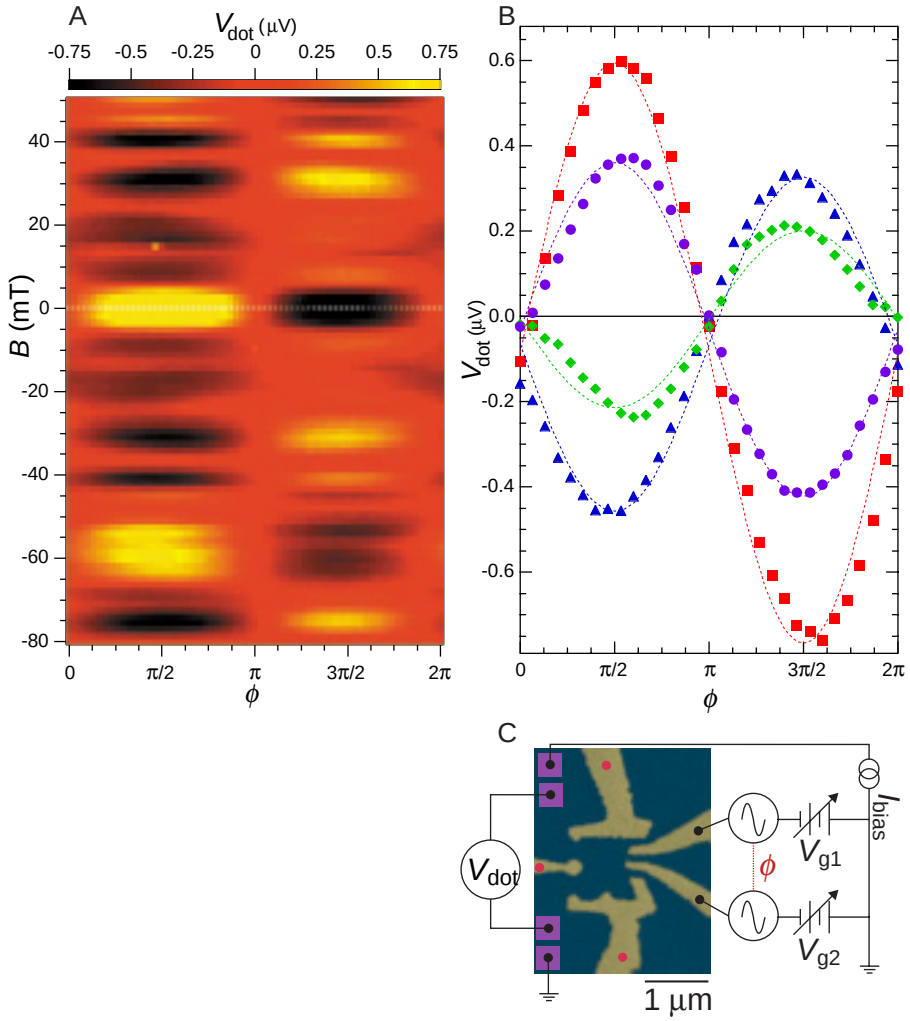

Figure 1.2: (A) Pumped dc voltage V_{dot} as a function of the phase difference ϕ between two shape-distorting ac voltages and magnetic field B. Note the sinusoidal dependence on ϕ and the symmetry about $B = 0$ (dashed white line). (B) $V_{dot}(\phi)$ for several different magnetic fields (solid symbols) along with fits of the form $V_{dot} = A_0 \sin\phi + B_0$ (dashed curves). (C) Schematic of the measurement setup and micrograph of device 1. I_{bias} is set to 0 for pumping measurements. Picture from Ref. [2]

classical analogy of this electronic transport mechanism ("quantum pump") was drawn: variation of the dot's shape squeezes electronic wave function in or out of the dot, thus 'pumping' electrons from one reservoir to another. These AC voltages result in DC current even for the reservoirs in equilibrium. However, a nonzero net current can be generated by at least two varying parameters, because a cycle of a single parameter-pump does not pump any charge. A schematic of the experiment is shown on the Fig. 1.2(C). For experimental reasons, the current was fixed at $I = 0$, and the voltage V was measured and found to be strongly dependent on phase difference ϕ between the varying parameters, see Fig. 1.2 (A,B). The quantum nature of pumped voltage is revealed in its random sign, see Fig. 1.2(B), for different samples.

1.2 Scattering matrix approach in transport through a dot

For description of the dot's transport properties we apply the aforementioned Scattering matrix formalism, where the matrix $\mathcal{S}$ characterizing the sample is a key quantity. Below we briefly describe this approach, first for the time-independent transport. A more complicated time-dependent scattering problem, extensively developed by Büttiker and coworkers [9], is considered later.

Take a mesoscopic sample connected to the reservoirs by several ideal reflectionless two-dimensional leads, see Fig. 1.3. A stationary configuration of impurities inside the dot defines the potential $V(\vec{r})$ that acts on the noninteracting electrons inside the dot and vanishes inside the leads. The electronic wavefunctions and spectrum are defined as solutions to Schrödinger equation with proper

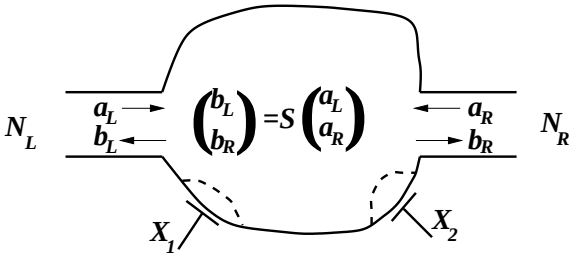

Figure 1.3: Two quantum point contacts with $N_{L,R}$ open channels connect the dot with reservoirs. The scattering modes of incoming $\mathbf{a}$ and outgoing $\mathbf{b}$ electrons from both sides are related via scattering matrix $\mathcal{S}$. Time-dependent perturbation of the dot's shape is governed via $X_{1,2}$ voltages on the gates.

boundary conditions. Far from the scatterer (the dot) these wavefunctions take their asymptotic values of incoming and outgoing plane-waves, defined by the quantization rules inside the leads. For the leads of width W the total momentum $p = \sqrt{2mE} = \hbar\sqrt{k_x^2 + k_y^2}$ is continuous, but $k_y = \pi n/W$ is quantized. The number N of the modes ("transversal channels") is limited due to finite kinetic energy E of electron. If the amplitudes $a_i, i = 1, 2, ..., N$ of incoming waves with energy E are defined, the solution of the Schrödinger equation gives amplitudes of outgoing waves $b_i, i = 1, 2..., N$. Hence the vector $\mathbf{b}(E) = (b_1, b_2, ..., b_N)^{\mathrm{T}}$ can be written up via the vector $\mathbf{a}(E) = (a_1, a_2, ..., a_N)^{\mathrm{T}}$ as

$$\mathbf{b}(E) = \mathcal{S}(E)\mathbf{a}(E). \tag{1.2}$$

The matrix $\mathcal{S}(E)$ can be interpreted in a following way: the matrix element $\mathcal{S}_{mn}$ describes the scattering amplitude for the electron incoming in the channel m to appear in outgoing channel n. For example, if m and n belong to the same (different) lead(s), the amplitudes $\mathcal{S}_{mn}$ describe reflection (transmission) amplitude, and it is common to write scattering matrix in the block form

$$\mathcal{S} = \begin{pmatrix} r & t \\ t' & r' \end{pmatrix}. \tag{1.3}$$

Due to flux conservation, $\mathcal{S}\mathcal{S}^\dagger = \mathbf{1}$, so the matrix $\mathcal{S}$ is unitary. In addition, if the Hamiltonian preserves time-reversal symmetry $t \to -t$, the complex-conjugate solution gives $\mathbf{a}(E) = \mathcal{S}^*(E)\mathbf{b}(E)$. Together with Eq. (1.2) this leads to $\mathcal{S}\mathcal{S}^* = 1$, so that the scattering matrix is unitary and symmetric, $\mathcal{S} = \mathcal{S}^{\mathrm{T}}$.

As the matrix $\mathcal{S}$ describes scattering between different channels, it is advantageous to use it in description of transport properties of mesoscopic samples. For example, famous Landauer formula expresses conductance G of a stationary mesoscopic sample at temperature $T = 0$ in linear regime in terms of scattering amplitudes t_{mn} of the transmission block of $\mathcal{S}(E_{\mathrm{F}})$ at Fermi energy [10]:

$$G = \frac{2e^2}{h}\mathrm{tr}\left(t^\dagger(E_{\mathrm{F}})t(E_{\mathrm{F}})\right). \tag{1.4}$$

The shot noise power S can be also expressed in a similar way in terms of applied voltage V as [10]:

$$S = \frac{e^3 V}{\pi\hbar}\mathrm{tr}\left(r^\dagger(E_{\mathrm{F}})r(E_{\mathrm{F}})t^\dagger(E_{\mathrm{F}})t(E_{\mathrm{F}})\right). \tag{1.5}$$

Eqs. (1.4, 1.5), expressed in terms of $\mathcal{S}$, allow one to find a sample-specific conductance G or noise S, but for a mesoscopic sample they might not be representative, especially for few-channel systems.

Statistical properties and correlations among several $\mathcal{S}$- matrix elements are necessary if one is interested in fluctuations and correlation functions of physical properties. For example, for an ensemble-averaged conductance, $\langle G\rangle$, one needs to know pair correlators of $\mathcal{S}$-matrix elements, but for its second moment a four-element correlators are required. For chaotic quantum dot attached to the ballistic QPC's a uniform distribution of $\mathcal{S}$-matrix over unitary group , "Dyson circular ensemble",

was proposed [11, 12, 13, 14, 15]:

$$P(\mathcal{S}) = \text{const.} \tag{1.6}$$

Its generalization for $N \times N$ matrix $\mathcal{S}$ of a dot with non-ideal contacts of non-zero reflection probability is given by "Poisson kernel" [16, 17, 8] as

$$P(\mathcal{S}) \propto \det \left|1 - \langle \mathcal{S}^\dagger \rangle \mathcal{S}\right|^{-\beta N + \beta - 2}. \tag{1.7}$$

The Eq. (1.7) reduces to Eq. (1.6) for $\langle \mathcal{S} \rangle = 0$. For large matrices, $N \to \infty$, the correlations tend to the Gaussian form and enable analytical calculation of transport properties using diagrammatic technique. For example, in this limit the weak localization correction to conductance becomes quite obvious to calculate, see Chapter 4.

In a more general situation of finite temperature, $T \neq 0$, knowledge of scattering matrix at different energies is necessary, typically inside the band of order T around Fermi energy E_{F}. Then the Landauer formula Eq (1.4) modifies to a convolution of $\mathcal{S}$ matrix elements with equilibrium Fermi distribution in the leads:

$$G \;=\; \frac{2e^2}{h} \int \mathrm{tr}\, \left(t^\dagger(E) t(E)\right) \left(\frac{-\partial f_{\mathrm{F}}(E)}{\partial E}\right) dE. \tag{1.8}$$

If the energy $k_{\mathrm{B}}T$ is negligible compared to energy scale on which the $\mathcal{S}$ matrix correlators change significantly (typically it is $N\Delta \ll E_{\mathrm{Th}}$), then $\mathcal{S}$ at Fermi level is sufficient. However, with time-dependent scattering one has to consider other energy scales involved.

In experiments, transport through a dot might be affected by a periodic variation of the dot's shape: the potential $V(\vec{r}, t)$ is governed by time-dependent parameters $X_i(t)$, see Fig. 1.3 and now the $\mathcal{S}$-matrix relates scattering states at different energies:

$$\mathbf{b}(E) = \int \mathcal{S}(E, E') \mathbf{a}(E') dE'. \tag{1.9}$$

In principle, if the frequency of variations ω is small enough, relevant energy differences are usually of order $|E - E'| \sim \omega$ and one can approximate $\mathcal{S}$ by a 'frozen' matrix $\mathcal{S}(E, t_0)$ calculated at particular time moment t_0, and consider corrections as perturbations, with relevant expansion parameter in small ω. Variations are slow if the dwell time $\tau_{\rm dwell}$ an electron spends inside the dot is much smaller then AC period $2\pi/\omega$.

For an open dot, the dwell time is defined by the number of escape channels N and mean level spacing Δ, so that the *adiabatic approximation* described above is valid for $\hbar\omega \ll N\Delta$. This condition is usually fulfilled in experiments up to Gigahertz frequencies $\hbar\omega/k_{\rm B} \sim 10^{-2}{\rm K} \ll \Delta/k_{\rm B} \sim 1$ K. In this approximation transport properties are expressed in terms of $\mathcal{S}(E, t_0)$ and its derivatives with respect to slow perturbations, $\partial\mathcal{S}(t_0)/\partial X$. Using the results of Brouwer *et al* [18, 19] where the distribution of these derivatives was related to that of Wigner-Smith time-delay matrix [20], a systematic approach to adiabatic transport allows one to find such time-dependent quantities as pumped current and its higher moments (noise etc).

Beyond the adiabatic regime, with $\hbar\omega \sim N\Delta$, one should either use the representation of two-energy dependent matrix $\mathcal{S}(E, E')$, Eq.(1.9) [21] or alternatively, use the time-dependent representation

$$\mathbf{b}_\alpha(t) \;=\; \int_{-\infty}^{+\infty} \mathcal{S}_{\alpha\beta}(t, t')\mathbf{a}_\beta(t')dt'. \tag{1.10}$$

In this thesis we apply this second approach. On one hand it allows a simple transformation to the mixed time-energy representation for comparison with adiabatic approximation results On the other, it does not give unnecessary complications for general ω, since it does not rely upon expansion in small frequency perturbation parameter.

The first part of this thesis, Chapters 2–4, is devoted to calculations of various

experimentally relevant transport properties of open quantum dots, both for adiabatic regime and beyond, and to the calculations of first several matrix element correlators. The latter are essential for the problems of noise calculations in a wide variety of regimes. In the Overview of this thesis, Section 1.4, we describe the problems solved in detail.

1.3 Spin-dependent transport through nanomagnets

In the last fifteen years a great attention was drawn to the spin-dependent transport through multilayered systems, where several ferromagnetic layers, usually thinner than 1 μm, were stacked between normal spacers. Resistance of such systems was explored and was found to strongly depend on relative orientation of the layers' magnetization vectors (GMR– Giant Magneto-Resistance). An electric current was flowing either in parallel to the layers' plane (CIP – current-in plane) [22] or perpendicular direction (CPP–current-perpendicular- to the plane) [23], see left panel of Fig. 1.4.

Resistance in the CIP geometry in wide films is much larger then in the CPP, but the CPP resistance scales as inverse area and may finally become larger then CIP. On sub-micron scales the CPP-geometry has several advantages over CIP. From experimental point of view, a typical resistance of an F-N-F system reaches $\sim 1\Omega$, comparable with usual CIP-resistance, but the effect of GMR is usually 2-4 times stronger [24]. This makes CPP sets possible candidates for the technological applications.

Theoretically, results of CPP-experiments are reasonably well explained using

simple intuitive spin-resistor model. The fact that a layer with magnetization $\mathbf{m}$ conducts electrons with spins $\mathbf{s}$ parallel ($\uparrow\uparrow$) to $\mathbf{m}$ better then antiparallel ($\uparrow\downarrow$) allows one to explain why resistance of stacked layers with parallel magnetizations $\mathbf{m_i}$ has a lower resistance then other configurations.

In the spin-resistor model, any magnet F with magnetization $\mathbf{m}$ serves as a resistor with resistivity $\rho_\uparrow$ and $\rho_\downarrow$ for spins $\uparrow$ and $\downarrow$ [22]; a normal spacer N is assumed to have a spin-independent resistivity. Currents of both spins are considered completely incoherent and can be fully defined once resistance of each element of electrical circuit is found. For example, a circuit for CPP through two identical magnetic layers is illustrated on the right panel of Fig. 1.4 : unequal spin-resistances R and r result in considerable GMR effect.

Although this model satisfactorily explains some experiments in GMR, its key assumption that there is no mixing between spins restricts one to systems of the size smaller then the spin-flip length, $L \ll l_{\rm sf}$; corrections to this theory due to finite $L/l_{\rm sf} \ll 1$ were introduced by Valet and Fert [25]. Secondly, this theory deals with magnetizations aligned on one axis, so that might be valid for collinear spin transport only.

The first condition is fulfilled in experiments on clean metals with weak spin-orbit scattering, *e.g.* Al, where $l_{\rm sf}$ reaches several hundred nanometers. However, a non-collinear situation requires a modified theory. In the experiments by Johnson [26], a multi-terminal experiment with three ferromagnets demonstrated that a noncollinear experimental set can be of interest as well. It was also recognized that for sufficiently thin layers with dimensions $L \ll l_{\rm sf}$ a strong GMR effect could rather come from interfacial spin-dependent resistances on the Normal-Ferromagnetic boundary than from bulk spin-resistors.

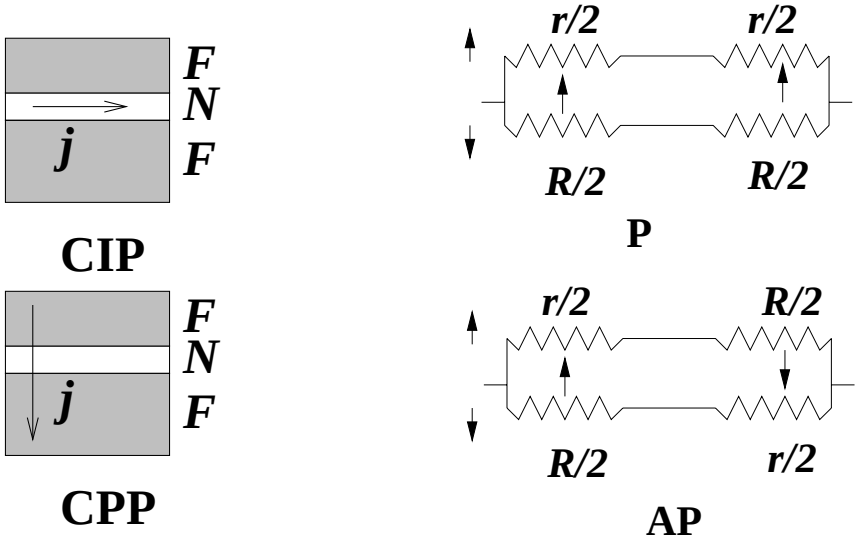

Figure 1.4: Left panel: Schematics of CIP and CPP experiment. Right panel: An example of spin-resistor circuit for CPP through a double-layered system. Spin $\mathbf{s}$ channels of $\uparrow$ and $\downarrow$ electrons pass through ferromagnetic layers of magnetization $\mathbf{m}$. Resistances R and r correspond to $\uparrow\downarrow$ ($\downarrow\uparrow$) and $\uparrow\uparrow$ ($\downarrow\downarrow$) configurations of $\mathbf{s}, \mathbf{m}$. In result, resistance of parallel configuration (top) $R_{\rm P} = Rr/(R+r)$ is less then that of antiparallel (bottom) $R_{\rm AP} = (R+r)/4$. The GMR$= R_{\rm AP}/R_{\rm P} - 1 = (R-r)^2/(4Rr)$.

Later this theory was modified by Brataas *et al.* [27] and Huertas-Hernando *et al.* [28]. Brataas *et al.* demonstrated that a multilayered system may be modelled by a set of resistors connecting nodes, either normal of ferromagnetic. Instead of two spin-dependent potentials of the spin-resistor model, the electronic non-equilibrium distribution function is characterized by charge- and three spin-dependent potentials $(\mu_e, \boldsymbol{\mu})$ for three spin components $\mathbf{s_x}, \mathbf{s_y}, \mathbf{s_z}$. Corresponding currents are defined as

$$j_\alpha = \frac{\sigma}{e}\nabla_\alpha \mu_e, \ \mathbf{j}_{s\alpha} = -\frac{\hbar\sigma}{2e^2}\nabla_\alpha \boldsymbol{\mu}_s, \quad \alpha = x, y, z. \tag{1.11}$$

The nodes are considered as good conductors with well defined spin-dependent potentials. Sum of incoming and outgoing spin currents is produced by external sources of spins, given by relaxation of existing nonequilibrium spin potential $\boldsymbol{\mu}$. Together with Kirchhoff law for charge currents, this results in

$$\sum_\alpha j_\alpha = 0, \ \sum_\alpha \mathbf{j}_{s\alpha} = \frac{\hbar\nu}{2}\frac{\boldsymbol{\mu}_s}{\tau_{\mathrm{sf}}}. \tag{1.12}$$

In continuous limit, the resistor model and Kirchhoff law become respectively diffusion equation for spin potential and Laplacian equation for electric potential, if the mean free path $l_{el} \ll l_{\mathrm{sf}}$ remains the least of all other length scales.

The authors of Ref. [27] also considered NF interface conductance in terms of spin-dependent scattering matrix $\mathcal{S}$. Only spin currents with $\uparrow, \downarrow$ spin directions were assumed to exist in the Ferromagnetic node, that is spin component perpendicular to $\mathbf{m}$ was filtered out on the NF boundary. With spin-flip on the boundary neglected, the scattering matrix $\mathcal{S}$ yields an expression that relates boundary jump in potentials $\mu_e, \boldsymbol{\mu}$ to currents on the normal side $j, \mathbf{j}$.

In the end, not only conventional real conductances for two spin directions $g_{\uparrow\uparrow}, g_{\downarrow\downarrow}$ are introduced, expected from the spin-resistor model as well, but also a complex conductance coefficient $g_{\uparrow\downarrow}$ [27]. This new parameter relates a spin-current $\mathbf{j}_{s\perp\mathbf{m}}$ of

the spin component perpendicular to the local magnetization $\mathbf{m}$ on the normal side of the boundary to the interfacial spin potential drop $\Delta\boldsymbol{\mu}$:

$$\mathbf{j}_{s\perp\mathbf{m},x} = \frac{-\hbar}{e^2}\left(\mathrm{Re}\, g_{\uparrow\downarrow}\mathbf{m}\times[\boldsymbol{\Delta\mu}\times\mathbf{m}] + \mathrm{Im}\,\mathbf{g}_{\uparrow\downarrow}[\mathbf{m}\times\boldsymbol{\Delta\mu}]\right). \tag{1.13}$$

Ab initio calculations of Ref. [29] demonstrated that for the most of experimentally relevant N-F surfaces $\mathrm{Re}\, g_{\uparrow\downarrow} \gg \mathrm{Im}\, g_{\uparrow\downarrow}$, so that the second term in Eq. (1.13) might be neglected.

Later, in 2002, Tserkovnyak *et al.* [3] considered the case when the magnetization $\mathbf{m}(t)$ of the layer is slowly rotating. In that case the scattering matrix approach with adiabatically slow time-dependent matrix $\mathcal{S}(t)$ can be used. Analogously to the "quantum pump" for pumped charge mechanism [1], varying components of $\mathbf{m}(t)$ serve as two external perturbations to pump spin currents through the NF boundaries into non-magnetic metal. Then the right hand side of Eq. (1.13) modifies for right (top sign) or left (bottom sign) NF surface as:

$$\begin{aligned}\mathbf{j}_{s\perp\mathbf{m},x} = {} & \frac{\hbar}{e^2}\mathrm{Re}\, g_{\uparrow\downarrow}\left(\Delta\boldsymbol{\mu}_s\times\mathbf{m}\mp\frac{\hbar}{2}\partial_t\mathbf{m}\right)\times\mathbf{m} \\ & + \frac{\hbar}{e^2}\mathrm{Im}\, g_{\uparrow\downarrow}\left(\Delta\boldsymbol{\mu}_s\times\mathbf{m}\mp\frac{\hbar}{2}\partial_t\mathbf{m}\right).\end{aligned} \tag{1.14}$$

Before this convenient description of spin transport in terms of $\mathcal{S}$-matrix was recognized, completely different methods allowed Slonczewski [30] and Berger [31] to predict in 1996 a new effect. They realized that for sufficiently thin magnetic layers the conduction electrons filtered by magnets might produce an observable feedback effect– exert a "spin-transfer torque" on magnetization vectors $\mathbf{m_i}$. Although their methods are somewhat different, the key idea is similar: for a trilayer FNF system with noncollinear magnetizations one should consider a spinor of the conduction electron spin $\mathbf{s}$ instead of an incoherent combination of spin currents of the spin-resistor model. Electrons entering the ferromagnet loose their perpendicular spin

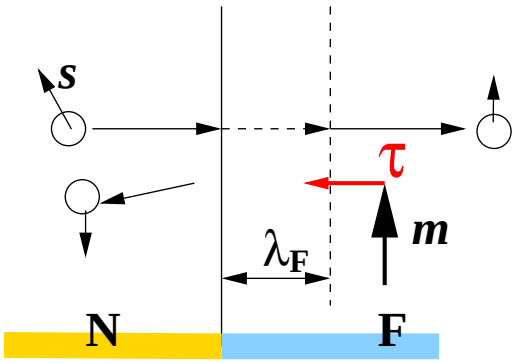

Figure 1.5: An electron with spin $\mathbf{s}$ is a coherent superposition of $\uparrow$ and $\downarrow$ parts. The $\uparrow$ component is transmitted and $\downarrow$ component is reflected. This filtering occurs on the length scales of $\sim \lambda_{\mathrm{F}}$ and the torque τ is exerted on the magnetization $\mathbf{m}$

component $\mathbf{s}_{\perp}$ when they pass through the boundary region. Since in a typical ferromagnet (Co, Ni, Fe) the band splitting for $\uparrow$ and $\downarrow$ spins is of order $\sim eV$, the Fermi wave-vector difference is large, $k_{\uparrow} - k_{\downarrow} \sim k_{\mathrm{F}}$. In result, on thicknesses of order λ_{F} the perpendicular component of the electron's spin is lost, see Fig. 1.5.

Indeed, for an electron incoming into the boundary layer a quantum-mechanical superposition of $\uparrow$ and $\downarrow$ states looses its coherence on the distances $\sim 2\pi/|k_{\uparrow} - k_{\downarrow}| \sim \lambda_{\mathrm{F}}$, which corresponds to rotation of the spin $\mathbf{s}$ on a random angle around $\mathbf{m}$. Summed over conduction electron spins, a perpendicular component of the spin curernt is randomized. Thus filtered spin-current component is absorbed by the ferromagnet as a torque acting on the vector $\mathbf{m}$. Since the boundary layer is thin, this model is called "surface spin-transfer torque".

As a key result, two ferromagnets with non-magnetic metal spacer between them act on each other by means of conduction electrons. If we assume spin-flip length l_{sf} in the normal spacer much longer then its size, a spin current carried by conduction electrons produces a torque which mainly lies inside the common plane of $\mathbf{m_{1,2}}$ and

thus aligns $\mathbf{m_1}$ along $\mathbf{m_2}$. The authors of Refs. [30, 31] predicted a torque $\vec{\tau}_{1\to 2}$ due to magnet with $\mathbf{m}_1$ on magnetization $\mathbf{m}_2$ in form of

$$\vec{\tau}_{1\to 2} \propto jp_1\mathbf{m}_1 \times [\mathbf{m}_2 \times \mathbf{m}_1], \tag{1.15}$$

the torque being proportional to the total electric current j and polarization coefficient $p_1 < 1$ due to the first magnet.

It is instructive to compare predictions of the theory by Slonczewski [30] and the circuit-theory [27, 28]. In the first one predicts the torque (1.15) to be completely in plane of magnetizations $\mathbf{m_{1,2}}$ involved, as long as in the circuit theory the 2nd term in the r.h.s. of (1.13) effectively gives some out-of-plane component of the torque.

With complete randomization of spins in the boundary layer, the angular momentum lost by the spin current would lie in the common plane of $\mathbf{m}, \mathbf{s}$, which corresponds to the first term in Eq.(1.13). The presence of the 2nd term in Eq.(1.13) means that some electrons are reflected from NF boundary layer before randomization is complete, and so their averaged spin rotates on a certain non-zero angle around $\mathbf{m}$. Theoretical assumptions of the circuit-theory [27] were substantiated by numerics of Stiles *et al.* [32]. They demonstrated that filtering is almost complete, which agrees with small ratio $\mathrm{Im}\, g_{\uparrow\downarrow}/\mathrm{Re}\, g_{\uparrow\downarrow} \ll 1$ found by Ref. [29].

Had one considered an alternative model of Ref. [33]– interaction between the layers in form of an effective magnetic field due to electronic build-up nearby, the torque would have only rotated $\mathbf{m_1}$ around $\mathbf{m_2}$. Another difference is that the spin-torque effect essentially depends on the charge current direction, whereas the effective-field effect does not. Experiments in Cornell [34] substantitated the spin-transfer theory by Slonczewski.

Qualitatively, the spin-torque induced effect in an FNF trilayer can be described as follows [35]: For simplicity, we restrict ourselves by the case when the left layer is

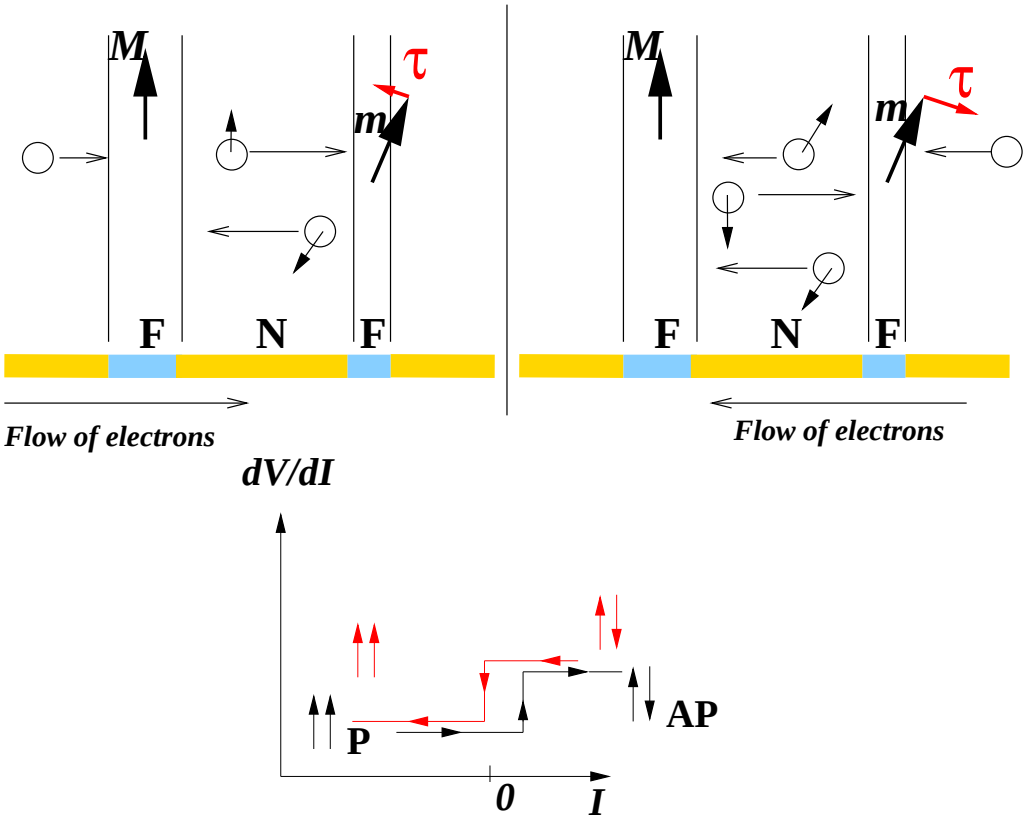

Figure 1.6: Top left panel: Electrons flowing from the left are polarized by the fixed layer and thus exert a spin-torque onto the thin layer towards the fixed layer magnetization. Top right panel: Electrons flowing from the right are reflected from the fixed layer, so that the net torque has the opposite sign and pulls the thin layer to the antiparallel configuration. Bottom panel: Qualitative plot for $dV/dI(I)$ of trilayer system at fixed small magnetic field. Ramping current from negative to positive values drives the system P $\rightarrow$ AP state by switching a free layer's magnetization at some value $I_+ > 0$. The reverse process switches back AP $\rightarrow$ P at $I_- < 0$

thick enough ("fixed layer") and keeps a constant magnetization **M**, but the right one is so thin ("free layer") that its magnetization **m** might change due to spin torque. Once the electrons move from the left (see the top left panel of Fig.1.6), the current in the normal spacer becomes spin polarized in the direction of **M**. As described above, a component of **M** perpendicular to **m** is absorbed by the thin layer as a torque acting on **m**. In result, the torque $\vec{\tau}$ pulls **m** *towards* **M**, making the *parallel* configuration P stable.

Reversely, if electrons are sent from the right (the top right panel of Fig.1.6) the net torque in the free layer comes from electrons reflected from the fixed magnet, but now their spins are directed preferentially opposite to **M**. This net torque pulls **m** *from* **M**, so that the *anti-parallel* state of magnets AP is more advantageous. There is a certain lower bound $I_{\pm}$ for the magnitudes of these switching currents because of Gilbert damping, which prevents any dynamics of the magnetization analogously to friction force. When the current becomes strong enough, a switching to the stable configuration occurs, which is usually observed as a feature in dV/dI characteristics due to GMR, see bottom panel in Fig. 1.6.

1.4 Overview of the thesis

Chapter 2: Pumped current and voltage for an adiabatic quantum pump

In this chapter we consider adiabatic pumping of electrons through an open quantum dot. As described in Sec. 1.1, the experiment [2] was performed at fixed current $I = 0$ and the averaged pumped voltage $\bar{V}$ was measured, see Fig. 1.2. On the other hand, an experiment might be carried out with $V = 0$ and non-zero current

$\bar{I}$ measured. We demonstrate that, even for very slow weak pumping, $\bar{I}$ and $\bar{V}$ are not simply related via dc conductance of the dot G as $\bar{I} = \bar{V}G$. The explanation lies in the fact that conductance G is also time-dependent, so that the product VG contain a rectified component due to AC components of V and G.

Therefore, we consider the statistical distribution of $\bar{d} = \bar{V}G - \bar{I}$. The scattering matrix formalism is applied to express transport properties via $\mathcal{S}$ matrix elements. Numerical integration over corresponding matrix ensemble yields the mesoscopic distribution of the voltage $\bar{V}$ or $\bar{d}$ in general case. Analytically, integrations can be performed for a single-channel, $N = 2$, or multi-channel, $N = \infty$, geometry. The distributions of $\bar{V}$, $\bar{d}$ and $\bar{I}$ are of similar width for experimentally relevant few-channel systems. In multichannel limit, $N \to \infty$, the distribution of $\bar{d}$ is much narrower than that of $\bar{V}$ or $\bar{I}$.

An important point of interpretation of experimental results Ref. [2] was raised by Brouwer [36], who proposed that the observed DC voltage was due to rectification of varying voltages, if they are capacitively connected to electronic reservoirs. If this is the case, pumped voltage and current are proportional to each other, with non-universal proportionality constant. However, an experimental exploration of $\bar{d}$ and its distribution $P(\bar{d})$ in few-channel dots may be useful to define whether it is the rectification effect or a true quantum pump which is observed in the experiment of Ref. [2].

The results were published in: M. L. Polianski and P. W. Brouwer Phys. Rev. B **64**, 075304 (2001).

Chapter 3: Noise through Quantum Pumps

First theoretical proposals and experimental realizations of the quantum pumping lead to a deeper investigations of the questions related to the pumped charge statistics (Full Counting Statistics (FCS)) of a given sample,and of pumped charge statistical properties in an ensemble of samples for various regimes of pumping frequency ω, temperature T and dwell time $\tau_{\rm dwell}$. Without addressing full FCS, we concentrate here in the Chapter 3 on its second moment, pumped noise S, and current-to-noise ratio I/S. We demonstrate that the noise through any mesoscopic sample in quantum pumping regime can be separated into the well-known equilibrium Nyquist thermal noise S_N and non-equilibrium pumping noise S_P. This last term, in the case of an open quantum dot, is the main subject of this Chapter.

For the experimentally relevant weak bilinear adiabatic regime $\hbar\omega, k_{\rm B}T \ll \hbar/\tau_{\rm dwell}$ the noise factorizes on frequency-temperature dependent coefficient $F(\omega, T)$ and a sample-specific contribution. The mesoscopic distribution of the latter is analyzed in detail for single- and multi-channel geometries. Full distributions $P(S)$ and $P(I/S)$ were found by numerical integration, and the ratio I/S was found to be limited, $I/S \leq 1$. In the multi-channel limit, $N \to \infty$ both distributions tended to Gaussian form, and fluctuations of noise S are analytically found small as $\sim 1/N$.

For $N \to \infty$, the noise S exhibits small fluctuations around an ensemble-averaged value, and in arbitrary pumping regime this value was found analytically. For the first time a pair correlator of time-dependent scattering matrix elements was found in diagrammatic technique method. It includes Diffuson $\mathcal{D}$ and Cooperon $\mathcal{C}$, analogous to ones in Hamiltonian approach.

The leading contribution to the noise due to Diffuson was considered for various regimes. Analogously to Ref. [37], a "heating temperature" T^* was introduced in

terms of pumping strength and frequency. This scale corresponds to broadening of the electron distribution function in the dot as a result of the time-dependent perturbations. Noise for various regimes of ω, T, T^* was considered both analytically and numerically and compared with previously obtained results. In particular, at strong pumping, $k_{\rm B}T^* \gg \hbar\omega$, the total noise was found to be dominated by either pumping noise $S_P \propto T^*$ or Nyquist noise $S_N \propto T$

The results were published in: M. L. Polianski and P. W. Brouwer, Phys. Rev. B **65**, 245314 (2002).

Chapter 4: Scattering matrix ensemble for time-dependent transport through a chaotic quantum dot

Important transport properties of a mesoscopic system are most elegantly expressed in terms of scattering matrix $\mathcal{S}$, see *e.g.* Eqs. (1.4,1.5) for conductance and shot noise of a stationary scatterer. However, a periodically perturbed sample, *e.g.* quantum dot, requires a modified treatment, with $\mathcal{S}$-matrix now dependent on two energy or two time arguments, see Eqs. (1.9,1.10). Until recently, there were no systematic attempts to find time-dependent $\mathcal{S}$ matrix distribution or, less ambitiously, to find matrix element correlators.

An alternative Hamiltonian approach was used in Ref. [37] to explore pumped current and noise, which invoked calculations of complicated diagrams, including Hikami box. Choice of approach is a matter of taste, but we demonstrate in this Chapter that the time-dependent $\mathcal{S}$ treatment of transport problems in multi-channel limit is more concise and efficient than the Floquet states formalism of two energy arguments [21] or aforementioned Hamiltonian approach of [37]. This Chapter establishes foundations of the scattering multi-channel matrix formalism with $\mathcal{S}$

matrix explicitly dependent on time.

First we consider a stationary scatterer and review known result for an energy-independent $\mathcal{S}$ matrix. Its elements have an almost Gaussian distribution with small non-Gaussian corrections of higher order in $1/N$. The pair- and four- matrix element correlations are sufficient to find a weak localization correction to conductance and conductance variance.

An energy-dependent stub model [10] with all energy dependence localized in a wide stub attached to the quantum dot (see Appendix C.2 for details) allows one to extend the $\mathcal{S}$ approach to single-energy argument matrices. In that case these correlators allow one to find, for example, a correlation of conductances at different energies. Their Fourier transform to time-representation gives a basis for a time-dependent scattering formalism.

With the time-dependent stub model, where time-dependent perturbation is localized in an attached stub, a pair correlators containing Diffuson $\mathcal{D}$ and Cooperon $\mathcal{C}$ of the previous chapter are derived in Appendix C.3, together with a four-element correlator. Although quite complicated, these general expressions are ready for plugging into any combination of time-dependent $\mathcal{S}(t,t')$. The pair correlators are used in examples of calculations of an ensemble-averaged weak-localization correction to the conductance of the periodically perturbed dot [38], of the white-noise perturbations [39]. The four-matrix correlator readily gives an averaged current-current correlator [37]. In a non-equilibrium situation a full noise is factorized on the shot noise S^S, Nyquist noise S^N, and pumping noise S^P, modified by external voltage V (equilibrium situation was considered in Chapter 3).

The results were published in: M. L. Polianski and P. W. Brouwer, J. Phys. A: Math. Gen. **36**, 3215 (2003).

Chapter 5: Current-induced transverse spin wave instability in a thin nanomagnet

The theoretical picture described in the Section 1.3 was substantiated by a series of experiments on trilayer systems in Cornell [34]. For one layer much thicker then the other, the spin torque rotated a thinner layer and led the system to the stable parallel (P) or anti-parallel (AP) configuration, cf. bottom of Fig. 1.6. An influence of applied magnetic field **H** was also extensively explored [40]. For a weak in-plane fields the dependence of dV/dI on current I clearly showed hysteretic switching, but at higher fields ~ 0.5 T the plot gained unexpected spiky and non-hysteretic behavior. This feature was attributed to spin-wave excitations created in a ferromagnet, and observed in computer simulations of mono-domain dynamics of Landau-Lifshitz-Gilbert equation with spin-torque term due to Slonczewski, see Eq. (1.15). Such spikes in dV/dI, see Fig. 1.7, upward or downward, are observed in many experiments, but their nature is not fully understood yet.

Motivated by this question, we considered a simpler system of a single thin ferromagnet attached to the reservoirs by normal contacts. Unlike many previous theoretical works on magnetization reversal, where two ferromagnets were considered as a one-dimensional system, we deal a single magnetic layer as essentially multi-dimensional and predict a new effect of transversal spin wave excitation. This is to be contrasted with a longitudal spin wave of 1d theoretical picture. An experimental signature of transversal vs. longitudal spin wave is a dip vs. peak in differential resistance dV/dI curve.

We show that a usual CPP-electric current through a thin ferromagnet can excite a spin-wave instability transverse to the current direction if source and drain contacts are not symmetric. The instability, which is driven by the current-induced "spin-

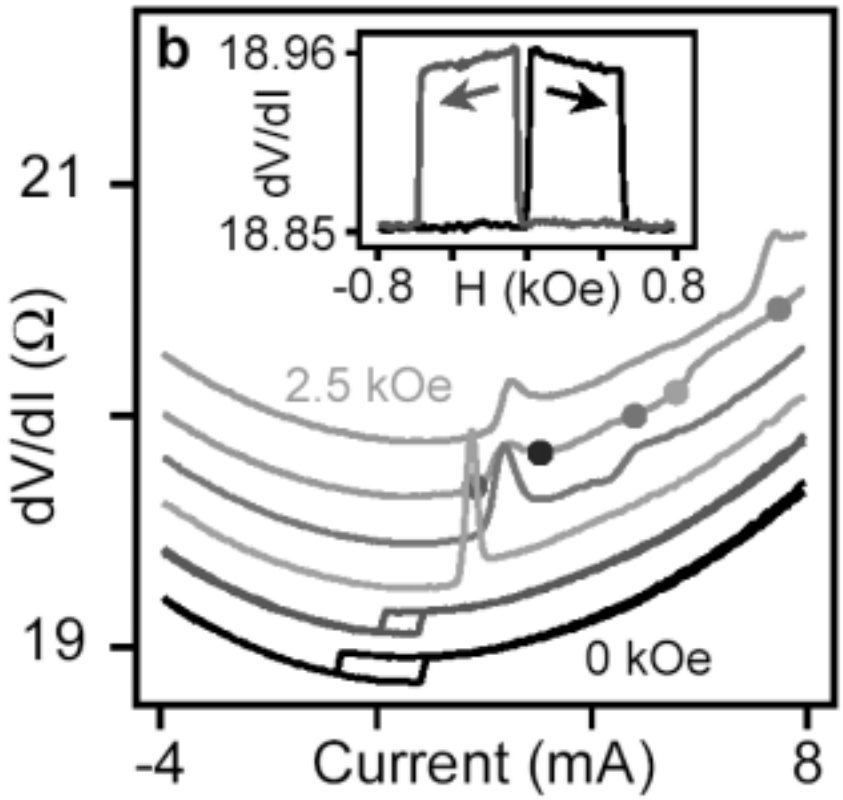

Figure 1.7: Differential resistance dV/dI was taken at various magnetic fields B for trilayer F-N-F system [40]. At low fields a clear hysteretic switching was observed, according to theoretical predictions, but at high fields a new unexpected peaks in dV/dI are found. The latter were attributed to uniform rotations of the thin magnet.

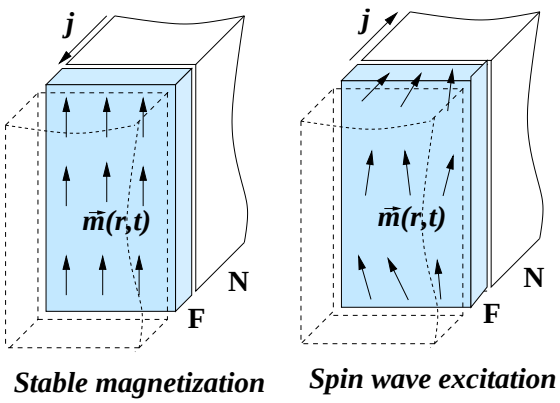

Figure 1.8: Left panel: One direction of electric current stabilizes the layer's magnetization. Right panel: Spin wave is excited inside the magnet if the current is sufficiently strong and electron flow from the larger normal lead to the smaller one.

transfer torque", exists for one current direction only, see Fig. 1.8

The excitation mechanism is based on probability for a spin, reflected from one point r of NF boundary, to diffuse to another point r' where the local magnetization $\mathbf{m}(r') \neq \mathbf{m}(r)$. Thus the spin $\mathbf{s}$ initially antiparallel to $\mathbf{m}(r)$ exerts a spin-torque on magnetization $\mathbf{m}(r')$, if $l_{\rm sf}$ in normal metal is much larger then the distance between r and r'. Since both transmitted and reflected electrons create a torque, the asymmetry becomes crucial: for example, if transmitted spins immediately sink into the electron reservoir close the magnet, the net torque is completely due to reflected electrons that *enhance* the spin-wave; in opposite situation the spin wave will be damped by torque due to the torque of transmitted spins.

The spin wave mode vector q, where the solution to Landau-Lifshitz-Gilbert equation becomes unstable, is a compromise between two competing mechanism opposing its excitation. For very small q modes magnetization $\mathbf{m}$ varies on the scales of $1/q$ and an electron should diffuse a large distance $\sim 1/q$ to exert a substantial spin torque. However, spin-flip processes, or finite spin-diffusion length $l_{\rm sf}$, strongly

limit a probability of such processes, so that critical current for small q grows as $I(q) \propto 1/q^2$. An $l_{\rm sf}$ inside Cu, fore example, is of order 100 nm, so the wavelength should be significantly smaller, $\lambda_{\rm SW} \ll 100$ nm.

On the other hand, large q are impossible because exchange energy $\propto q^2$ does not allow creation of fast modulation of $\mathbf{m}$ inside the ferromagnet. A relevant length scale is completely defined by physical properties of the ferromagnet and is usually referred to as "domain wall thickness", typically of order several nanometers, so that $\lambda_{\rm SW} \gg 5$ nm.

Currently, experimenters work either with wide films or nanopillars, the the transversal dimensions of the latter are typically $\sim$ 70 nm. One might expect that the spin waves we predict can be readily observed in experiment with highly asymmetric normal leads attached to a thin magnetic film. Indeed, this effect was recently explored in experiments in New-York University [41], and the theory of this Chapter was found in very good agreement with experimental observations.

The results presented in this Chapter were published in: M. L. Polianski and P. W. Brouwer, Phys. Rev. Lett. **92**, 026602. (2004)

Bibliography

[1] P. W. Brouwer, Phys. Rev. B **58**, 10135 (1998).

[2] M. Switkes *et al.*, Science **283**, 1905 (1999).

[3] Ya. Tserkovnyak, A. Brataas, and G. E. W. Bauer, Phys. Rev. Lett. **88**, 117601 (2002), Phys. Rev. B **66**, 224403 (2002).

[4] C. W. J. Beenakker, Rev. Mod. Phys. **69**, 731 (1997).

[5] M. L. Mehta, *Random Matrices*, (Academic, New York, 1991).

[6] J. J. M. Verbaarschot, H. A. Weidenmüller, and M. R. Zirnbauer, Phys. Rep. **129**, 367 (1985).

[7] C. H. Lewenkopf and H. A. Weidenmüller, Ann. Phys. **212**, 53 (1991).

[8] P. W. Brouwer, Phys. Rev. B **51**, 16878 (1995).

[9] M. Büttiker, A. Prêtre and H. Thomas, Phys. Rev. Lett. **70**, 4114 (1993); M. Büttiker J. Phys. Condens. Matter **5**, 9361 (1993); M. Büttiker, H. Thomas and A. Prêtre, Z. Phys. B **94**, 133 (1994); M. Büttiker and T. Christen, *Quantum Transport in Semiconductor Submicron Structures, NATO ASI Ser. E* vol 326 ed B Kramer (Dordrecht: Kluwer), 263 (1996); M. Büttiker, J. Low Temp. Phys. **118**, 519 (2000).

[10] Y. M. Blanter and M. Büttiker, Phys. Rep. **336**, 1 (2001).

[11] R. Blümel and U. Smilansky, Phys. Rev. Lett. **60**, 477 (1988).

[12] R. Blümel and U. Smilansky, Phys. Rev. Lett. **64**, 241 (1990).

[13] U. Smilansky, in *Chaos and Quantum Physics*, edited by M.-J. Giannoni, A. Voros, and J. Zinn-Justin (North-Holland, Amsterdam, 1991).

[14] H. U. Baranger and P. A. Mello, Phys. Rev. Lett. **73**, 142 (1994).

[15] R. A. Jalabert, J.-L. Pichard, and C. W. J. Beenakker, Europhys. Lett. **27**, 255 (1994).

[16] P. A. Mello in *Mesoscopic Quantum Physics*, edited by E. Akkermans, G. Montambaux, J.-L. Pichard, and J. Zinn-Justin (North-Holland, Amsterdam, 1995).

[17] P. A. Mello, P. Pereyra, and T. H. Seligman, Ann. Phys. **161**, 254 (1985).

[18] P. W. Brouwer *et al.*, Phys. Rev. Lett. **79**, 913 (1997).

[19] P. W. Brouwer, K. M. Frahm, and C. W. J. Beenakker, Phys. Rev. Lett. **78**, 4737 (1997); *Waves in Random Media* **9**, 91 (1999).

[20] E. P. Wigner, Phys. Rev. **98**, 145 (1955), and F. T. Smith, Phys. Rev. **118**, 349 (1960).

[21] M. Moskalets and M. Büttiker , Phys. Rev. B **66**, 035306(2002).

[22] M. N. Baibich *et al.*, Phys. Rev. Lett. **61**, 2472 (1988); G. Binash *et al.*, Phys. Rev. B **39**, 4828 (1989).

[23] W. P. Pratt *et al.*, Phys. Rev. Lett., **66**, 3060 (1991).

[24] J. Bass and W. P. Pratt, Jr., Physica B, **321**, 1 (2002).

[25] T. Valet and A. Fert, Phys. Rev. B **48**, 7099 (1993).

[26] M. Johnson, Phys. Rev. Lett. **70**, 2142 (1993).

[27] A. Brataas, Yu. V. Nazarov, and G. E. W. Bauer, Phys. Rev. Lett. **84**, 2481 (2000).

[28] D. Huertas-Hernando *et al.*, Phys. Rev. B **62**, 5700 (2000).

[29] K. Xia *et al.*, Phys. Rev. B **65**, 220401 (2002).

[30] J. Slonczewski, J. Magn. Magn. Mater. **159**, L1 (1996).

[31] L. Berger, Phys. Rev. B **54**, 9353 (1996).

[32] M. D. Stiles and A. Zangwill, Phys. Rev. B **66**, 014407 (2002).

[33] C. Heide, Phys. Rev. Lett. **87**, 197201 (2001), Phys. Rev. B **65**, 054401 (2002).

[34] E. B. Myers *et al.*, Science **285**, 867 (1999); J. A. Katine*et al.*, Phys. Rev. Lett. **84**, 3149 (2000); F. J. Albert*et al.*, Phys. Rev. Lett. **89**, 226802 (2002).

[35] X. Waintal *et al.*, Phys. Rev. B **62**, 12317 (2000).

[36] P. W. Brouwer, Phys. Rev. B **63**, 121303 (2001).

[37] M. G. Vavilov, V. Ambegaokar, and I. L. Aleiner, Phys. Rev. B **63**, 195313 (2001).

[38] M. G. Vavilov and I. L. Aleiner, Phys. Rev. B **60**, R16311 (1999).

[39] H. U. Baranger and P. A. Mello, Phys. Rev. B **51**, 4703 (1995); I. L. Aleiner and A. I. Larkin, Phys. Rev. B **54**, 14423 (1996); P. W. Brouwer and C. W. J. Beenakker, Phys. Rev. B **55**, 4695 (1997).

[40] S. I. Kiselev *et al.*, Nature **425**, 380 (2003).

[41] B. Oezyilmaz *et al.*, cond-mat/0403367.

Chapter 2

Pumped current and voltage for an adiabatic quantum pump

2.1 Introduction

An electron pump is a device that converts a periodic variation of its characteristics into a time-independent electric current.[1] Such characteristics can be "macroscopic", like the charge on the device or the conductance of point contacts, or "microscopic", such as the location of a scatterer or the magnetic flux threading the sample. When there are two characteristics of the device that can be varied harmonically with a frequency ω and phase difference ϕ, pumping of electrons already occurs in the adiabatic limit $\omega \to 0$. In that case the pumped current is proportional to $\omega \sin \phi$, and changes sign when the phase relationship between the parameters is reversed. Adiabatic electron pumps have been realized experimentally in (arrays of) Coulomb blockaded quantum dots, using the voltages on plunger gates, and/or the transparencies of the contacts as pumping parameters.[2, 3, 4]

In this Chapter, we consider an adiabatic electron pump that consist of a semi-

conductor quantum dot coupled to two electron reservoirs by means of ballistic point contacts.[5] Variation of two gate voltages allow for small changes of the shape of the dot, and thus for the flow of a dc current. Following a proposal by Spivak *et al.*,[6] such a device has been built and investigated by Switkes *et al.*[7] The device of Ref. [7] is referred to as an "adiabatic quantum pump", because the variation of the gate voltages predominantly affects the quantum interference of the electrons in the quantum dot, not their classical trajectories. An important property of the quantum dot used in the experiment of Ref. [7] is that its classical dynamics is chaotic. As a result, the magnitude and the sign of the expected pumped current $\bar{I}$ are subject to mesoscopic fluctuations. Since these fluctuations are large, the mean $\langle \bar{I} \rangle$ and variance $\langle \bar{I}^2 \rangle$ are insufficient to describe the ensemble, and one needs to know the entire probability distribution $P(\bar{I})$.

Theoretical analysis has focused on the dc current $\bar{I}$ pumped through the dot [8, 9, 10, 11, 12, 13],

$$\bar{I} = \frac{1}{T} \int_0^T dt I(t), \tag{2.1}$$

$T = 2\pi/\omega$ being the period of the pumping cycle. However, experimentally, the preferred measurement is that of the dc voltage $\bar{V}$ that the electron pump generates,[7]

$$\bar{V} = \frac{1}{T} \int_0^T dt V(t). \tag{2.2}$$

Naively, one might expect that, for small pumping amplitudes, $\bar{I}$ and $\bar{V}$ are related via the dot's conductance G as $\bar{I} = \bar{V}G$. However, as we show in this Chapter, this naive "Ohm's law" is not always true, depending on whether the pumping frequency ω is small or large compared to the charge-relaxation rate γ of the reservoirs. (For adiabatic pumping, ω must always be small compared to the charge relaxation rate of the quantum dot.) For $\omega \ll \gamma$ and if the number N of propagating channels in the point contacts between the quantum dot and the electron reservoirs is small, the

pumped current $\bar{I}$ and the difference $\bar{D} = \bar{V}G - \bar{I}$ can actually be of comparable magnitude.

A qualitative explanation why the pumped voltage and current are not related via the simple relation $\bar{V}G - \bar{I}$ in the limit $\omega \ll \gamma$ follows from the observation that both the pumped current and the pumped voltage have dc and ac components. For slow pumping, the electron pump generates a bias voltage that counteracts both the dc and ac currents generated in the dot. Since the conductance G itself also varies in time, $V_{\rm ac}G$ has a dc component. It is this additional rectified dc component of the current that is responsible for the difference between $\bar{V}G$ and $\bar{I}$ for an adiabatic electron pump. When pumping is faster than the charge relaxation rate of the reservoirs, no ac bias voltage is generated to balance the ac current, and the difference between $\bar{V}G$ and $\bar{I}$ disappears.

The purpose of this Chapter is to find the distribution of the difference $\bar{V}G - \bar{I}$ between pumped current and pumped voltage for adiabatic pumping of electrons through a chaotic quantum dot and to compare it to the distributions of $\bar{I}$ and $\bar{V}$. For a chaotic dot, these distributions have a universal form, independent of details of the pumping mechanism or the shape of the quantum dot. In section 2.2 we use the scattering approach to present a quantitative theory for the pumped voltage $\bar{V}$, and the difference $\bar{D} = \bar{V}G - \bar{I}$. In section 2.3 we then evaluate the distribution of $\bar{V}G - \bar{I}$ for an ensemble of chaotic quantum dots, using random matrix theory.

2.2 Pumped current and voltage

We consider a quantum dot coupled to two electron reservoirs via point contacts, see Fig. 2.1. The shape of the quantum dot is varied periodically by variation of two gate voltages, represented by dimensionless parameters X_1 and X_2. Alternatively, X_1 or

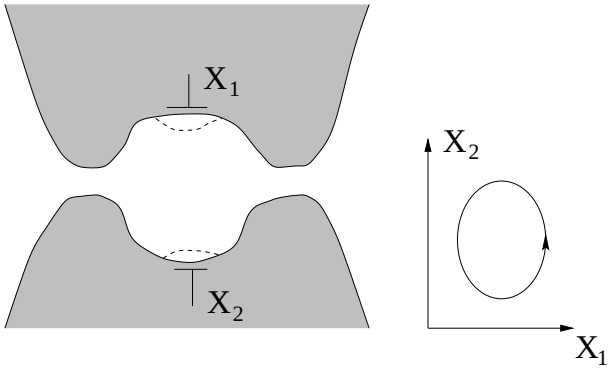

Figure 2.1: Schematic of a chaotic quantum dot whose shape can be changed by varying gate voltages X_1 and X_2 (left). In one cycle X_1 and X_2 trace out a contour in (X_1, X_2) space (right).

X_2 can represent the value of an applied magnetic field, or any other parameter that characterizes the quantum dot.

As discussed in the introduction, the electron pump can be characterized experimentally via a direct measurement of the pumped current, or via a measurement of the voltage $V(t)$ between the two reservoirs generated as a result of the pumping of charge through the quantum dot.[14]

A formula for the dc current has been derived in Refs. [8, 9]. To derive a formula for the dc voltage $\bar{V}$, we introduce a simple model for the quantum dot and the two electron reservoirs, see Fig. 2.2. The dot and the reservoirs 1, 2 are connected to a screening gate via capacitances C and C_1, C_2. Following Refs. [15, 16], we introduce the emissivity $e\delta q(m)/\delta X_j$, which is the charge that exits the dot through point contact m $(m = 1, 2)$ when the parameter X_j $(j = 1, 2)$ is changed adiabatically by an amount δX_j. Then the total current flowing through contacts 1 and 2 reads

$$I_1(t) = e\sum_{i=1}^{2} \frac{\delta q(1)}{\delta X_i}\frac{dX_i}{dt} + [V_1(t) - V_2(t)]G, \tag{2.3}$$

$$I_2(t) = e\sum_{i=1}^{2}\frac{\delta q(2)}{\delta X_i}\frac{dX_i}{dt} + [V_2(t) - V_1(t)]G, \tag{2.4}$$

where G is the dc cconductance of the quantum dot. Here we assume that all variations are made slowly on the scale of the dwell time of the quantum dot.

When current is measured, the voltages of the two reservoirs are equal, $V_1(t) = V_2(t)$. Hence the dc current $\bar{I}$ can be found from integration of Eq. (2.3) or (2.4).[8] Using Stokes' theorem, $\bar{I}$ can be rewritten as an integral over the surface area S enclosed by the contour of the parameters X_1 and X_2 in the (X_1, X_2) plane,

$$\bar{I} = \frac{e\omega}{2\pi}\int dX_1 dX_2 \bar{i}(X_1, X_2), \tag{2.5}$$

where

$$\begin{aligned}\bar{i} &= \frac{\partial}{\partial X_2}\frac{\partial q(1)}{\partial X_1} - \frac{\partial}{\partial X_1}\frac{\partial q(1)}{\partial X_2} \\ &= -\frac{\partial}{\partial X_2}\frac{\partial q(2)}{\partial X_1} + \frac{\partial}{\partial X_1}\frac{\partial q(2)}{\partial X_2}.\end{aligned} \tag{2.6}$$

When voltage is measured, the result depends on whether variation of the parameters X_1 and X_2 is fast or slow compared to the charge relaxation rates $\gamma_{1,2} \sim G/C_{1,2}$ of the reservoirs. Combining Eq. (2.3) with $I_1 = C_1 dV_1(t)/dt$, $I_2 = C_2 dV_2(t)/dt$ one obtains

$$\frac{d(V_1 - V_2)}{dt} = \sum_{i=1}^{2}\left(\frac{e}{C_1}\frac{\delta q(1)}{\delta X_i} - \frac{e}{C_2}\frac{\delta q(2)}{\delta X_i}\right)\frac{dX_i}{dt} + \left(\frac{G}{C_1} + \frac{G}{C_2}\right)(V_1 - V_2). \tag{2.7}$$

If the variation is fast compared to $\gamma_{1,2}$ (but still slow compared to the charge relaxation rate of the quantum dot), the voltage difference $V_1 - V_2$ is essentially time independent and takes the value

$$\bar{V} = \bar{I}/\bar{G}, \tag{2.8}$$

where $\bar{G}$ is the conductance averaged over one cycle,

$$\bar{G} = \frac{1}{T}\int_0^T dt G(X_1(t), X_2(t)). \tag{2.9}$$

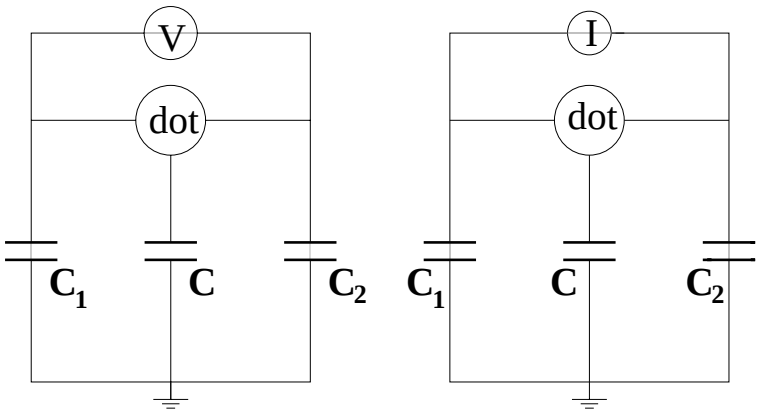

Figure 2.2: Equivalent circuit for a measurement of the pumped voltage through the dot (left) and of the pumped current (right). C_i and C are geometrical capacitances of the $i-$th reservoir and the dot.

In the opposite limit $\omega \ll \gamma_{1,2}$, which is the case we'll consider in the remainder of the Chapter, the r.h.s. of Eq. (2.7), which is proportional to $\gamma_{1,2}$, must vanish, so that $I_1(t) = \eta I_2(t)$, where $\eta = C_1/C_2$ is a numerical coefficient describing the capacitive division between the two reservoirs. Combining this with Eq. (2.3), we find

$$V_1(t) - V_2(t) = \frac{e}{G(1+\eta)} \sum_{i=1}^{2} \left(\frac{\delta q(1)}{\delta X_i} \frac{dX_i}{dt} - \eta \frac{\delta q(2)}{\delta X_i} \frac{dX_i}{dt} \right)$$

The dc voltage $\bar{V}$ is then found by integration over the period T, with the result

$$\bar{V} = \frac{h\omega}{4\pi e} \int dX_1 dX_2 \bar{v}(X_1, X_2), \tag{2.10}$$

$$\begin{aligned} \bar{v} = & \frac{1}{1+\eta} \left[\frac{\partial}{\partial X_2} (\frac{1}{g} \frac{\partial q(1)}{\partial X_1}) - \frac{\partial}{\partial X_1} (\frac{1}{g} \frac{\partial q(1)}{\partial X_2}) \right] \\ & - \frac{\eta}{1+\eta} \left[\frac{\partial}{\partial X_2} (\frac{1}{g} \frac{\partial q(2)}{\partial X_1}) - \frac{\partial}{\partial X_1} (\frac{1}{g} \frac{\partial q(2)}{\partial X_2}) \right], \end{aligned} \tag{2.11}$$

where $g = hG/2e^2$ is the dimensionless conductance. For small harmonic variations of the parameters, $X_1(t) = \delta X_1 \cos(\omega t)$ and $X_2(t) = \delta X_2 \cos(\omega t + \phi)$, the integrations

are trivial, and one finds

$$\bar{I} = \frac{1}{2} e\omega \delta X_1 \delta X_2 \bar{i} \sin\phi \tag{2.12}$$

for the pumped current, and

$$\bar{V} = \frac{h\omega}{4e} \delta X_1 \delta X_2 \bar{v} \sin\phi \tag{2.13}$$

for the pumped voltage.

If the conductance G were constant in a cycle, i.e., G would not depend on X_1 and X_2, Eqs. (2.6) and (2.11)–(2.13) give the identity $\bar{V}G = \bar{I}$: the pumped current measured at zero bias and the pumped voltage measured at zero current are related by Ohm's law. However, in general G does depend on X_1 and X_2, and this "Ohm's law" does not hold. The deviation is described by the difference

$$\bar{D} = \bar{V}G - \bar{I}. \tag{2.14}$$

For small δX_1 and δX_2, we find from Eqs. (2.6), (2.11),

$$\bar{D} = \frac{1}{2} e\omega \delta X_1 \delta X_2 \bar{d} \sin\phi, \tag{2.15}$$

$$\begin{aligned} \bar{d} = {} & \frac{1}{1+\eta} \left[\frac{1}{g} \frac{\partial g}{\partial X_1} \frac{\partial q(1)}{\partial X_2} - \frac{1}{g} \frac{\partial g}{\partial X_2} \frac{\partial q(1)}{\partial X_1} \right] \\ & - \frac{\eta}{1+\eta} \left[\frac{1}{g} \frac{\partial g}{\partial X_1} \frac{\partial q(2)}{\partial X_2} - \frac{1}{g} \frac{\partial g}{\partial X_2} \frac{\partial q(2)}{\partial X_1} \right]. \end{aligned} \tag{2.16}$$

The derivatives to X_1 and X_2 appearing in the above formulae are derivatives taken at constant values of the electro-chemical potential μ of the reservoirs. These are not necessarily equal to derivatives taken at a constant value of the (self-consistent[1]) electrostatic potential $V_{\rm sc}$ inside the quantum dot. (The self-consistent

[1] Corrections to the self-consistent description are small as $1/N_{\rm ch}$, where $N_{\rm ch}$ is the total number of channels connecting the dot to the reservoirs, including spin degeneracy, see I. L. Aleiner, P. W. Brouwer, and L. I. Glazman, Phys. Rep. **358**, 309 (2002). Even for single-channel point contacts, one has $N_{\rm ch} = 4$, and the quantitative effect of these corrections is small.

electrostatic potential is meant in the sense of a mean-field approximation of the electron-electron interactions, see Refs. [14, 15, 16] for details.) Changes of $V_{\rm sc}$ occur in a pumping cycle, because the total charge on the dot may vary during the pumping cycle. For technical reasons, it is preferred to treat $V_{\rm sc}$, or, equivalently, the kinetic energy $E = \mu - V_{\rm sc}$, as an independent parameter, and to take derivatives at constant E. The above equations for pumped voltage and current can be rewritten using derivatives at constant E if we substitute the parametric derivatives $\partial/\partial X_1$ and $\partial/\partial X_2$ in Eqs. (2.6), (2.11), and (2.16) by[15, 16]

$$\left.\frac{\partial}{\partial X}\right|_{\mu} \rightarrow \left.\frac{\partial}{\partial X}\right|_{E} + \frac{\partial E}{\partial X}\frac{\partial}{\partial E}, \tag{2.17}$$

$$\frac{\partial E}{\partial X_i} = -\frac{\partial q/\partial X_i}{C/2e^2 + \partial q/\partial E}. \tag{2.18}$$

Here C is the capacitance of the quantum dot. In Eq. (2.17), we abbreviated

$$\frac{\partial q}{\partial X_j} = \frac{\partial q(1)}{\partial X_j} + \frac{\partial q(2)}{\partial X_j}. \tag{2.19}$$

For a realistic quantum dot, the charging energy e^2/C is much larger than the mean level spacing Δ. In that limit, one finds that the dot charge remains constant during the pumping cycle, $I_1(t) = -I_2(t)$ for all time. As a consequence, the pumped voltage $\bar{V}$ and the difference $\bar{D} = \bar{V}G - \bar{I}$ lose their dependence on the capacitive division η.

In the absence of inelastic processes and for low temperatures (temperature T below the mean level spacing Δ in the quantum dot), the emissivities $\partial q(m)/\partial X_j$ and the conductance G can be expressed in terms of the scattering matrix S of the quantum dot and its derivatives to X_1, X_2, and E. The matrix S has dimension $2N$, where N is the number of propagating channels in each point contact; it is unitary (unitary symmetric) in the presence (absence) of a time-reversal symmetry breaking magnetic field. The derivatives of S are parameterized via hermitian matrices R,

R_j, defined as [2]

$$R = -i\frac{\Delta}{2\pi}\frac{\partial S}{\partial E}S^\dagger,\ R_j = -i\frac{\partial S}{\partial X_j}S^\dagger.$$

Then the emissivities $\partial q(m)/\partial E,\ \partial q(m)/\partial X$, $m = 1, 2$, are given by [16]

$$\frac{\partial q(m)}{\partial E} = \frac{1}{\Delta}\mathrm{Re\ tr}\, P_m R, \tag{2.20}$$

$$\frac{\partial q(m)}{\partial X_j} = \frac{1}{2\pi}\mathrm{Re\ tr}\, P_m R_j. \tag{2.21}$$

Here $P_1 = 1 - P_2$ is a diagonal matrix with elements $(P_1)_{jj} = 1$ if $j \leq m$ and zero otherwise. The dc conductance g is given by the Landauer formula,

$$g = \mathrm{tr}\, S^\dagger P_1 S P_2. \tag{2.22}$$

In the next section, we shall study the distribution of the dimensionless difference $\bar{d} = \bar{v}g - \bar{i}$ for the case of a chaotic quantum dot.

2.3 Distribution of $\bar{D} = \bar{V}G - \bar{I}$

For an ensemble of chaotic quantum dots, the statistical distribution of the scattering matrix and its derivatives is known from the literature.[18] It takes its simplest form when the derative of S is not parameterized by the matrices R_j, R, but by the symmetrized derivatives Q, Q_j,

$$Q = S^{-1/2}RS^{1/2},\ Q_j = S^{-1/2}R_jS^{1/2}.$$

In the prensence of time-reversal symmetry (labeled by the Dyson parameter $\beta = 1$), the matrices Q, Q_1, and Q_2 are real symmetric. When time-reversal symmetry is broken by a magnetic field ($\beta = 2$), Q, and Q_1, and Q_2 are hermitian. For ideal

[2] The matrix $-i(\partial S/\partial E)S^\dagger = 2\pi R/\Delta$ is the Wigner-Smith time-delay matrix, see [19]

contacts, the joint distribution $P(S, Q, Q_1, Q_2)$ reads [18]

$$\begin{aligned} P &\propto \left(1 + \frac{2e^2}{C\Delta}\mathrm{tr}\, Q\right) \Theta(Q)(\det Q)^{-N/2-2(\beta N+2-\beta)} \\ &\quad \times \exp\left[-\frac{\beta}{2}\mathrm{tr}\,\left(Q^{-1}\right)\right] \exp\left[-\frac{\beta}{16}\mathrm{tr}\,\left(\left(Q^{-1}Q_1\right)^2 + \left(Q^{-1}Q_2\right)^2\right)\right], \quad (2.23) \end{aligned}$$

where $\Theta(Q) = 1$ if all eigenvalues of Q are positive and $\Theta(Q) = 0$ otherwise. The capacitance C appears in the distribution because the ensemble is obtained by sweeping an external gate voltage, not the self-consistent energy E.[17]

To find the distribution $P(\bar{d})$, we first integrate over Q_1 and Q_2 at fixed S and Q, and then over S and Q. The first integration can be done analytically, since, for fixed Q, Q_1 and Q_2 are Gaussian random matrices, see Eq. (2.23). The result of this integration takes a simple form,

$$P(\bar{d}) = \left\langle \frac{1}{2\sigma} e^{-|\bar{d}|/\sigma} \right\rangle_{S,Q}, \quad (2.24)$$

where the brackets indicate the average over S and Q that remains to be done. In equation (2.24) σ is positive function of S and Q, given by

$$\begin{aligned} \sigma^2 &= \left(\frac{16}{\beta g}\right)^2 \left([\mathrm{tr}\, A^2 + \frac{\delta_{\beta,1}}{2}\mathrm{tr}\,(PRSPR^T S^\dagger - \right. \\ &\quad \left. - PRPR)]\ \mathrm{tr}\, B^2 - (\mathrm{tr}\, AB)^2 \right), \quad (2.25) \end{aligned}$$

where we abbreviated

$$\begin{aligned} A &= R\left(P - \frac{\mathrm{tr}\, PR}{C\Delta/2e^2 + \mathrm{tr}\, R}\right), \\ B &= R\left(\Lambda - \frac{\mathrm{tr}\, \Lambda R}{C\Delta/2e^2 + \mathrm{tr}\, R}\right), \end{aligned}$$

and $P = (P_1 - \eta P_2)/(1+\eta)$, $\Lambda = i(P_1 S P_2 S^\dagger - S P_2 S^\dagger P_1)$.

For the remaining integrations over S and Q we consider two limiting cases: multichannel point contacts ($N \gg 1$) and single channel point contacts ($N = 1$).

2.3.1 Single-channel contacts

For $N = 1$ the remaining number of variables is small, and can be integrated over numerically, using the distribution (2.23).[3] Results for the (physically relevant) limit $C\Delta \ll e^2$ are shown in Fig. 2.3. In this limit, the distribution $P(\bar{d})$ does not depend on the capacitive division η between the reservoirs. The results for larger values of C are not very different from those shown in Fig. 2.3. This is illustrated in the inset of Fig. 2.3, where we have shown the distribution $P(\bar{d})$ for the case of large capacitance $C\Delta \gg e^2$ and asymmetric reservoirs (capacitive division $\eta = 0$). For $\bar{d}$ close to zero, the distribution shows a cusp with a logarithmically divergent derivative at $\bar{d} = 0$. For $\bar{d} \gg 1$, the distribution $P(\bar{d})$ has power-law tails. For $C\Delta \ll e^2$ they are as follows[4]

$$P(\bar{d}) \propto \begin{cases} \bar{d}^{-3}, & \beta = 1, \\ \bar{d}^{-3} \log \bar{d}, & \beta = 2. \end{cases} \tag{2.26}$$

The tails of the distribution correspond to samples with an anomalously large eigenvalue of Q, corresponding to an anomalously large dwell time τ_D:[19] a value of $\bar{d}$ in the tail of the contribution typically corresponds to a dwell time $\tau_D \sim \tau_H \bar{d}^{2/\beta}$, $\tau_H = \hbar/\Delta$ being the Heisenberg time. Since configurations with anomalously large dwell times are more sensitive to dephasing or thermal smearing, such perturbations will truncate the tails for $\bar{d} \sim (\tau_\phi/\tau_H)^{\beta/2}$ or $\bar{d} \sim (\tau_H T)^{-\beta/2}$.

For comparison, we have also calculated the distribution of the pumped current $\bar{i}$ and voltage $\bar{v}$. For single-channel contacts, the distribution again takes the form (2.24), with σ replaced by σ_i and σ_v, respectively. Expressions for σ_i and σ_v can

[3] The numerical method to generate random matrices according to the distribution (2.23) is outlined in J. N. H. J. Cremers and P. W. Brouwer, Phys. Rev. B **65**, 115333 (2002).

[4] The tails of the distribution depend on the value of the capacitance C. In the non-interacting limit $C\Delta \gg e^2$ and $\eta = 0$, they read $P(\bar{d}) \propto \bar{d}^{-2}$ for $\beta = 1$ and $P(\bar{d}) \propto \bar{d}^{-3} \log \bar{d}$ for $\beta = 2$.

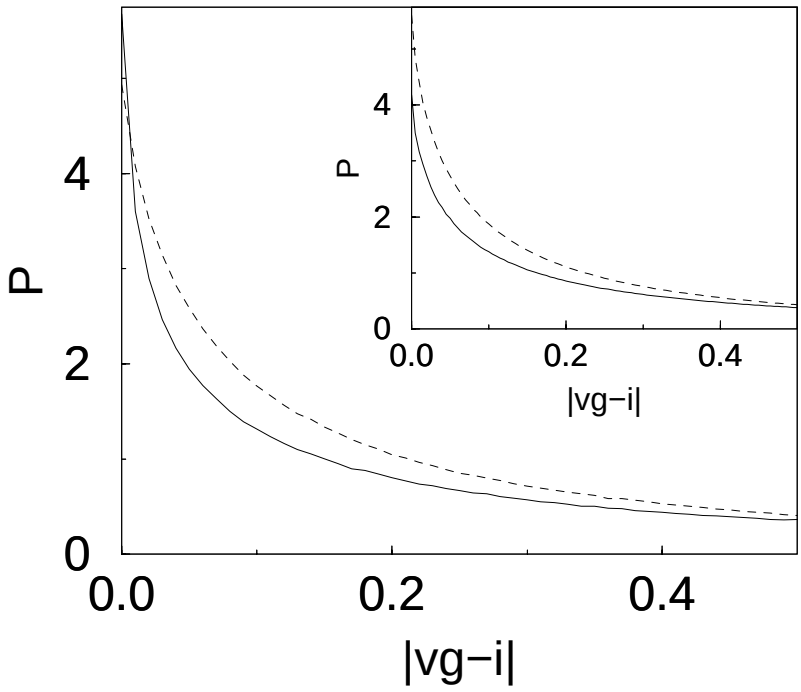

Figure 2.3: Distribution of the normalized difference $\bar{d} = \bar{v}g - \bar{i}$ between pumped voltage $\bar{v}$ and pumped current $\bar{i}$ for single-channel point contacts, for the physically relevant limit $C\Delta \ll e^2$ (main figure). The opposite limit $C\Delta \gg e^2$ is shown in the inset for the case $\eta = 0$. Presence (absence) of time-reversal symmetry $\beta = 1$ ($\beta = 2$) is shown solid (dashed).

be found in the Appendix A. The resulting distributions are shown in Fig. 2.4. (The distribution of the current was calculated previously in Ref. [8].) The main conclusion upon comparison of Figs. 2.3 and 2.4 is that, for single-channel point contacts, the distributions of $\bar{i}$ and of $\bar{d} = \bar{v}g - \bar{i}$ have comparable widths. Hence, for $N = 1$, deviations from "Ohm's law", as characterized by $\bar{d} = \bar{v}g - \bar{i}$ are of the same order as the pumped current $\bar{i}$ itself.

2.3.2 Multi-channel contacts

The distribution of $\bar{d}$ in the limit $N \gg 1$ can be directly obtained from Eq. (2.24). The integration over the unitary matrix U of eigenvectors of R and over the scattering matrix S is performed using the method of Ref. [20]. For the remaining integration over the eigenvalues $\tau_i, i = 1, \ldots, 2N$, of the matrix R it is sufficient to know their density,[18]

$$\rho(\tau) = \sum_{j=1}^{2N} \langle \delta(\tau_j - \tau) \rangle = \frac{N}{\pi\tau^2} \sqrt{(\tau_+ - \tau)(\tau - \tau_-)}, \tag{2.27}$$

where $\tau_\pm = (3 \pm \sqrt{8})/2N$. The result is

$$\langle \sigma^2 \rangle = \frac{4}{\beta N^4} \left[1 + \frac{4}{\beta} \left(\frac{1-\eta}{1+\eta} \right)^2 \left(\frac{\Delta}{\Delta + 2e^2/C} \right)^2 \right]. \tag{2.28}$$

[The $1/N^4$ prefactor in Eq. (2.28) follows from a contribution $\propto 1/N^2$ from the factor g^{-2} in Eq. (2.25) and a factor $1/N$ from each of the traces $\mathrm{tr}\, A^2$ and $\mathrm{tr}\, B^2$ in that same equation; the term $(\mathrm{tr}\, AB)^2$ in Eq. (2.25) does not contribute to $\langle \sigma^2 \rangle$ to leading order in $1/N$.] Calculation of higher moments of σ shows that fluctuations of σ are small compared to the average as $N \to \infty$. Hence, we can conclude that the distribution of $\bar{d}$ in multi-channel limit is of the Poissonian form (2.24), with σ^2 given by Eq. (2.28).

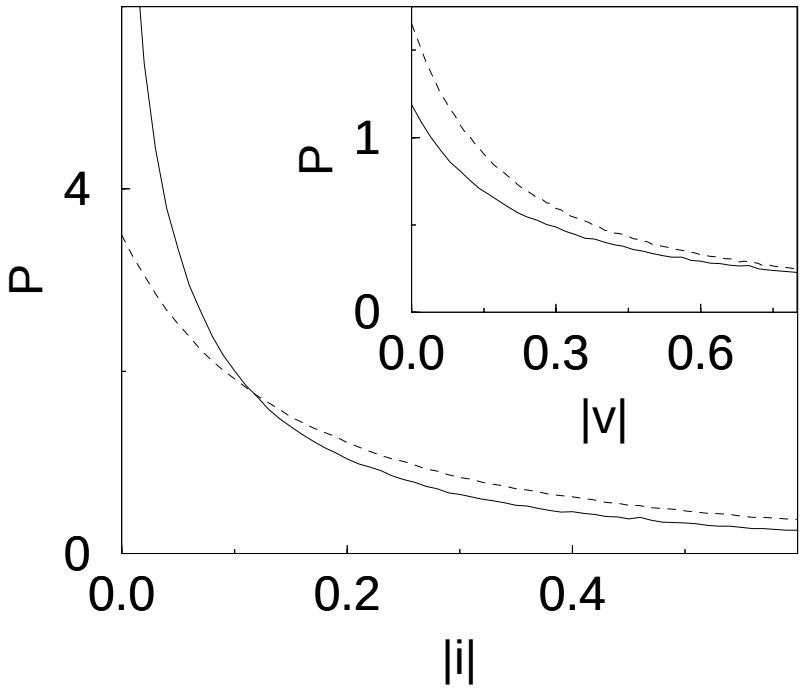

Figure 2.4: Distribution of normalized pumped current $\bar{i}$ and (inset) voltage $\bar{v}$ for single-channel contacts. Presence (absence) of time-reversal symmetry $\beta = 1$ ($\beta = 2$) is shown solid (dashed).

This is to be contrasted with the distribution of the pumped current $\bar{i}$, which is Gaussian for large N, with zero mean and with root mean square[8, 10]

$$\langle \bar{i}^2 \rangle^{1/2} = \frac{1}{\pi N}. \tag{2.29}$$

Hence we conclude that, for large N, typically $\bar{d}$ is a factor $\sim N$ smaller than the pumped current, and can be neglected in a measurement. Hence, in the limit $N \to \infty$ the expectation of "Ohm's law" $\bar{v}g = \bar{i}$ holds, and one readily concludes that the pumped voltage $\bar{v}$ has a Gaussian distribution with zero mean and with root mean square

$$\langle \bar{v}^2 \rangle^{1/2} = \frac{2}{\pi N^2}. \tag{2.30}$$

In summary, for adiabatic pumping of electrons through a chaotic quantum dot, we have derived expressions of the pumped current $\bar{I}$ (in case of a current measurement) or the pumped voltage $\bar{V}$ (in case of a voltage measurement) in terms of the scattering matrix of the quantum dot. Pumped current and voltage are not simply related by the dot's conductance G. We have calculated the distribution of the difference $\bar{V}G - \bar{I}$ for small pumping amplitudes, which is universal for a chaotic quantum dot. If the number N of propagating channels in the contacts between the quantum dot and the reservoirs is one, $\bar{I}$ and $\bar{V}G - \bar{I}$ can be of the same size; if $N \gg 1$, $\bar{V}G - \bar{I}$ is typically a factor N smaller than $\bar{I}$. Our results are valid in the limit of slow pumping, where the pumping frequency ω is much smaller than the charge relaxation rate γ of the reservoirs. If $\omega \gg \gamma$, the difference $\bar{V}G - \bar{I}$ is suppressed.

The results obtained here are important in view of the interpretation of the experiment of Ref. [7]. The observations of that experiment can also be explained if the observed dc voltage is the result of rectification of ac displacement currents gen-

erated by the time-dependent gate voltages that should drive the electron pump.[21] Therefore, it is important to identify signatures that distinguish adiabatic pumping from mere rectification of displacement currents. For the case of a current measurement, two such signatures are the magnetic field symmetry and the typical size of the pumped current.[10, 21] Except for the case $N = 1$, our results allow to translate these signatures to a voltage measurement as well.[5] Further, the relation between pumped voltage and pumped current provides a third signature of a adiabatic pumping: For few-channel point contacts, $\bar{I}$, $\bar{V}G$, and the difference $\bar{V}G - \bar{I}$ are all random and of comparable magnitude for a quantum pump, while, if the dc signal is due to rectification, there is a fixed relationship $\bar{I} \propto G^2\bar{V}$, the proportionality constant being non-universal.[21]

[5]For single-channel contacts $N = 1$, $\bar{v}$ is expressed in terms of the scattering matrix S as

$$\bar{v} = \frac{1}{(1+\eta)} \frac{2}{|S_{12}|^4} \mathrm{Im} \left(\frac{\partial S_{11}}{\partial X_1} \frac{\partial S_{11}^*}{\partial X_2} - \eta \frac{\partial S_{22}}{\partial X_1} \frac{\partial S_{22}^*}{\partial X_2} \right).$$

Since $S(B) = S^T(-B)$ under reversal of a magnetic field B, this equation results in $\bar{v}(-B) = \bar{v}(B)$. There is no such magnetic field symmetry of the pumped voltage for $N > 1$.

Bibliography

[1] D. Thouless, Phys. Rev. B **27**, 6083 (1983).

[2] L. P. Kouwenhoven *et al.*, Phys. Rev. Lett. **67**, 1626 (1991).

[3] H. Pothier *et al.*, Europhys. Lett. **17**, 249 (1992).

[4] T. H. Oosterkamp *et al.*, Phys. Rev. Lett. **78**, 1536 (1997).

[5] For reviews, see L. P. Kouwenhoven *et al.*, in *Mesoscopic Electron Transport*, edited by L. L. Sohn, L. P. Kouwenhoven, and G. Schön (Kluwer, Dordrecht, 1997); C. W. J. Beenakker, Rev. Mod. Phys. **69**, 731 (1997); Y. Alhassid, Rev. Mod. Phys. **72**, 895 (2000).

[6] B. Spivak, F. Zhou, and M. T. Beal Monod, Phys. Rev. B **51**, 13226 (1995).

[7] M. Switkes *et al.*, Science **283**, 1905 (1999).

[8] P. W. Brouwer, Phys. Rev. B **58**, 10135 (1998).

[9] F. Zhou, B. Spivak, and B. Altshuler, Phys. Rev. Lett. **82**, 608 (1999).

[10] T. A. Shutenko, I. L. Aleiner, and B. L. Altshuler Phys. Rev. B **61**, 10366 (2000).

[11] A. V. Andreev and A. Kamenev, Phys. Rev. Lett. **85**, 1294 (2000).

[12] I. L. Aleiner, B. L. Altshuler, and A. Kamenev, Phys. Rev. B **62**, 10373 (2000).

[13] J. E. Avron *et al.*, Phys. Rev. B **62**, 10618 (2000).

[14] M. Büttiker and T. Christen, in *Quantum Transport in Semiconductor Submicron Structures*, edited by B. Kramer, NATO ASI Series **326** (Kluwer, Dordrecht, 1996).

[15] M. Büttiker, A. Prêtre, and H. Thomas, Phys. Rev. Lett. **70**, 4114 (1993).

[16] M. Büttiker, J. Phys. Condens. Matter **5**, 9361 (1993); M. Büttiker, H. Thomas, and A. Prêtre, Z. Phys. B **94**, 133 (1994).

[17] P. W. Brouwer *et al.*, Phys. Rev. Lett. **79**, 913 (1997).

[18] P. W. Brouwer, K. M. Frahm, and C. W. J. Beenakker, Phys. Rev. Lett. **78**, 4737 (1997); *Waves in Random Media* **9**, 91 (1999).

[19] E. P. Wigner, Phys. Rev. **98**, 145 (1955), and F. T. Smith, Phys. Rev. **118**, 349 (1960).

[20] P. W. Brouwer and C. W. J. Beenakker, J. Math. Phys **37**, 4904 (1996).

[21] P. W. Brouwer, Phys. Rev. B **63**, 121303 (2001).

Chapter 3

Noise through Quantum Pumps

3.1 Introduction

A periodic perturbation of a confined electron system may produce a direct current. The initial theoretical proposals [1, 2] and experimental realizations [3, 4, 5] for electron pumps were for a pump where the spectrum is gapped and the charge pumped in one cycle quantized and not subject to fluctuations. Recently, attention has shifted to pumps that are well connected to electron reservoirs, and, hence, do not have a gapped excitation spectrum [6, 7, 8, 9]. If the pump relies on a time-dependent perturbation that mainly affects the quantum-mechanical phases of the electrons, and not their classical trajectories, it is referred to as a "quantum electron pump". Such a quantum pump was fabricated by Switkes *et al.* [10].

The current that is pumped through a quantum electron pump is subject to mesoscopic fluctuations and to quantum or thermal fluctuations (noise). Mesoscopic fluctuations of the current refer to the fact that the magnitude and direction of the time-averaged current vary from sample to sample. For a quantum pump built from a chaotic quantum dot, as is the case in the experiment of Ref. [10], the mesoscopic

current fluctuations were investigated for various regimes of temperature, pumping amplitude and dot conductances [8, 9, 11, 12, 13, 14]. On the other hand, noise — quantum and thermal fluctuations of the current — is a property of the current pumped through a particular realization of an electron pump. Noise in an electron pump is best described by the fluctuations of the charge pumped through the system in a certain number of pumping cycles. The statistics of such charge fluctuations was studied in Refs. [15, 16, 17, 18, 19, 20, 21, 22] for temperatures and pumping frequencies much smaller than the inverse dwell time (escape rate) of electrons in the quantum dot.

In this Chapter, we consider the mesoscopic fluctuations of the noise. We do not impose any restrictions on the relative magnitudes of temperature T, pumping frequency ω, escape rate γ and pumping amplitude. This is important, as in an experimental realization of a quantum pump, T and γ are usually comparable, while both are much larger than ω. Furthermore, the experiment of Ref. [10] has addressed both the cases of weak pumping, where the pumped current $\bar{I} \ll e\omega$ and strong pumping, where $\bar{I} \gg e\omega$. Previous works by Andreev and Kamenev [15] and Levitov [16] addressed the full counting statistics, but at temperatures $kT \ll \hbar\omega$ only. The mean square charge fluctuations for $\hbar\omega, kT \ll \gamma$ (but including the case $\hbar\omega \approx kT$) and weak pumping were considered very recently by Moskalets and Büttiker [22].

Denoting the quantum-mechanical average with a bar $\overline{\cdots}$, the quantum and thermal fluctuations of the pumped charge are described by

$$S = \frac{1}{\tau_0}\left[\overline{Q}^2 - (\overline{Q})^2\right]. \tag{3.1}$$

Here τ_0 is the observation time and Q is the total charge pumped through the dot in the time τ_0. The noise in an electron pump can be divided onto a Nyquist-Johnson

component S^N and pumping component S^P. The former is the thermal equilibrium noise due to the thermal fluctuations of electrons in the leads, and depends on the electron temperature T in the leads and the time-averaged conductance $\bar{G}$ of the quantum dot through the fluctuation-dissipation theorem,

$$S^N = 2kT\bar{G}. \tag{3.2}$$

The pumping contribution S^P, in contrast, is a true non-equilibrium noise due to the perturbation of electrons *inside* the dot. As we shall discuss in Sec. 3.3, this contribution to the noise can be seen as arising due to the heating of electrons inside the dot as a result of the time-dependent perturbation.

In the adiabatic regime $\hbar\omega \ll \gamma$ one needs to vary at least two system parameters periodically in order to generate a direct current. Current noise, however, is already generated if only one parameter is varied. The problem of current noise (and full counting statistics) for a single time-dependent scatterer with frequency $\hbar\omega \ll \gamma$ was addressed by Levitov and coworkers [19, 20]. Our results can be used to compute the mesoscopic fluctuations of the current in that case. We find that the main effect of the second time-dependent parameter in a true electron pump is to reduce the mesoscopic fluctuations of the noise.

This Chapter is organized as follows: A formal expression for the noise in terms of the time-dependent scattering matrix of the dot $\mathcal{S}$ is derived in Sec. 3.2. Section 3.3 considers the mesoscopic fluctuations of the noise through a chaotic quantum dot with two (or more) time-dependent parameters. For an adiabatic quantum pump at temperature $kT \ll \gamma$ we consider the full distribution of the mesoscopic fluctuations of the noise in Sec. 3.3.1. We focus on the cases of a quantum dot with single-channel and many-channel point contacts. For a dot with many-channel point contacts, the sample-to-sample fluctuations of the noise are much smaller than the average. In

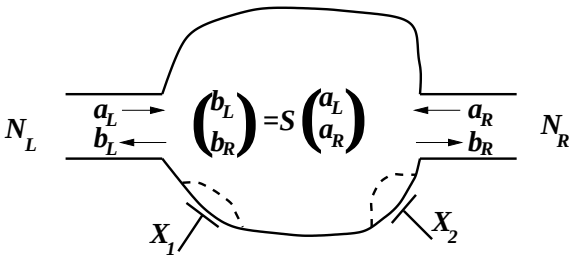

Figure 3.1: Schematic drawing of the quantum dot and the leads. There are N_L (N_R) propagating modes in the left (right) contact. The shape of the dot is controlled by the voltages of two shape-defining gates. The vectors $\mathbf{a}_{L,R}$ and $\mathbf{b}_{L,R}$ of annihilation operators for the incoming and outgoing states, respectively, in the left (L) and right (R) leads are related by the scattering matrix $\mathcal{S}$.

Sec. 3.3.2 we then present the ensemble-averaged noise for a dot with many-channel point contacts at arbitrary temperature and pumping strength. In the Appendix B we give some details of the

3.2 General formalism

We consider fluctuations of charge transmitted the sample during the observation time τ_0. The sample is connected to electron reservoirs through two point contacts with N_L and N_R open channels, respectively, see Fig. 3.1. It is subject to a periodic perturbation at frequency $\omega/2\pi$; The perturbation is described by specifying the time-dependence of parameters $X_1(t)$, $X_2(t)$, ..., $X_n(t)$ characterizing Hamiltonian of the sample. The electrons in the two reservoirs are held at the same chemical potential μ and temperature T at all times during the pumping cycle.

We calculate the noise of the quantum pump using the scattering formalism of Büttiker [23]. In Büttiker's original application there are no time-dependent

perturbations, so that the system is described by a scattering matrix that depends on energy, but not on time. On the other hand, as long as pumping frequencies and temperatures much smaller than the escape rate γ are considered, the system with a time-dependent perturbation can be described using a scattering matrix that depends on time, but not on energy [15, 16, 19, 20, 21, 22]. When kT, $\hbar\omega$ and γ are all comparable, one needs to use a scattering matrix $\mathcal{S}$ that depends on both time and energy, or, equivalently, that depends on two times or two energies. Here we shall make use of a formulation with a scattering matrix $\mathcal{S}(t,t')$ that depends on two times. This formulation was used to calculate the the time-averaged conductance and pumped current in the Ref. [13]. The formalism is equivalent to the two-energy scattering formalism developed by Büttiker and coworkers for time-dependent transport through mesoscopic structures [24, 25, 26, 27].

The scattering matrix $\mathcal{S}(t,t')$ relates the annihilation [creation] operators $\mathbf{a}_\alpha(t)$ $[\mathbf{a}^\dagger(t)]$ and $\mathbf{b}_\alpha(t)$ $[\mathbf{b}^\dagger_\alpha(t)]$ of incoming states and outgoing states in channel $\alpha = 1,\ldots,2N$ of the leads (the index α includes the spin degree of freedom),

$$\mathbf{b}_\alpha(t) = \int_{-\infty}^{+\infty} \mathcal{S}_{\alpha\beta}(t,t')\mathbf{a}_\beta(t')dt', \tag{3.3}$$

$$\mathbf{b}^\dagger_\alpha(t) = \int_{-\infty}^{+\infty} \mathbf{a}^\dagger_\beta(t')(\mathcal{S}^\dagger(t',t))_{\beta\alpha}dt'. \tag{3.4}$$

Here the indices α and β label the propagating channels in the point contact contacting the dot to the left and right reservoirs for $\alpha,\beta = 1,\ldots,2N_L$ and $\alpha,\beta = 2N_L+1,\ldots,2N$, respectively. The $2N\times 2N$ matrices $\mathcal{S}^\dagger$ and $\mathcal{S}$ are related as

$$\Big(\mathcal{S}^\dagger(t',t)\Big)_{\alpha\beta} = \mathcal{S}^*_{\beta\alpha}(t,t'). \tag{3.5}$$

Causality requires that $\mathcal{S}(t,t') = 0$ if $t < t'$. We restrict our attention to the case where spin rotation invariance is preserved, and, hence, $\mathcal{S}$ is proportional to the 2×2 unit matrix in spin grading.

The expression for the current $\mathbf{I}_L$ in the left lead is

$$\mathbf{I}_L(t) \;=\; e\sum_{\alpha=1}^{2N_L}\left[\mathbf{a}_\alpha^\dagger(t)\mathbf{a}_\alpha(t)-\mathbf{b}_\alpha^\dagger(t)\mathbf{b}_\alpha(t)\right]. \tag{3.6}$$

A similar expression holds for the current $\mathbf{I}_R$ in the right lead. Although the currents $\mathbf{I}_L(t)$ and $-\mathbf{I}_R(t)$ in the left and right leads do not need to be equal at every instance of the pumping cycle, their integrals over one pumping cycle are. (The charge on the dot is conserved after each cycle.) Hence, since we are only interested in the time-averaged charge $\bar{Q}$ pumped through the dot and the charge noise S, we can replace the expression for the current operator by a suitable combination of $\mathbf{I}_L$ and $\mathbf{I}_R$,

$$\mathbf{I}(t) \;=\; \frac{N_R}{N}\mathbf{I}_L(t)-\frac{N_L}{N}\mathbf{I}_R(t)=e\sum_{\alpha,\beta=1}^{2N}\left(\mathbf{a}_\alpha^\dagger(t)\Lambda_{\alpha\beta}\mathbf{a}_\beta(t)-\mathbf{b}_\alpha^\dagger(t)\Lambda_{\alpha\beta}\mathbf{b}_\beta(t)\right). \tag{3.7}$$

Here Λ is a diagonal matrix with elements

$$\Lambda_{\alpha\alpha}=\begin{cases} N_R/N & \alpha=1,\ldots,2N_L,\\ -N_L/N & \alpha=2N_L+1,\ldots,2N.\end{cases} \tag{3.8}$$

In terms of the current operator $\mathbf{I}$, the time-averaged pumped current I reads

$$I=\frac{1}{\tau_0}\int_0^{\tau_0}dt\overline{\mathbf{I}}(t), \tag{3.9}$$

where the observation time τ_0 is an integer number of pumping cycles. The noise S is defined as [cf. Eq. (3.1)]

$$S=\frac{1}{\tau_0}\int_0^{\tau_0}dtdt'\left(\overline{\mathbf{I}(\mathbf{t})\mathbf{I}(\mathbf{t'})}-\overline{\mathbf{I}}(t)\overline{\mathbf{I}}(t')\right). \tag{3.10}$$

In the leads, the electron distribution function is given by the Fourier transform $f(t)$ of the Fermi function,

$$\begin{aligned}\overline{\mathbf{a}_\beta^\dagger(t')\mathbf{a}_\alpha(t)} &= \delta_{\alpha\beta}f(t'-t),\\ \overline{\mathbf{a}_\beta(t')\mathbf{a}_\alpha^\dagger(t)} &= \delta_{\alpha\beta}\tilde{f}(t-t'),\end{aligned} \tag{3.11}$$

where we defined

$$\tilde{f}(t) = \delta(t) - f(t). \tag{3.12}$$

Averages involving four creation/annihilation operators are calculated using Wick's theorem, see, e.g., Ref. [23]. Using Eq. (3.3) to eliminate the operators $\mathbf{b}(t)$ and $\mathbf{b}^\dagger(t)$ from Eq. (3.7) and Eq. (3.11) to compute the quantum-mechanical expectation values, we find the average current

$$I = \frac{1}{\tau_0} e \int_0^{\tau_0} dt \int dt_1 dt_2 f(t_1 - t_2) \mathrm{tr} \left[\mathcal{S}^\dagger(t_1, t) \Lambda \mathcal{S}(t, t_2) - \delta(t - t_1) \Lambda \delta(t - t_2) \right],$$

and the noise

$$S = S^N + S^P, \tag{3.13}$$

where the Nyquist-Johnson and pumping contributions S^N and S^P read

$$\begin{aligned} S^N &= \frac{2e^2}{\tau_0} \int_0^{\tau_0} dt dt' \int dt_1 dt_2 f(t_1 - t') \tilde{f}(t' - t_2) \, \mathrm{tr} \left[\delta(t - t_1) \Lambda^2 \delta(t - t_2) \right. \\ &\quad \left. - \mathcal{S}^\dagger(t_1, t) \Lambda \mathcal{S}(t, t_2) \Lambda \right], \end{aligned} \tag{3.14}$$

$$\begin{aligned} S^P &= \frac{e^2}{\tau_0} \int_0^{\tau_0} dt dt' \int dt_1 dt_2 dt_1' dt_2' f(t_1 - t_2') \tilde{f}(t_1' - t_2) \\ &\quad \times \mathrm{tr} \left[\mathcal{S}^\dagger(t_1, t) \Lambda \mathcal{S}(t, t_2) \mathcal{S}^\dagger(t_1', t') \Lambda \mathcal{S}(t', t_2') \right. \\ &\quad \left. - \delta(t - t_1) \delta(t' - t_1') \Lambda^2 \delta(t - t_2) \delta(t' - t_2') \right]. \end{aligned} \tag{3.15}$$

(These equations can also be derived using the Keldysh formalism, see Ref. [28].) Equation (3.15) coincides with the result of Andreev and Kamenev in the extreme low-temperature adiabatic limit $kT \ll \hbar\omega \ll \gamma$. [15]

For adiabatic pumping, $\hbar\omega \ll \gamma$, Equation (3.13) is equivalent to the time-averaged current of Refs. [8] and [9]. The Nyquist-Johnson contribution to the noise is related to the time-averaged conductance $\bar{G}$ of the system at temperature T, see Refs. [29, 30] and Eq. (3.2) above.

3.2.1 Bilinear adiabatic pumping

Of particular interest is the case when the perturbation is slow compared to the (elastic) escape rate γ of the electrons from the sample into the reservoirs. This is the regime of the adiabatic quantum pump of Ref. [10]. In this approximation it is advantageous to use an analog of the Wigner transform for the matrix $\mathcal{S}(t,t')$:

$$\mathcal{S}(\varepsilon,t)=\int_{-\infty}^{+\infty}dt'e^{-i\varepsilon(t-t')}\mathcal{S}(t,t'). \tag{3.16}$$

Up to corrections of order $\hbar\omega/\gamma$, the matrix $\mathcal{S}(\varepsilon,t)$ is equal to the "instantaneous" scattering matrix $\mathcal{S}_X(\varepsilon)$, which is obtained by "freezing" all parameters X_j to their values at time t [31].[1]

If, in addition to being adiabatic, the parameters X_j, $j=1,\ldots,n$, undergo only small excursions from their average value, which we set to zero, we may further expand in X_j. To find the noise it is sufficient to expand $\mathcal{S}$ up to the second order in X. Arranging the parameters X_j in an n-component vector $\mathcal{X}=(X_1,\ldots,X_n)^{\mathrm{T}}$, we thus find

$$\begin{aligned} S^P &= \frac{e^2}{4\tau_0}\int_0^{\tau_0}dtdt'\int_{-\infty}^{+\infty}\frac{d\varepsilon}{2\pi}\int_{-\infty}^{+\infty}\frac{d\varepsilon'}{2\pi}\left[f(\varepsilon)\tilde{f}(\varepsilon')+f(\varepsilon)\tilde{f}(\varepsilon')\right] \\ &\quad\times\cos\left[(\varepsilon-\varepsilon')(t-t')\right]\left[(\mathcal{X}^{\mathrm{T}}(t)-\mathcal{X}^{\mathrm{T}}(t'))\mathcal{K}(\varepsilon,\varepsilon')(\mathcal{X}(t')-\mathcal{X}(t))\right], \end{aligned} \tag{3.17}$$

where $\tilde{f}(\varepsilon)=1-f(\varepsilon)$ and the $n\times n$ matrix $\mathcal{K}$ reads

$$\mathcal{K}_{ij}(\varepsilon,\varepsilon') = \mathrm{tr}\left[\Lambda^2\mathcal{R}_i(\varepsilon)\mathcal{R}_j(\varepsilon)+\Lambda^2\mathcal{R}_j(\varepsilon')\mathcal{R}_i(\varepsilon')-2\Lambda\mathcal{R}_i(\varepsilon)\Lambda\mathcal{R}_j(\varepsilon')\right], \tag{3.18}$$

$$\mathcal{R}_j(\varepsilon) = -i\frac{\partial\mathcal{S}_X(\varepsilon)}{\partial X_j}\mathcal{S}_X^\dagger(\varepsilon). \tag{3.19}$$

For $kT\ll\gamma$, Eq. (3.17) coincides with the result found by Moskalets and Büttiker. [22]

[1] The first order correction in an expansion in powers of $\hbar\omega/\gamma$ is given in Appendix C of Ref. [13]. See also B. Wang *et al.*, Phys. Rev. B **65**, 073306 (2002), and O. Entin-Wohlman, A. Aharony, and Y. Levinson, Phys. Rev. B **65**, 195411 (2002).

In the bilinear regime and at zero temperature, the time-averaged current I and the noise S^P are sufficient to define the total counting statistics of the pump [16]: To lowest order in the excursions of the parameters X_j, the pumping cycles are statistically independent. A pumping cycle is characterized by quantum-mechanical probabilities P_R and P_L that an electron is pumped from left to right or from right to left, respectively. Both P_R and P_L are small, of order X^2, and one has $I = (e\omega/2\pi)(P_L - P_R)$, $S^P = (e^2\omega/2\pi)(P_L + P_R)$.

For a typical quantum dot with capacitance C and mean level spacing Δ, the charging energy $e^2/2C \gg \Delta$. The derivatives in Eq. (3.19) should be taken at a constant value of the chemical potential μ, which, in the Hartree approximation, is equal to sum of the electron's kinetic energy and the electrostatic potential. In the absence of electron-electron interactions all derivatives are taken at constant value of the kinetic energy. As we prefer to take derivatives at constant kinetic energy (i.e., at constant ε) in both cases, we substitute the parametric derivatives as [24, 32].

$$\left.\frac{\partial}{\partial X}\right|_{\mu} \;\to\; \left.\frac{\partial}{\partial X}\right|_{\varepsilon} - \left(\frac{\frac{1}{2}\mathrm{tr}\,\mathcal{R}_i}{\frac{\pi C}{e^2} - \frac{i}{2}\mathrm{tr}\,\frac{\partial \mathcal{S}_X}{\partial \varepsilon}\mathcal{S}_X^\dagger}\right)\frac{\partial}{\partial \varepsilon}\,. \tag{3.20}$$

Equation (3.20) differs from a similar expression in Ref. [8] by factor of 1/2 in front of the traces because of the double size of matrix $\mathcal{S}$ as a result of the inclusion of spin.

3.3 Application to chaotic quantum dots

We now consider the mesoscopic fluctuations of the pumping noise S^P for the case of a chaotic quantum dot. The quantum dot is characterized by a mean level spacing Δ, escape rate $\gamma = N\Delta/2\pi$, Thouless energy $E_{\mathrm{Th}} = \hbar/\tau_{\mathrm{erg}} \gg \Delta$, and capacitance C, with charging energy $e^2/2C \gg \Delta$. It is coupled to two electron reservoirs via

ballistic point contacts with N_L and N_R channels each, see Fig. 3.1.

The dot is driven by periodically varying parameter(s) X_i, $i = 1, \ldots, n$ with frequency ω, cf. Fig. 3.1. In the experiment of Ref. [10], the parameters X_i correspond to the voltages on external gates that control the dot shape. The precise relation between the parameters X used in the theory and in the experiment is not known a priori, but can be established using independent measurements of, e.g., the derivative of the conductance [32] or the rate of change of the position of Coulomb blockade peaks when the point contacts between the dot and the reservoirs are pinched off [13]. Following Refs. [8, 11, 13], we will assume that the different parameters X_i correspond to different perturbations of which the matrix elements between states (of the closed dot) within a Thouless energy from the Fermi level $\varepsilon = 0$ are Gaussian and independently distributed. We choose the scale for the parameters X_i such that the mean square derivative $\langle(\partial\varepsilon_\mu/\partial X_i)(\partial\varepsilon_\mu/\partial X_j)\rangle = \delta_{ij}\Delta^2/\pi^2$, where Δ is the mean level spacing and ε_μ is an energy level in the closed dot.

The transmitted charge Q is measured during a time τ_0, which we will assume to be a large number of pumping cycles. This requirement of large observations is discussed in detail in Ref. [20]. For short observation times boundary effects related to switching processes in the system need to be taken into account.

3.3.1 Weak adiabatic low temperature pumping

If not only the frequency $\hbar\omega$ is much smaller than the escape rate γ, but also $kT \ll \gamma$, the scattering matrix $S(\varepsilon, t)$ in Eq. (3.17) can be taken at the Fermi level $\varepsilon = 0$, and we find the simple result

$$S^P = \frac{e^2}{2\tau_0}\int_0^{\tau_0} dtdt' f(t-t')\tilde{f}(t'-t)(\mathcal{X}(t)-\mathcal{X}(t'))^{\mathrm{T}}\mathcal{K}(\mathcal{X}(t')-\mathcal{X}(t)), \quad (3.21)$$

$$\mathcal{K}_{ij} = \mathrm{tr}\left(\Lambda^2\mathcal{R}_i\mathcal{R}_j + \Lambda^2\mathcal{R}_j\mathcal{R}_i - 2\Lambda\mathcal{R}_i\Lambda\mathcal{R}_j\right). \quad (3.22)$$

We now consider the case of two parameters, $\mathcal{X}(t) = (X_1(t), X_2(t))^{\mathrm{T}}$:

$$X_1(t) = X_1 \cos(\omega t),\ X_2(t) = X_2 \cos(\omega t + \phi), \tag{3.23}$$

in more detail. For this case, Eq. (3.21) is factorized into a factor $F(T, \omega)$ that depends on the relevant time and energy scales, and a sample specific contribution,

$$S^P = e^2 F(T, \omega) \left(\mathcal{K}_{11} X_1^2 + \mathcal{K}_{22} X_2^2 + 2 \cos\phi\ \mathcal{K}_{12} X_1 X_2 \right). \tag{3.24}$$

To find the integral $F(T, \omega)$ for the physically relevant limit of long observation times $\tau_0 \gg 1/T$, we note that in this limit the distribution function $f(t)$ is given by Fourier transform of the equilibrium Fermi distribution function,

$$f(t) = \int \frac{d\varepsilon}{2\pi\hbar} \frac{e^{i\varepsilon t/\hbar}}{e^{\varepsilon/kT} + 1} = \frac{ikT}{2\hbar \sinh(\pi k T t/\hbar)}. \tag{3.25}$$

Substitution into Eq. (3.21) then yields

$$F = \frac{\omega}{2\pi} \left(\coth \frac{\hbar\omega}{2kT} - \frac{2kT}{\hbar\omega} \right). \tag{3.26}$$

The result (3.24) with F given by Eq. (3.26) coincides with the theory of Moskalets and Büttiker [22].

The physical meaning of the function $F(T, \omega)$ with becomes clear once it is written in energy representation,

$$\begin{aligned} F = \int \frac{d\varepsilon}{4\pi\hbar} \Bigg(& f(\varepsilon + \frac{\hbar\omega}{2}) \tilde{f}(\varepsilon - \frac{\hbar\omega}{2}) - 2 f(\varepsilon) \tilde{f}(\varepsilon) \\ & + f(\varepsilon - \frac{\hbar\omega}{2}) \tilde{f}(\varepsilon + \frac{\hbar\omega}{2}) \Bigg). \end{aligned} \tag{3.27}$$

Equation (3.27) measures the change in the number of equilibrium electron-hole pairs due to absorption and emission of the pumping field quantum $\hbar\omega$. At temperatures $kT \ll \hbar\omega$ the Fermi distribution is sharp, and $F = \omega/2\pi$. At high $kT \gg \hbar\omega$, the Fermi distribution is smooth on the scale $\sim \omega$, so that F is small, $F \sim \hbar\omega^2/kT$.

Fluctuations of the noise are described by the second factor in Eq. (3.24), which varies from sample to sample. To find the mesoscopic fluctuations of the noise, we use the joint distribution of the matrices $\mathcal{R}_i$ $(i = 1, 2)$ derived in Ref. [33]. The resulting distribution of this mesoscopic contribution depends on two parameters,

$$C_l = \frac{2}{N}(X_1^2 + X_2^2), \quad C_c = \frac{4}{N} X_1 X_2 \sin\phi. \tag{3.28}$$

Equality $C_c = C_l$ is achieved if $X_1 = X_2$ and $\phi = \pi/2$, corresponding to the circular contour in the (X_1, X_2) plane. Below we consider the noise distribution for a quantum dot with single-channel point contacts ($N_L = N_R = 1$), and for a dot with many-channel point contacts ($N_L, N_R \gg 1$) separately.

Two channel geometry, $N = 2$

For small N, the full distribution of the noise can be obtained using the method of Ref. [34] to numerically generate the matrices $\mathcal{R}_1$ and $\mathcal{R}_2$ according to the appropriate distribution, see Appendix B for details. Figure 3.2 shows the distribution of the noise power S^P and the current-to-noise ratio I/S^P for a quantum dot with single-channel leads ($N = 2$) for the case $C_l = C_c$. The distributions are shown with and without time-reversal symmetry (TRS). For reference we have also included the distributions for the case $e^2/C \ll \Delta$ of weak electron-electron interactions inside the dot. The case $C_c < C_l$ (i.e., the dependence on the phase difference ϕ) is illustrated in Fig. 3.3. The current-to-noise ratio shown in Figs. 3.2 and 3.3 accounts for the pumping noise S^P only. The Nyquist-Johnson noise S^N presents a different noise source, which will dominate over the pumping noise if $kT \sim \hbar\omega\sqrt{C_l}$.

We note that the distributions of S^P and I/S^P are highly non-Gaussian. In particular, the mean $\langle S^P \rangle$ of the noise distribution is dominated by the algebraic tail for large S^P, and is not representative of the distribution itself. [For example, in the

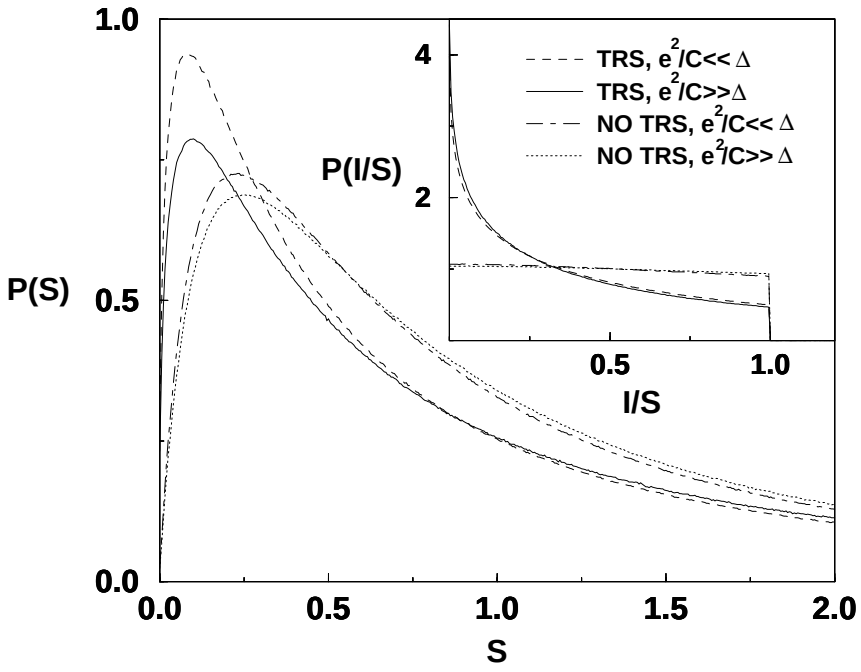

Figure 3.2: Main panel: Distribution of pumping noise S^P for a chaotic quantum dot with single-channel point contacts and two time-dependent parameters X_1 and X_2 given by Eq. (3.23) with $C_l = C_c$. [The parameters C_l and C_c are defined in Eq. (3.28).] The noise is measured in units of $e^2 C_l F$. The plots are with and without time-reversal symmetry (TRS) and for $e^2/C \ll \Delta$ (weak electron-electron interactions inside the dot) or $e^2/C \gg \Delta$. Inset: Distribution of the current-to-noise ratio I/S^P, measured in units of $\omega/(2\pi Fe)$. There is no divergence at $I/S^P \to 0$.

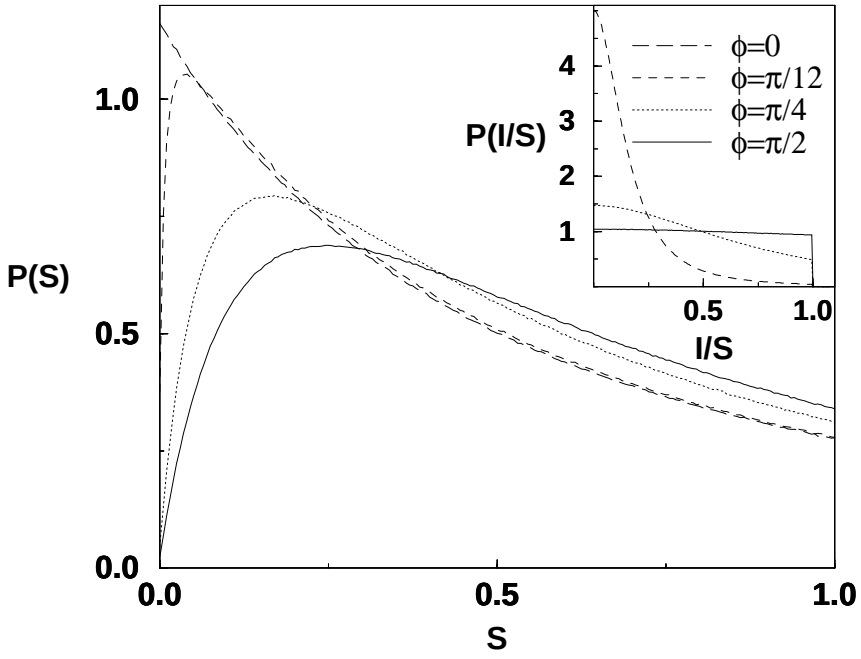

Figure 3.3: Distribution of the pumping noise S^P (main panel) and the current-to-noise ratio I/S^P (inset) for a quantum dot with two single channel point contacts and broken time-reversal symmetry, for various values of C_c/C_l. The values of C_c/C_l shown are $C_c/C_l = 1$, $\sin(\pi/4)$, $\sin(\pi/12)$, and 0. If the variations of the parameters X_1 and X_2 have equal amplitudes, this corresponds to phase difference $\phi = \pi/2$, $\pi/4$, $\pi/12$, and 0, respectively. The noise S^P is measured in units of $e^2 C_l F$ and the current I is measured in units of $eC_l\omega/2\pi$. For $C_c = 0$, $P(I/S^P)$ is a delta function at $I/S^P = 0$ (not shown).

absence of time-reversal symmetry and for $e^2/C \ll \Delta$, the mean $\langle S^P \rangle = 8/3(e^2 C_l F)$, while the most probable value is for $S^P \approx 0.5(e^2 C_l F)$.] We also note that, while the phase difference ϕ affects the typical size of the time-averaged pumped current $I \propto e\omega C_c$ but not the form of the distribution, changing ϕ has a small effect on the average noise $\langle S^P \rangle$, but changes the shape of the noise distribution significantly, see Fig. 3.3. In particular, the probability to find small S^P is significantly higher for ϕ close to zero than for $\phi \sim \pi/2$. The reason for this difference is that the case $\phi \sim \pi/2$ corresponds to noise generated by two independent sources, while ϕ close to zero corresponds to only a single noise source. Furthermore, the current-noise ratio I/S^P has a maximum at $I/S^P = e$, as was predicted by Levitov [16]. For a quantum dot with single-channel point contacts, there is a finite probability density to achieve this optimum current-to-noise ratio, as is seen in the inset of Fig. 3.2. For point contacts with more than one channel, the probability density to attain the maximum value $I/S^P = e$ vanishes [16], see, e.g. Fig. 3.4.

Multichannel limit, $N \gg 1$

For large N, the ensemble average and variance of the noise can be expressed in terms of an integral over the unitary group and over the eigenvalues of the Wigner-Smith time-delay matrix $\mathcal{R} = -i\hbar(\partial S/\partial\varepsilon)S^\dagger$ [35]. These integrals can be calculated using the method of Ref. [36] and Chapter 2, together with asymptotic expressions for the density and two-point correlations of the eigenvalues of the Wigner-Smith time-delay matrix, see Appendix B for details.

The result is

$$\langle S^P \rangle = 2e^2 F g \left(1 + \frac{2}{N}\delta_{\beta,1}\right) C_l, \tag{3.29}$$

$$\operatorname{var} S^P = \frac{g(2e^2F)^2}{N}\left(3\left[1 + (1+2\delta_{\beta,1})\frac{2g}{N}\right]C_l^2 - \left[1 + (1+4\delta_{\beta,1})\frac{g}{N}\right]C_c^2\right). \tag{3.30}$$

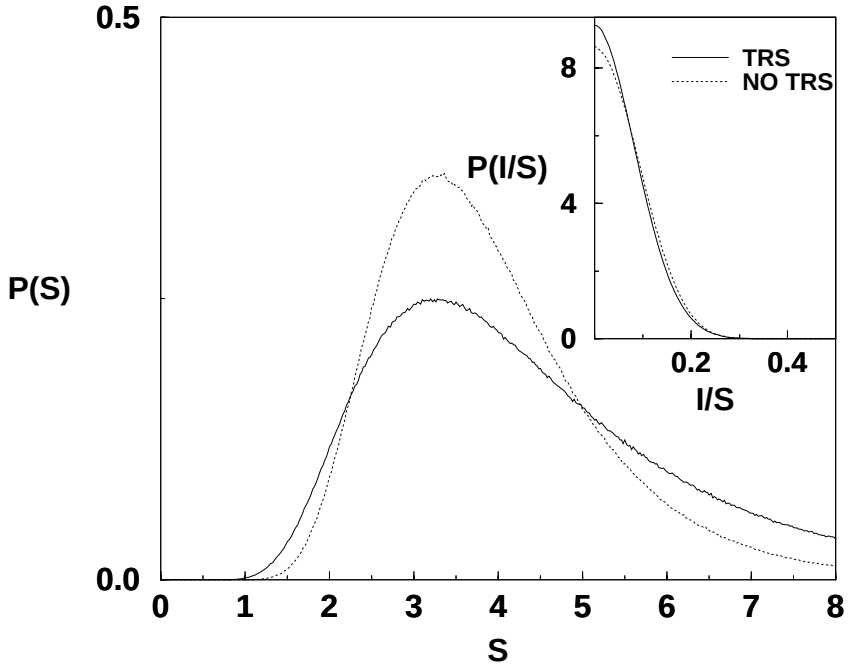

Figure 3.4: The same as Fig. 3.2 for a quantum dot with $N_L = N_R = 5$. Curves with weak and strong electron-electron interaction are indistinguishable.

where we abbreviated $g = N_L N_R/N$. The factor F depends on ω and T and was defined in Eq. (3.26). Note that the fluctuations of S^P are a factor $\sim 1/N$ smaller than the average. Higher cumulants of the noise are even smaller, so that we conclude that, for $N \gg 1$, the noise distribution becomes sharply peaked at the average $\langle S^P \rangle$ and that the remaining sample-to-sample fluctuations are Gaussian.

In Fig. 3.4 we show the results of a numerical calculation of the distribution noise S^P and the current-to-noise ratio I/S^P for a dot with $N_L = N_R = 5$, $N = 10$. This value of N can be seen as intermediate between the small-N regime, where the distributions are strongly non-Gaussian and the large-N regime where the distributions are Gaussian. We note that for $N = 10$ the noise distribution still has pronounced tails for large S^P.

3.3.2 Noise at arbitrary pumping for multichannel dots

In this subsection we consider a general time dependence and amplitude of the parameters X_j. We limit ourselves to the calculation of the ensemble averaged noise, since the mesoscopic fluctuations of the noise are smaller than the average by a factor $1/N$ if $N \gg 1$, see Eq. (3.29).

For a calculation of the ensemble average noise $\langle S^P \rangle$, we need to know the correlation functions of scattering matrix elements $\mathcal{S}_{\alpha\beta}(t,t')$ for an ensemble of chaotic quantum dots. The indices α and β refer to the "orbital" channels as well as to the spin of the electrons. In order to discriminate between the orbital and spin degrees of freedom, we set $\alpha = (i,\sigma)$, where $\sigma = \pm 1$ refers to spin and $i = 1,\ldots,N$ denotes the orbital channels, $i = 1,\ldots,N_L$ for channels in the left point contact and $i = N_L+1,\ldots,N$ for channels in the right point contact. In this notation, the scattering matrix $\mathcal{S}_{\alpha\beta} = \mathcal{S}^{\rm o}_{ij}\delta_{\sigma\sigma'}$ is proportional to the 2×2 unit matrix in spin space. The correlator of the orbital part $S^{\rm o}_{ij}$ reads

$$\begin{aligned}\langle \mathcal{S}^{\rm o}_{ij}(t,t')\mathcal{S}^{\rm o*}_{kl}(\tau,\tau')\rangle &= \delta(t-t'-\tau+\tau')\Big[\delta_{ik}\delta_{jl}\,\mathcal{D}(\frac{t+\tau}{2},t'+\frac{\tau-t}{2},\tau-t)\\ &\quad +\delta_{il}\delta_{jk}\,\mathcal{C}(\frac{t+\tau}{2},t'+\frac{\tau-t}{2},\tau-t)\Big], \qquad (3.31)\end{aligned}$$

with $\mathcal{D}$ and $\mathcal{C}$ given by

$$\begin{aligned}\mathcal{D}(t_1,t_2,\tau) &= \Theta(t_1-t_2)\exp\left\{-\int_{t_2}^{t_1}\frac{\Delta d\xi}{2\pi\hbar}\left[N_d + 2\,(\mathcal{X}^{\rm T}(\xi-\tau/2)-\mathcal{X}^{\rm T}(\xi+\tau/2))\right.\right.\\ &\quad \left.\left.\times(\mathcal{X}(\xi-\tau/2)-\mathcal{X}(\xi+\tau/2))\right]\right\}, \qquad (3.32)\\ \mathcal{C}(t_1,t_2,\tau) &= \Theta(t_1-t_2)\exp\left\{-\int_{t_2-\tau/2}^{t_1-\tau/2}\frac{\Delta d\eta}{2\pi\hbar}\left[N_c + 2\,(\mathcal{X}^{\rm T}(\eta)-\mathcal{X}^{\rm T}(t_1+t_2-\eta))\right.\right.\\ &\quad \left.\left.\times(\mathcal{X}(\eta)-\mathcal{X}(t_1+t_2-\eta))\right]\right\}. \qquad (3.33)\end{aligned}$$

Here $\Theta(z) = 1$ if $z > 0$ and 0 otherwise and we abbreviated

$$N_d = N, \quad N_c = N + 2x^2, \qquad (3.34)$$

where $x \propto (\Phi/\Phi_0)(\tau_{\rm erg}\Delta)^{-1/2}$ is a dimensionless parameter describing the magnetic flux penetrating the quantum dot and Φ_0 the flux quantum [37]. The unitary ensemble, when time-reversal symmetry is fully broken, corresponds to the limit $x \to \infty$.

In the literature, two equivalent approaches have been taken to calculate correlators such as Eq. (3.31) above, the Hamiltonian and scattering approaches [37]. In the Hamiltonian approach the fundamental object is the random Hamiltonian of the closed chaotic quantum dot and the Green functions related to it. Once the scattering matrix $\mathcal{S}$ is expressed in terms of Green functions, the correlator (3.31) can be analyzed by standard diagrammatic techniques. The two terms $\mathcal{C}$ and $\mathcal{D}$ then appear as the cooperon and diffuson contributions. The fundamental object of the scattering approach is a statistical model for the scattering matrix $\mathcal{S}$ of an ensemble of dots. Equivalence of both methods, including the parametric and energy dependence of $\mathcal{S}$ is shown in Ref. [33]. A derivation of Eq. (3.31) using the scattering approach is given in Chapter 4. We refer to Ref. [28] for a discussion based on the Hamiltonian approach.

Knowing the correlator (3.31), we can find the ensemble-averaged noise $\langle S^P \rangle$,

$$\begin{aligned} \langle S^P \rangle &= \frac{2e^2 g}{\tau_0} \int_0^{\tau_0} dt\ dt' f(t-t')\tilde{f}(t'-t) \\ &\quad \times \left(\left[\int_0^\infty \mathcal{D}(\frac{t+t'}{2}, \frac{t+t'}{2} - \frac{\hbar\zeta}{\gamma}, t'-t)\ d\zeta \right]^2 - 1 \right), \end{aligned} \tag{3.35}$$

where $g = N_L N_R/N$ is the dot conductance, $\gamma = N\Delta/2\pi$ the escape rate, and we assumed $\tau_0 \gg 1/\omega, \hbar/\gamma$. The Cooperon term $\mathcal{C}$ of Eq. (3.31) does not appear in $\langle S^P \rangle$ to leading order in $1/N$; its contribution is a factor $1/N$ smaller, see, e.g., Eq. (3.29).

Equation (3.35) gives the ensemble-averaged noise for arbitrary ω, T, and γ, and for arbitrary excursions of the parameters X_j. We now investigate Eq. (3.35)

for the case that there are two time-dependent parameters X_1 and X_2 with time dependence given by Eq. (3.23). In order to distinguish regimes of "weak" (bilinear) and "strong" pumping, we introduce the energy scale [13, 30]

$$kT^* = \hbar\omega\sqrt{C_l}. \tag{3.36}$$

The meaning of the energy scale kT^* becomes clear when we view the pumping process as "diffusion in energy space": carriers absorb or emit energy quanta of size $\hbar\omega$ at a rate $X^2\Delta/\hbar$ [13]. Weak (bilinear) pumping corresponds to the case when the probability to absorb or emit one or more quanta is small, i.e., to the regime $X^2\Delta \ll \gamma$ or $kT^* \ll \hbar\omega$. For $kT^* \gg \hbar\omega$ many quanta are absorbed or emitted, so that the carriers in the dot shift their energies by an amount $\sim \hbar\omega\sqrt{X^2\Delta/\gamma} \sim T^*$. If T^* exceeds the temperature T of the electrons in the leads, the time-dependent potentials in the dot lead to significant "heating" of the electrons inside the dot and T^* can be viewed as an effective electron temperature inside the dot. The latter regime is referred to as "strong" pumping.

For weak pumping, $kT^* \ll \hbar\omega$, we can expand $\mathcal{D}$ to first order in X^2 and we recover the result Eq. (3.29), now without a restriction on the temperature T. For strong pumping, $kT^* \gg \max\{\hbar\omega, kT\}$, a simple expression for the noise power can be obtained if pumping is adiabatic, $\hbar\omega \ll \gamma$. In that case, we note that $\mathcal{D}$ in Eq. (3.35) contains the fast decay $\sim \exp(-\zeta)$ and a slowly varying contribution from the time-dependence of the parameters X_j. Since the X_j vary slowly on the time scale $\hbar/\gamma$, the integration over ζ can be done, and the result is

$$\begin{aligned}\langle S^P\rangle &= \frac{2e^2 g}{\tau_0}\int_0^{\tau_0} dt'dt\, f(t'-t)\tilde{f}(t-t') \\ &\quad\times\left[\left(\frac{N}{N+2(\mathcal{X}^{\mathrm{T}}(t)-\mathcal{X}^{\mathrm{T}}(t'))(\mathcal{X}(t)-\mathcal{X}(t'))}\right)^2-1\right].\end{aligned} \tag{3.37}$$

In the limit of low temperatures, $kT \ll \hbar\omega$ (and, as before, assuming long observa-

tion times $\hbar/\tau_0 \ll kT, \hbar\omega$), Eq. (3.37) yields

$$\langle S^P \rangle = \frac{e^2 g\omega}{\pi} \frac{[1+6C_l(1+C_l(1-S^2))]\ \mathbf{E}(k) - [1+2C_l(1-S)]\ \mathbf{K}(k)}{\pi[1+2C_l(1-S)]\sqrt{1+2C_l(1+S)}}, \quad (3.38)$$

where $\mathbf{E}(k)$ and $\mathbf{K}(k)$ are full elliptic integrals of the 2nd and 3rd kind, respectively, and we abbreviated

$$S = \sqrt{1-\left(\frac{C_c}{C_l}\right)^2}, \quad k^2 = \frac{4C_l\ S}{1+2C_l(1+S)}. \quad (3.39)$$

In the special case that the two time-dependent parameters $X_1(t)$ and $X_2(t)$ have equal amplitudes, $S = |\cos\phi|$. The dependence of the averaged noise in Eq. (3.38) on the ratio C_c/C_l (i.e., on the phase difference ϕ) is weak. For the case $C_c = 0$ ($\phi = 0$) we find the asymptotes

$$\langle S^P \rangle = e^2 g \frac{\omega}{\pi} C_l = e^2 g \frac{(kT^*)^2}{\pi\hbar^2\omega} \quad \text{if } kT^* \ll \hbar\omega, \quad (3.40)$$

$$\langle S^P \rangle = e^2 g \frac{3\omega}{\pi^2}\sqrt{\frac{C_l}{2}} = e^2 g \frac{3}{\pi^2\hbar\sqrt{2}} kT^* \quad \text{if } kT^* \gg \hbar\omega. \quad (3.41)$$

For the case $C_c = 0$, but at arbitrary temperatures kT, Eq. (3.37) yields

$$\langle S^P \rangle = e^2 g\omega \left(\frac{2kT}{\hbar\omega}\right)^2 \int_0^\infty \frac{d\zeta}{\sinh^2(2\pi kT\zeta/\hbar\omega)} \left\{1 - \frac{\hbar\omega}{\sqrt{(\hbar\omega)^2 + 4(kT^*)^2\sin^2\zeta}} + \frac{2(kT^*)^2\hbar\omega\sin^2\zeta}{\left[(\hbar\omega)^2 + 4(kT^*)^2\sin^2\zeta\right]^{3/2}}\right\}. \quad (3.42)$$

The low temperature asymptotics can be easily obtained from this result, and reproduce the Eqs. (3.40,3.41) for $kT^* \ll \hbar\omega$ or $kT^* \gg \hbar\omega$. For intermediate values of $kT^*/\hbar\omega$ and $kT/\hbar\omega$, Eq. (3.42) is plotted in Fig. 3.5. As long as both $\hbar\omega$ and kT are much smaller than kT^*, the integral (3.42) is dominated by $\zeta \ll \hbar\omega/kT^* \ll 1$, so that the strong pumping asymptote of Eq. (3.41) is reached, irrespective of ω or T.

An analytical expression for $\phi \neq 0$ can, in principle, be obtained from Eq. (3.37) as well. The qualitative behavior as a function of pumping strength and temperature

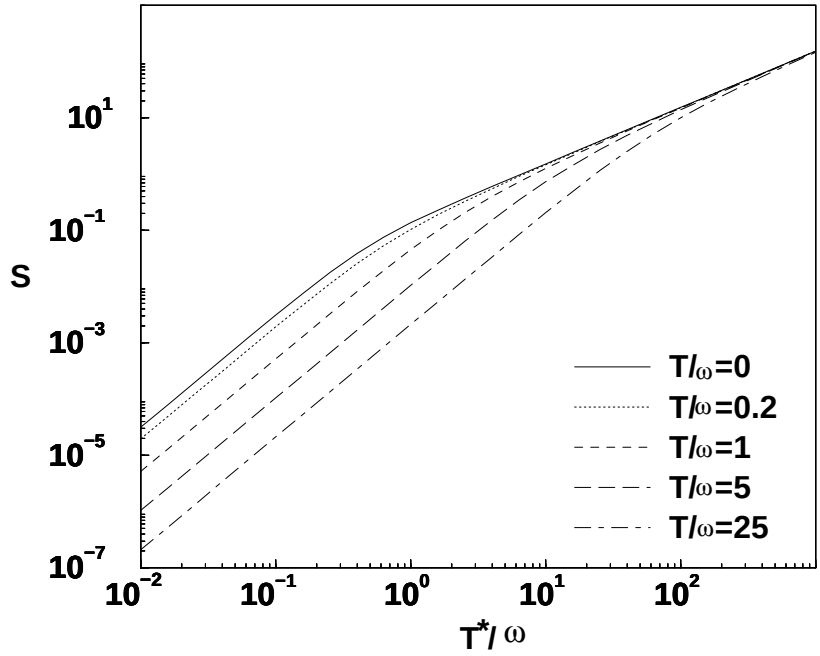

Figure 3.5: Noise $\langle S^P \rangle$ in units of $e^2 g\omega$, as a function of the dimensionless pumping strength $kT^*/\hbar\omega$ and for various choices $kT/\hbar\omega$.

is similar to that shown in Fig. 3.5 for the case $\phi = 0$. The limit of strong pumping should converge to the limit Eq. (3.38) of $T = 0$, similarly to the case $\phi = 0$ studied above.

Here we calculated the current noise generated in a quantum pump using a scattering matrix formalism with a scattering matrix $\mathcal{S}(t, t')$ that depends on two times. With this formalism, we could consider arbitrary pumping frequency ω, temperature T, escape rate γ, and pumping strength X. We then calculated the average and variance of the noise for an ensemble of quantum pumps consisting of a chaotic quantum dot.

One issue that has received considerable attention recently is the question whether one can build a noiseless quantum pump [38]. While our results for the bilinear

pumping regime show that there is a finite (mesoscopic) probability for zero noise, it is not possible to have no noise and a finite pumped current at the same time in the bilinear regime [16, 39], cf. Figs. 3.2 and 3.3. This is different beyond the bilinear regime, where a quantized, and, hence, noiseless pump has been proposed using a pumping contour that encircles a resonance in an almost closed quantum dot [40].

We note that both the equilibrium Nyquist-Johnson noise S^N and the pumping noise S^P depend on the available energy window. For pumping noise, that energy window is the heating temperature T^*, see Eq. (3.36); for Nyquist-Johnson noise it is the temperature T of the electron reservoirs. The results (3.29) and (3.38)–(3.42) allow us to compare the Nyquist-Johnson and pumping contributions to the averaged noise. In the experimentally relevant case that $\hbar\omega \ll kT$, both noise contributions are proportional to the (dimensionless) dot conductance g, but the Nyquist-Johnson noise scales as T, while the pumping noise scales as T^* if $T^* \gg T$ and as T^{*2}/T if $T^* \ll T$. The Nyquist-Johnson and pumping contributions to the noise are comparable at $T \sim T^*$. An experiment cannot separate the two contributions to the noise, since it measures the total noise power. The pumping contribution to the noise is dominant as long as $T \ll T^*$.

Bibliography

[1] D. Thouless, Phys. Rev. B **27**, 6083 (1983).

[2] Q. Niu, Phys. Rev. Lett. **64**, 1812 (1990).

[3] L. P. Kouwenhoven *et al.*, Phys. Rev. Lett. **67**, 1626 (1991).

[4] H. Pothier *et al.*, Europhys. Lett. **17**, 249 (1992).

[5] T. H. Oosterkamp *et al.*, Phys. Rev. Lett. **78**, 1536 (1997).

[6] V. I. Fal'ko and D. E. Khmelnitskii, Zh. Eksp. Teor. Fiz. **95**, 328 (1989) [Sov. Phys. JETP **68**, 186 (1989)].

[7] B. Spivak, F. Zhou, and M. T. Beal Monod, Phys. Rev. B **51**, 13226 (1995).

[8] P. W. Brouwer, Phys. Rev. B **58**, 10135 (1998).

[9] F. Zhou, B. Spivak, and B. Altshuler, Phys. Rev. Lett. **82**, 608 (1999).

[10] M. Switkes *et al.*, Science **283**, 1905 (1999).

[11] T. A. Shutenko, I. L. Aleiner, and B. L. Altshuler Phys. Rev. B **61**, 10366 (2000).

[12] J. E. Avron *et al.*, Phys. Rev. B **62**, 10618 (2000).

[13] M. G. Vavilov, V. Ambegaokar, and I. L. Aleiner, Phys. Rev. B **63**, 195313 (2001).

[14] M. Blaauboer and E. J. Heller, Phys. Rev. B **64**, 241301 (2001).

[15] A. V. Andreev and A. Kamenev, Phys. Rev. Lett. **85**, 1294 (2000).

[16] L. S. Levitov, cond-mat/0103617 (2001)

[17] A. V. Andreev and E. G. Mishchenko, Phys. Rev. B **64**, 233316 (2001).

[18] L. S. Levitov and G. B. Lesovik, Zh. Eksp. Teor. Fiz. **58**, 225 (1993) [JETP Lett. **58**, 230 (1993)].

[19] L. S. Levitov, H. Lee, and G. B. Lesovik, J. Math. Phys. **37**, 4845 (1996).

[20] D. A. Ivanov and L. S. Levitov, Pis'ma Zh. Eksp. Teor. Fiz. **58**, 450 (1993) [JETP Lett. **58**, 461 (1993)]; D. A. Ivanov, H. Lee and L. S. Levitov, Phys. Rev. B **56**, 6839 (1997).

[21] Yu. Makhlin and A. D. Mirlin, Phys. Rev. Lett. **87**, 276803 (2001).

[22] M. Moskalets and M. Büttiker, Phys. Rev. B **66** , 035306 (2002).

[23] M. Büttiker, Phys. Rev. B **46**, 12485 (1992); Phys. Rev. Lett, **65**, 2901 (1990); Phys. Rev. B **45**, 3807 (1992).

[24] M. Büttiker, A. Prêtre, and H. Thomas, Phys. Rev. Lett. **70**, 4114 (1993).

[25] M. Büttiker, J. Phys. Condens. Matter **5**, 9361 (1993); M. Büttiker, H. Thomas, and A. Prêtre, Z. Phys. B **94**, 133 (1994).

[26] M. Büttiker and T. Christen, in *Quantum Transport in Semiconductor Submicron Structures*, B. Kramer ed., NATO ASI Ser. E, Vol. 326 (Kluwer, Dordrecht, 1996).

[27] Y. M. Blanter and M. Büttiker, Phys. Rep. **336**, 1 (2001).

[28] M. G. Vavilov, Ph.D. Thesis, Cornell University, (2001).

[29] M. G. Vavilov and I. L. Aleiner, Phys. Rev. B **60**, R16311 (1999); **64**, 085115 (2001).

[30] V. I. Yudson, E. Kanzieper, and V. E. Kravtsov, Phys. Rev. B **64**, 045310 (2001).

[31] M. Büttiker and R. Landauer, Phys. Rev. Lett. **49**, 1739 (1982).

[32] P. W. Brouwer *et al.*, Phys. Rev. Lett. **79**, 913 (1997).

[33] P. W. Brouwer, K. M. Frahm, and C. W. J. Beenakker, Phys. Rev. Lett. **78**, 4737 (1997); *Waves in Random Media* **9**, 91 (1999).

[34] J. N. H. J. Cremers and P. W. Brouwer, Phys. Rev. B **65** , 115333 (2002).

[35] E. P. Wigner, Phys. Rev. **98**, 145 (1955), and F. T. Smith, Phys. Rev. **118**, 349 (1960).

[36] P. W. Brouwer and C. W. J. Beenakker, J. Math. Phys **37**, 4904 (1996).

[37] C. W. J. Beenakker, Rev. Mod. Phys. **69**, 731 (1997).

[38] J.E. Avron *et al.*, Phys. Rev. Lett. **87**, 236601 (2001).

[39] A. Alekseev, cond-mat/0201474.

[40] Y. Levinson, O. Entin-Wohlman, and P. Wölfle, Phys. Rev. Lett. **85**, 634 (2000).

Chapter 4

Scattering matrix ensemble for time-dependent transport through a chaotic quantum dot

Random matrix theory can be used to describe the transport properties of a chaotic quantum dot coupled to leads. In such a description, two approaches have been taken in the literature, considering either the Hamiltonian of the dot or its scattering matrix as the fundamental random quantity of the theory. In this Chapter, we calculate the first four moments of the distribution of the scattering matrix of a chaotic quantum dot with a time-dependent potential, thus establishing the foundations of a "random scattering matrix approach" for time-dependent scattering. We consider the limit that the number of channels N coupling the quantum dot the reservoirs is large. In that limit, the scattering matrix distribution is almost Gaussian, with small non-Gaussian corrections. Our results reproduce and unify results for conductance and pumped current previously obtained in the Hamiltonian approach. We also discuss an application to current noise.

4.1 Introduction

From a statistical point of view, energy levels and wavefunctions in semiconductor quantum dots and metal grains, or eigenfrequencies and eigenmodes of microwave cavities, share a remarkable universality. With proper normalization, correlation functions of energy levels or wavefunctions for an ensemble of macroscopically equivalent, but microscopically distinct samples depend on the fundamental symmetries of the sample only; they do not depend on sample shape or volume, or on the impurity concentration. The same universality appears for correlators of eigenvalues and eigenfunctions of large matrices with randomly chosen elements [1, 2, 3]. Originally, such "random matrices" were introduced by Wigner and Dyson to describe the universal features of spectral correlations in heavy nuclei [4, 5]. Theoretical predictions from random matrix theory have been verified in experiments on semiconductor quantum dots and chaotic microwave cavities, and with the help of numerical simulations [6, 7, 8, 9]; for the case of a disordered quantum dot, the validity of random matrix theory has been proven by field-theoretic methods [10].

Open samples, such as semiconductor quantum dots coupled to source and drain reservoirs by means of ballistic point contacts or microwave cavities coupled to ideal waveguides, do not have well-resolved energy levels or wavefunctions. They are characterized by means of a continuous density of states and by their transport properties, such as conductance or shot noise power. Within random-matrix theory, two approaches have been taken to describe open samples [37]. In both approaches, transport properties are described in terms of the sample's scattering matrix $\mathcal{S}$. The first approach is the "random Hamiltonian approach". In this approach, the scattering matrix is expressed in terms of a random Hermitean matrix H, which represents the Hamiltonian of the closed sample. Averages or fluctuations of trans-

port properties are then calculated in terms of the known statistical distribution of the random matrix H [12, 13]. In the second approach, the "random scattering matrix approach", the scattering matrix $\mathcal{S}$ itself is considered the fundamental random quantity. It is taken from Dyson's "circular ensemble" of uniformly distributed random unitary matrices [14, 15, 16, 17, 18], or a generalization known as the "Poisson kernel" [2, 19, 20]. Both approaches were shown to be equivalent [13, 20]. Hence, in the end, which method to use is a matter of taste.

Recently, there has been interest in transport through chaotic quantum dots with a time-dependent Hamiltonian. Switkes *et al.* fabricated a "quantum electron pump" consisting of a chaotic quantum dot of which the shape could be changed by two independent parameters [10]. Periodic variation of the shape then causes current flow through the quantum dot, hence the name "electron pump". Motivated by theoretical predictions of Vavilov and Aleiner [22, 23], Huibers *et al.* looked at the effect of microwave radiation on the quantum interference corrections to the conductance of a quantum dot [24]. The presence of a time-dependent potential will cause the ratio of universal conductance fluctuations with and without time-reversal symmetry to be less than two if the typical frequency of the fluctuations is of the order of the electron escape rate from the quantum dot [23, 30, 26, 27]. (By the Dyson-Mehta theorem [28], the ratio is two in the absence of a time-dependent perturbation [37].)

A scattering matrix formalism to describe time-dependent transport was developed by Büttiker and coworkers [29, 30, 31, 32, 33]. The scattering matrix formalism for time-dependent scattering is more complicated than the formalism for time-independent scattering, since energy is no longer conserved upon scattering from a cavity or quantum dot with a time-dependent potential. In the adiabatic

limit, when the frequency ω of the time-dependent variations is small compared to the escape rate from the quantum dot, the theory can be formulated in terms of the scattering matrix $\mathcal{S}$ and its derivative to energy [32]. However, a theory that describes arbitrary frequencies ω must be formulated in terms of a scattering matrix $\mathcal{S}(\varepsilon, \varepsilon')$ that depends on two energy arguments, or, equivalently, a matrix $\mathcal{S}(t, t')$ depending on two time arguments [22].

Random matrix theory can be used to describe the statistics of time-dependent transport if the time dependence is slow on the scale of the time $\tau_{\rm erg}$ needed for ergodic exploration of the quantum dot. In several recent papers [22, 23, 30, 26, 27, 11, 13], the calculation of time-dependent transport properties for an ensemble of chaotic quantum dots was done using a variation of the "random Hamiltonian approach": the time-dependent scattering matrix $\mathcal{S}(t, t')$ is first expressed in terms of a time-dependent Hermitean matrix $H(t)$, which is the sum of a time-independent random matrix and a time-dependent matrix which does not need to be random; the ensemble average is then calculated by integrating H over the appropriate distribution of random matrices. It is the purpose of this Chapter to develop a "random scattering matrix approach" for time-dependent scattering, using the distribution of the scattering matrix $\mathcal{S}(t, t')$, not the Hamiltonian $H(t)$, as the starting point for further calculations.

For time-independent scattering, the distribution of the elements of the scattering matrix is given by the circular ensembles from random matrix theory (or, for a quantum dot with non-ideal leads, by the Poisson kernel). In the limit that the dimension N of the scattering matrix becomes large, the scattering matrix distribution can be well approximated by a Gaussian, whereas non-Gaussian correlations can be accounted for in a systematic expansion in $1/N$ [20]. For the calculation of transport

properties (conductance, shot noise power), the Gaussian approximation is usually sufficient; knowledge of the underlying "full" scattering matrix distribution is not required. Here, we take a similar approach for time-dependent transport. We show that, for large N, elements of the scattering matrix $\mathcal{S}(t,t')$ are almost Gaussian random numbers, for which non-Gaussian correlations can be taken into account by means of a systematic expansion in $1/N$. We calculate the second moment of the distribution and the leading non-Gaussian correction.

This Chapter is organized as follows: In section 4.2 we review the scattering matrix approach for time-independent scattering. The case of time-dependent scattering is considered in section 4.3. Applications are discussed in section 4.4. Details of the calculation and an extension to the case of quantum dots with nonideal contacts can be found in the appendices. The second moment of the scattering matrix distribution calculated here was used in reference [37] to compute the shot noise power of a quantum electron pump.

4.2 Time-independent scattering

We first summarize important facts about the distribution of the scattering matrix $\mathcal{S}$ for time-independent scattering.

For large matrix size N, the scattering matrix elements $\mathcal{S}_{ij}$ have a Gaussian distribution with small non-Gaussian correlations. Mathematically, this is a consequence of the fact that $\mathcal{S}$ is distributed according to the circular ensemble from random matrix theory or, for a quantum dot with non-ideal leads, the Poisson kernel [36]. In a semiclassical picture, the Gaussian distribution of the scattering matrix elements follows from the central limit theorem, when $\mathcal{S}_{ij}$ is written as a sum over many paths, where the contribution of each path contains a random phase factor

[14, 15, 16, 38, 39]. The small non-Gaussian corrections follow because the full scattering matrix satisfies the constraint of unitarity, which is not imposed in the semiclassical formulation.[1]

The Gaussian part of the distribution is characterized by the first two moments. In the main text, we focus on the case of a quantum dot coupled to the outside world via ideal leads. In this case, the first moment vanishes,

$$\langle \mathcal{S}_{ij} \rangle = 0. \tag{4.1}$$

The case of nonideal leads, for which $\langle \mathcal{S}_{ij} \rangle \neq 0$, is discussed in the Appendix C.1. The second moment of the scattering matrix distribution depends on the presence or absence of time-reversal symmetry (TRS),

$$W_1^{ij;kl} = \langle \mathcal{S}_{ij} \mathcal{S}^*_{kl} \rangle \;=\; \frac{1}{N} \times \begin{cases} (\delta_{ik}\delta_{jl} + \delta_{il}\delta_{jk}) & \text{with TRS,} \\ \delta_{ik}\delta_{jl} & \text{without TRS,} \end{cases} \tag{4.2}$$

up to corrections of relative order $1/N$ in the presence of time-reversal symmetry. All averages involving unequal powers of $\mathcal{S}$ and $\mathcal{S}^*$ vanish. Equation (4.2) is for spinless particles or for electrons with spin in the absence of spin-orbit coupling. (In the latter case, the scattering matrix has dimension $2N$ and is of the form $\mathcal{S} \otimes \mathbf{1}_2$, where $\mathbf{1}_2$ is the 2×2 unit matrix in spin space and the $N \times N$ matrix $\mathcal{S}$ describes scattering between orbital scattering channels.) We do not consider the case of broken spin-rotation symmetry, when $\mathcal{S}$ is a random matrix of quaternions [1].

Non-Gaussian correlations of scattering matrices are of relative order $1/N$ or less.

[1] Averages or correlation functions of certain transport properties which, at first sight, would require knowledge of the fourth moment of the scattering matrix distribution, can be formulated in terms of the second moment only, using unitarity of the scattering matrix. This way, the average and fluctuations of the conductance of a chaotic quantum dot have been calculated using the semiclassical approach, see, e.g., references [42, 43].

The leading non-Gaussian correlations are described by the cumulant [40, 41, 36]

$$W_2^{i_1 j_1, i_2 j_2; k_1 l_1, k_2 l_2} = \langle \mathcal{S}_{i_1 j_1} \mathcal{S}_{i_2 j_2} \mathcal{S}^*_{k_1 l_1} \mathcal{S}^*_{k_2 l_2} \rangle - \langle \mathcal{S}_{i_1 j_1} \mathcal{S}^*_{k_1 l_1} \rangle \langle \mathcal{S}_{i_2 j_2} \mathcal{S}^*_{k_2 l_2} \rangle - \langle \mathcal{S}_{i_1 j_1} \mathcal{S}^*_{k_2 l_2} \rangle \langle \mathcal{S}_{i_2 j_2} \mathcal{S}^*_{k_1 l_1} \rangle . \quad (4.3)$$

In the absence of time-reversal symmetry and for $N \gg 1$, the cumulant W_2 is given by

$$W_2 = -\frac{1}{N^3} \left(\delta_{i_1 k_1} \delta_{j_1 l_2} \delta_{i_2 k_2} \delta_{j_2 l_1} + \delta_{i_1 k_2} \delta_{j_1 l_1} \delta_{i_2 k_1} \delta_{j_2 l_2} \right) . \quad (4.4)$$

In the presence of time-reversal symmetry, W_2 is found by the addition of 14 more terms to equation (4.4), corresponding to the permutations $i_2 \leftrightarrow j_2$, $k_1 \leftrightarrow l_1$, and $k_2 \leftrightarrow l_2$,

$$\begin{aligned} W_2 = -\frac{1}{N^3} (& \delta_{i_1 k_1} \delta_{j_1 l_2} \delta_{i_2 k_2} \delta_{j_2 l_1} + \delta_{i_1 k_2} \delta_{j_1 l_1} \delta_{i_2 k_1} \delta_{j_2 l_2} + \delta_{i_1 k_1} \delta_{j_1 l_2} \delta_{j_2 k_2} \delta_{i_2 l_1} \\ & + \delta_{i_1 k_2} \delta_{j_1 l_1} \delta_{j_2 k_1} \delta_{i_2 l_2} + \delta_{i_1 l_1} \delta_{j_1 l_2} \delta_{i_2 k_2} \delta_{j_2 k_1} + \delta_{i_1 k_2} \delta_{j_1 k_1} \delta_{i_2 l_1} \delta_{j_2 l_2} \\ & + \delta_{i_1 l_1} \delta_{j_1 l_2} \delta_{j_2 k_2} \delta_{i_2 k_1} + \delta_{i_1 k_2} \delta_{j_1 k_1} \delta_{j_2 l_1} \delta_{i_2 l_2} + \delta_{i_1 k_1} \delta_{j_1 k_2} \delta_{i_2 l_2} \delta_{j_2 l_1} \\ & + \delta_{i_1 l_2} \delta_{j_1 l_1} \delta_{i_2 k_1} \delta_{j_2 k_2} + \delta_{i_1 k_1} \delta_{j_1 k_2} \delta_{j_2 l_2} \delta_{i_2 l_1} + \delta_{i_1 l_2} \delta_{j_1 l_1} \delta_{j_2 k_1} \delta_{i_2 k_2} \\ & + \delta_{i_1 l_1} \delta_{j_1 k_2} \delta_{i_2 l_2} \delta_{j_2 k_1} + \delta_{i_1 l_2} \delta_{j_1 k_1} \delta_{i_2 l_1} \delta_{j_2 k_2} + \delta_{i_1 l_1} \delta_{j_1 k_2} \delta_{j_2 l_2} \delta_{i_2 k_1} \\ & + \delta_{i_1 l_2} \delta_{j_1 k_1} \delta_{j_2 l_1} \delta_{i_2 k_2}) . \end{aligned} \quad (4.5)$$

We refer to reference [36] for higher-order cumulants and finite-N corrections to W_1 and W_2.

Although equations (4.2) and (4.3) do not specify the full scattering matrix distribution — for that one would need to know all cumulants —, they are sufficient to calculate the average and variance of most transport properties. As an example, we consider a quantum dot connected to source and drain reservoirs by means of two ballistic point contacts with N_1 and N_2 propagating channels per spin direction

at the Fermi level, with $N = N_1 + N_2$. The zero-temperature conductance is given by the Landauer formula, which we write as [42]

$$G = \frac{2e^2}{h}\left(\frac{N_1 N_2}{N} - \operatorname{tr}\mathcal{S}\Lambda\mathcal{S}^\dagger\Lambda\right), \tag{4.6}$$

where $\mathcal{S}$ is the $N \times N$ scattering matrix and Λ is an $N \times N$ diagonal matrix with

$$\Lambda_{ij} = \frac{\delta_{ij}}{N} \times \begin{cases} N_2 & \text{if } 1 \le i \le N_1, \\ -N_1 & \text{if } N_1 < i \le N. \end{cases} \tag{4.7}$$

For large N, the second term in equation (4.6) is a small and fluctuating quantum correction to the classical conductance of the quantum dot. Using equations (4.2) and (4.4), the average and variance of the conductance for $N \gg 1$ then follow as

$$\langle G\rangle = \frac{2e^2}{h}\left(\frac{N_1 N_2}{N} - \delta_{\beta,1}\frac{N_1 N_2}{N^2}\right), \tag{4.8}$$

$$\operatorname{var} G = \frac{4e^4}{h^2}\left(\frac{N_1^2 N_2^2}{N^4}\right)(1 + \delta_{\beta,1}), \tag{4.9}$$

where the symmetry parameter $\beta = 1$ or 2 with or without time-reversal symmetry, respectively.

In the derivation of equations (4.8) and (4.9) it is important that the matrix Λ is traceless. This ensures that the non-Gaussian cumulant (4.4) does not contribute to $\operatorname{var} G$, despite the fact that calculation of $\operatorname{var} G$ involves an average over a product of four scattering matrices. Similarly, the $\mathcal{O}(N^{-2})$ corrections to the second moment W_1 of equation (4.2) in the presence of time-reversal symmetry do not contribute to the average conductance to order N^0.

So far we have only considered elements of the scattering matrix at one value of the Fermi energy ε (and of the magnetic field, etc.). If one wants to calculate averages involving scattering matrices at different energies, one needs to know the joint distribution of the scattering matrix $\mathcal{S}(\varepsilon)$ at different values of ε. To date,

no full solution to this problem is known for $N > 1$. However, for large N, the joint distribution of scattering matrix elements $\mathcal{S}_{ij}$ at different values of the Fermi energy or other parameters continues to be well approximated by a Gaussian, while unitarity causes non-Gaussian corrections that are small as $1/N$. As before, the Gaussian part of the distribution is specified by its first and second moment. The first moment is zero for a quantum dot with ideal leads; the second moment reads [2]

$$\begin{aligned} W_1^{ij;kl}(\varepsilon;\varepsilon') &= \langle \mathcal{S}_{ij}(\varepsilon)\mathcal{S}_{kl}(\varepsilon')^*\rangle \\ &= \frac{1}{N-\mathrm{i}(\varepsilon-\varepsilon')} \times \begin{cases} (\delta_{ik}\delta_{jl}+\delta_{il}\delta_{jk}) & \text{with TRS,} \\ \delta_{ik}\delta_{jl} & \text{without TRS.} \end{cases} \end{aligned} \tag{4.10}$$

Here, and below, we measure energy in units of $\Delta/2\pi$, where Δ is the mean spacing between the spin-degenerate energy levels in the quantum dot without the leads. Equation (4.10) was originally derived using semiclassical methods [14, 15, 16, 38, 39] and in the Hamiltonian approach of random-matrix theory [12, 44, 45]. A derivation using the random scattering matrix approach is given in reference [46] and in Appendix C.2. In the absence of time-reversal symmetry, the leading non-Gaussian correlations are described by the cumulant

$$\begin{aligned} W_2^{i_1j_1,i_2j_2;k_1l_1,k_2l_2}(\varepsilon_1,\varepsilon_2;\varepsilon_1',\varepsilon_2') &= \langle S_{i_1j_1}(\varepsilon_1)S_{i_2j_2}(\varepsilon_2)S^*_{k_1l_1}(\varepsilon_1')S^*_{k_2l_2}(\varepsilon_2')\rangle \\ &\quad - \langle S_{i_1j_1}(\varepsilon_1)S^*_{k_1l_1}(\varepsilon_1')\rangle\langle S_{i_2j_2}(\varepsilon_2)S^*_{k_2l_2}(\varepsilon_2')\rangle \\ &\quad - \langle S_{i_1j_1}(\varepsilon_1)S^*_{k_2l_2}(\varepsilon_2')\rangle\langle S_{i_2j_2}(\varepsilon_2)S^*_{k_1l_1}(\varepsilon_1')\rangle \\ = -\frac{(\delta_{i_1k_1}\delta_{j_1l_2}\delta_{i_2k_2}\delta_{j_2l_1}+\delta_{i_1k_2}\delta_{j_1l_1}\delta_{i_2k_1}\delta_{j_2l_2})\,(N-\mathrm{i}(\varepsilon_1+\varepsilon_2-\varepsilon_1'-\varepsilon_2'))}{(N-\mathrm{i}(\varepsilon_1-\varepsilon_1'))(N-\mathrm{i}(\varepsilon_1-\varepsilon_2'))(N-\mathrm{i}(\varepsilon_2-\varepsilon_1'))(N-\mathrm{i}(\varepsilon_2-\varepsilon_2'))}. \end{aligned} \tag{4.11}$$

In the presence of time-reversal symmetry, 14 terms corresponding to the permutations $i_2 \leftrightarrow j_2$, $k_1 \leftrightarrow l_1$, and $k_2 \leftrightarrow l_2$ have to be added to equation (4.11), respectively,

[2] For the second moment, an exact solution was obtained using the supersymmetry approach, see reference [12].

as in equation (4.5) for the energy-independent case. A derivation of equation (4.11) is given in Appendix C.2.

Equations (4.10) and (4.11) can be used to calculate averages and correlation functions for transport properties that involve scattering matrices at different energies. As an example, using equation (4.10) for the second moment of the scattering matrix distribution, the conductance autocorrelation function is found as [44, 45]

$$\langle G(\varepsilon_1)G(\varepsilon_2)\rangle - \langle G(\varepsilon_1)\rangle\langle G(\varepsilon_2)\rangle \;=\; \frac{4e^2N_1^2N_2^2}{h^2N^2}\frac{(1+\delta_{\beta,1})}{N^2+(\varepsilon_1-\varepsilon_2)^2}. \qquad (4.12)$$

4.3 Time-dependent scattering

For time-dependent scattering, the energies of incoming and scattered particles do not need to be equal. In order to describe scattering from a time-dependent scatterer, we use a scattering matrix $\mathcal{S}(t,t')$ with two time arguments. (We prefer to use the formulation with two time arguments instead of a formulation in which $\mathcal{S}$ has two energy arguments, since the former allows us to describe an arbitrary time-dependence of the perturbations.) For a quantum dot coupled to leads with, in total, N scattering channels, the two-time scattering matrix $\mathcal{S}(t,t')$ relates the annihilation operators $\mathbf{a}_i(t)$ and $\mathbf{b}_i(t)$ of incoming states and outgoing states in channel $i = 1,\ldots,N$,

$$\begin{aligned}\mathbf{b}_i(t) &= \sum_{j=1}^{N}\int_{-\infty}^{+\infty}\mathcal{S}_{ij}(t,t')\mathbf{a}_j(t')dt',\\ \mathbf{b}_i^\dagger(t) &= \sum_{j=1}^{N}\int_{-\infty}^{+\infty}\mathbf{a}_j^\dagger(t')(\mathcal{S}^\dagger(t',t))_{ji}dt'.\end{aligned} \qquad (4.13)$$

Causality imposes that

$$\mathcal{S}(t,t') = 0 \quad \text{if } t<t'. \qquad (4.14)$$

Unitarity is ensured by the condition

$$\sum_{j=1}^{N} \int dt (\mathcal{S}^\dagger(t'',t))_{ij} \mathcal{S}_{jk}(t,t') = \delta(t''-t')\delta_{ik},$$
$$\sum_{j=1}^{N} \int dt \mathcal{S}_{ij}(t'',t)(\mathcal{S}^\dagger(t,t'))_{jk} = \delta(t''-t')\delta_{ik}, \tag{4.15}$$

where the Hermitian conjugate scattering matrix $\mathcal{S}^\dagger(t',t)$ is defined as

$$\left(\mathcal{S}^\dagger(t',t)\right)_{ij} = \mathcal{S}^*_{ji}(t,t'). \tag{4.16}$$

For a quantum dot without time-independent potential, the scattering matrix $\mathcal{S}^0(t,t')$ depends on the difference $t-t'$ only. (In this section, we use a superscript "0" to indicate that $\mathcal{S}^0$ is a scattering matrix for time-independent scattering.) It is related the scattering matrix in energy representation by Fourier transform,

$$\mathcal{S}^0(t,t') = \frac{1}{2\pi\hbar}\int_{-\infty}^{\infty} d\varepsilon\, \mathcal{S}^0(\varepsilon) \mathrm{e}^{i\varepsilon(t-t')/\hbar}. \tag{4.17}$$

Borrowing results from the previous section, we infer that the elements of $\mathcal{S}^0(t,t')$ have a distribution that is almost Gaussian — the Fourier transform of a Gaussian is a Gaussian as well —, but with non-Gaussian correlations that are small as $N \to \infty$. Fourier transforming equation (4.10), we obtain the variance of the distribution [47]

$$\langle \mathcal{S}^0_{ij}(t,t')\mathcal{S}^{0*}_{kl}(s,s')\rangle = \delta(t-t'-s+s')\theta(t-t')\mathcal{D}^0(t-t') \times \begin{cases} (\delta_{ik}\delta_{jl}+\delta_{il}\delta_{jk}) & \text{with TRS,} \\ \delta_{ik}\delta_{jl} & \text{without TRS.} \end{cases} \tag{4.18}$$

Here, time is measured in units of $2\pi\hbar/\Delta$ and the function $\mathcal{D}^0$ is given by

$$\mathcal{D}^0(\tau) = \mathrm{e}^{-N\tau}. \tag{4.19}$$

Fourier transform of equation (4.11) gives the leading non-Gaussian contribution,

$$W_2^{0;i_1j_1,i_2j_2;k_1l_2,k_2l_2}(t_1,t_1';t_2,t_2';s_1,s_1';s_2,s_2')$$

$$
\begin{aligned}
&= \langle \mathcal{S}^0_{i_1 j_1}(t_1, t_1') \mathcal{S}^0_{i_2 j_2}(t_2, t_2') \mathcal{S}^{0*}_{k_1 l_1}(s_1, s_1') \mathcal{S}^{0*}_{k_2 l_2}(s_2, s_2') \rangle \\
&- \langle \mathcal{S}^0_{i_1 j_1}(t_1, t_1') \mathcal{S}^{0*}_{k_1 l_1}(s_1, s_1') \rangle \langle \mathcal{S}^0_{i_2 j_2}(t_2, t_2') \mathcal{S}^{0*}_{k_2 l_2}(s_2, s_2') \rangle \\
&- \langle \mathcal{S}^0_{i_1 j_1}(t_1, t_1') \mathcal{S}^{0*}_{k_2 l_2}(s_2, s_2') \rangle \langle \mathcal{S}^0_{i_2 j_2}(t_2, t_2') \mathcal{S}^{0*}_{k_1 l_1}(s_1, s_1') \rangle \qquad (4.20) \\
&= \left(\delta_{i_1 k_1} \delta_{j_1 l_2} \delta_{i_2 k_2} \delta_{j_2 l_1} + \delta_{i_1 k_2} \delta_{j_1 l_1} \delta_{i_2 k_1} \delta_{j_2 l_2}\right) \mathcal{F}^0(t_1 - t_1'; t_2 - t_2'; s_1 - s_1'; s_2 - s_2') \\
&\times \delta(t_1 - t_1' + t_2 - t_2' - s_1 + s_1' - s_2 + s_2') \theta(t_1 - t_1') \theta(t_2 - t_2') \theta(s_1 - s_1'),
\end{aligned}
$$

with

$$
\mathcal{F}^0(\tau_1; \tau_2; \tau_3; \tau_4) \;=\; [N \min(\tau_1, \tau_2, \tau_3, \tau_4) - 1] \mathrm{e}^{-N(\tau_1 + \tau_2)}. \qquad (4.21)
$$

Note that, in view of the delta function in equation (4.20), the function $\mathcal{F}^0$ depends on three time variables only. Despite the redundancy, we keep the four time arguments for notational convenience. As before, in the presence of time-reversal symmetry, the expression for the cumulant is obtained by adding terms that are obtained after interchanging $i_2 \leftrightarrow j_2$, $k_1 \leftrightarrow l_1$, and $k_2 \leftrightarrow l_2$, cf. Eq. (4.5).

In order to calculate the defining cumulants W_1 and W_2 for the case of a chaotic quantum dot with a time-dependent potential, we need a statistical model for the scattering matrix distribution for time-dependent scattering. Such a model can be provided by the Hamiltonian approach [22], or, alternatively, by extending the "stub model" of references [46, 48, 49] to the case of time-dependent scattering[3]. In the latter approach, the $N \times N$ scattering matrix $\mathcal{S}(t, t')$ is written in terms of an $M \times M$ random matrix $\mathcal{U}(t, t')$ (with $M \gg N$) and a $(M-N) \times (M-N)$ random Hermitian matrix H,

$$
\mathcal{S} = P\mathcal{U}(1 - R\mathcal{U})^{-1} P^\dagger, \quad R = Q^\dagger \mathrm{e}^{-2\pi \mathrm{i} H/M\Delta} Q. \qquad (4.22)
$$

[3]The stub model is similar in spirit to the "quantum graph", the spectral statistics of which is known to follow random-matrix theory [50].

Here P is an $N \times M$ matrix with $P_{ij} = \delta_{i,j}$ and Q is an $(M-N) \times M$ matrix with $Q_{ij} = \delta_{i+N,j}$. The scattering matrices $\mathcal{S}(t,t')$ and $\mathcal{U}(t,t')$ depend on two time indices, and the matrix products involving $\mathcal{U}(t,t')$ in equation (4.22) also imply integration over intermediate times. The Hermitian matrix H depends on a single time argument and models both time-independent and time-dependent perturbations to the Hamiltonian of the quantum dot. The matrix $\mathcal{U}(t,t')$ depends on the time difference $t-t'$ only and satisfies the constraint of unitarity, equation (4.15) above. As the effect of a time-reversal symmetry breaking magnetic field will be included in H, cf. equation (4.26) below, we further require that the matrix $\mathcal{U}$ is time-reversal symmetric,

$$\mathcal{U}_{ij}(t-t') = \mathcal{U}_{ji}(t-t'). \tag{4.23}$$

The statistical distribution of the matrix $\mathcal{U}$ is the same as that of the scattering matrix of a chaotic quantum dot coupled to a lead with M channels, but without magnetic field and time-dependent potential. Hence, the first nonvanishing moments of the distribution are given by equations (4.18) and (4.20) above, with $\mathcal{S}^0$ replaced by $\mathcal{U}$ and N by M.

The physical idea behind equation (4.22) is that the time-dependent part of the potential is located in a "stub" (a closed lead), see figure 4.1. The number of channels in the stub is $M-N$. The matrix $\mathcal{U}$ is the $M \times M$ scattering matrix of the quantum dot without the stub; the scattering matrix $\mathcal{S}$ is the scattering matrix of the entire system consisting of the dot and the stub, taking into account the time-dependent scattering from the stub. The matrix R represents the time-dependent scattering matrix for scattering from the stub. The stub is chosen to be small compared to the quantum dot, so that reflection from the stub can be regarded instantaneous — that's why the matrix $R(t)$ depends on a single time argument only. At the

end of the calculation, we take the limit $M \to \infty$. This limit ensures that the dwell time in the dot, which is proportional to $1/N$, is much larger than the time of ergodic exploration of the dot-stub system, which is proportional to $1/M$. It is only in this limit that the scattering matrix acquires a universal distribution which is described by random matrix theory. Once the limit $M \to \infty$ is taken, the spatial separation of chaotic scattering (described by the $M \times M$ scattering matrix $\mathcal{U}$) and the interaction with the time-dependent potential (described by the time-dependent reflection matrix R) no longer affects the distribution of the scattering matrix $\mathcal{S}$ and the scattering matrix distribution found using the stub model becomes identical to that with a spatially distributed time-dependent potential in the Hamiltonian approach.

A similar model has been used to describe the parametric dependence of the scattering matrix in the scattering matrix approach [46, 48, 51]. For the parametric dependence of $\mathcal{S}$, equivalence of the "stub" model and the Hamiltonian approach was shown in reference [49]. The calculational advantage of the "stub" model is that, for a quantum dot with ideal leads, the vanishing of the first moment $\langle \mathcal{S}_{ij} \rangle = 0$ is manifest throughout the calculation, while it requires fine-tuning of parameters at the end of the calculation in the Hamiltonian approach.

The matrix H in equation (4.22) can be written as a sum of three terms, de-

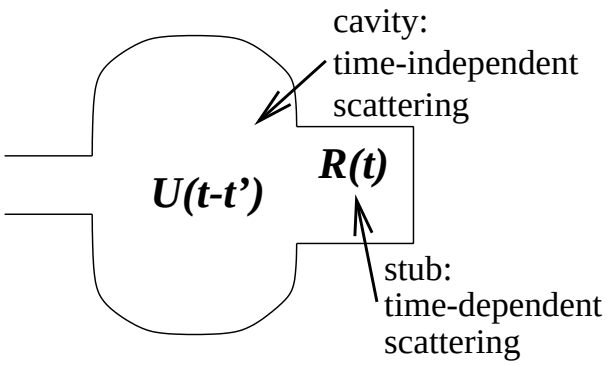

Figure 4.1: Cartoon of the picture behind equation (4.22): Scattering from the chaotic quantum dot with the time-dependent potential is modelled as scattering from a chaotic quantum dot with time-independent potential and a stub with time-dependent potential.

scribing three different perturbations to the Hamiltonian of the quantum dot[4]

$$H = V(t)\mathbf{1} + H_{\rm shape} + H_{\rm magn}. \tag{4.24}$$

The first term in equation (4.24) represents an overall shift of the potential $V(t)$ in the quantum dot. The second term represents the effect of a variation of the shape of the quantum dot,

$$H_{\rm shape}(t) = \sum_{j=1}^{n} x_j(t)\frac{X_j\Delta}{\pi} \tag{4.25}$$

Here the x_j $(j = 1, \ldots, n)$ are n time-dependent parameters governing the shape

[4]In the Hamiltonian approach, the parameters $x_1(t)$, $x_2(t)$, $V(t)$, and $\alpha(t)$ of equations (4.24)–(4.27) correspond to time-dependent variations of the form

$$\mathcal{H}(t) = S + V(t)\mathbf{1} + \frac{\rm i}{\sqrt{2M}}\alpha(t)A + \sum_{j=1}^{n}\frac{1}{\sqrt{M}}x_j(t)X_j,$$

where S and X_j are real symmetric random $M\times M$ matrices, $j = 1, \ldots, n$, A is a real antisymmetric random $M\times M$ matrix, and $\mathbf{1}$ is the $M\times M$ unit matrix. The off-diagonal elements of these random matrices are Gaussian random numbers with zero mean and unit variance. The diagonal elements of S and X_j have twice the variance of the off-diagonal elements.

of the quantum dot, and the X_j are real symmetric random $(M-N)\times(M-N)$ matrices with $\mathrm{tr}\, X_i X_j = M^2\delta_{ij}$, $i,j=1,\ldots,n$. Having more than one parameter to characterize the dot's shape is important for applications to quantum pumping [21, 52, 53, 54]. The third term in equation (4.24) represents the parametric dependence of the Hamiltonian on a magnetic flux Φ through the quantum dot

$$H_{\mathrm{magn}}(t) = \mathrm{i}\alpha(t)\frac{A\Delta}{\pi\sqrt{2}}, \tag{4.26}$$

where A is a random antisymmetric $(M-N)\times(M-N)$ matrix with $\mathrm{tr}\, A^{\mathrm{T}}A = M^2$. For a dot with diffusive electron motion (elastic mean free path l, dot size $L \gg l$) one has

$$\alpha^2 = \kappa\left(\frac{e\Phi(t)}{hc}\right)^2\frac{\hbar v_F l}{L^2\Delta}, \tag{4.27}$$

where κ is a constant of order unity and Φ the flux through the quantum dot. One has $\kappa = 4\pi/15$ for a diffusive sphere of radius L and $\kappa = \pi/2$ for a diffusive disk of radius L [55]. For ballistic electron motion with diffusive boundary scattering, the mean free path l in equation (4.27) is replaced by $5L/8$ and $\pi L/4$ for the cases of a sphere and a disk, respectively. (For the ballistic case, the value of α^2 reported in reference [55] is incorrect, see reference [56].) In order to ensure the validity of the random matrix theory, the time dependence of the parameters x_j and α should be slow on the scale of the ergodic time τ_{erg} of the quantum dot.

Note that the description (4.22)–(4.27) contains the dependence on a magnetic field explicitly. Having the full dependence on the magnetic field at our disposal, we no longer need to distinguish between the cases of presence and absence of time-reversal symmetry.

Expanding equation (4.22) in powers of R, the scattering matrix $\mathcal{S}$ is calculated as a sum over "trajectories" that involve chaotic scattering in the quantum dot and reflections from the stub. Since different "trajectories" involve different channels

in the stub at different times, each term in the expansion carries a random phase, determined by the random phases of the elements of $\mathcal{U}$. Hence, elements $\mathcal{S}_{ij}$ will have a distribution that is almost Gaussian for large N, since they are sums over many contributions with random phases. Unitarity, imposed by the constraint (4.15) for the matrix $\mathcal{U}$ and the form of the matrices $\mathcal{S}$ and R in equation (4.22) R, leads to corrections to the Gaussian distribution that are small as N becomes large.

The Gaussian part of the distribution of the time-dependent scattering matrix $\mathcal{S}(t,t')$ is specified by the second moment,

$$W_1^{ij;kl}(t,t';s,s') = \langle \mathcal{S}_{ij}(t,t')\mathcal{S}^*_{kl}(s,s')\rangle, \tag{4.28}$$

whereas the leading non-Gaussian corrections are described by the cumulant

$$\begin{aligned} &W_2^{i_1j_1,i_2j_2;k_1l_1,k_2l_2}(t_1,t_1';t_2,t_2';s_1,s_1';s_2,s_2') \\ &= \langle \mathcal{S}_{i_1j_1}(t_1,t_1')\mathcal{S}_{i_2j_2}(t_2,t_2')\mathcal{S}^*_{k_1l_1}(s_1,s_1')\mathcal{S}^*_{k_2l_2}(s_2,s_2')\rangle \\ &- \langle \mathcal{S}_{i_1j_1}(t_1,t_1')\mathcal{S}^*_{k_1l_1}(s_1,s_1')\rangle\langle \mathcal{S}_{i_2j_2}(t_2,t_2')\mathcal{S}^*_{k_2l_2}(s_2,s_2')\rangle \\ &- \langle \mathcal{S}_{i_1j_1}(t_1,t_1')\mathcal{S}^*_{k_2l_2}(s_2,s_2')\rangle\langle \mathcal{S}_{i_2j_2}(t_2,t_2')\mathcal{S}^*_{k_1l_1}(s_1,s_1')\rangle. \end{aligned} \tag{4.29}$$

The central result of this Chapter is a calculation of the cumulants W_1 and W_2 for time-dependent scattering. Details of the calculation are reported in Appendix C.3. For the second moment W_1 we find

$$\begin{aligned} W_1^{ij;kl}(t,t';s,s') &= \delta(t-t'-s+s')\theta(t-t') \\ &\quad \times \left[\delta_{ik}\delta_{jl}\mathcal{D}(t,t';s,s') + \delta_{il}\delta_{jk}\mathcal{D}(t,t';s',s)\right], \end{aligned} \tag{4.30}$$

with

$$\begin{aligned} \mathcal{D}(\tau,\sigma;\tau',\sigma') = \exp\Bigg[&-N|\tau-\sigma| - \frac{2\pi}{\Delta}\int_0^{|\tau-\sigma|} d\xi\,\left(V(\sigma+\eta\xi) - V(\sigma'+\eta'\xi)\right) \\ &+ 2\sum_j \left[x_j(\sigma+\eta\xi) - x_j(\sigma'+\eta'\xi)\right]^2 + \left[\eta\alpha(\sigma+\eta\xi) - \eta'\alpha(\sigma'+\eta'\xi)\right]^2\Bigg], \end{aligned} \tag{4.31}$$

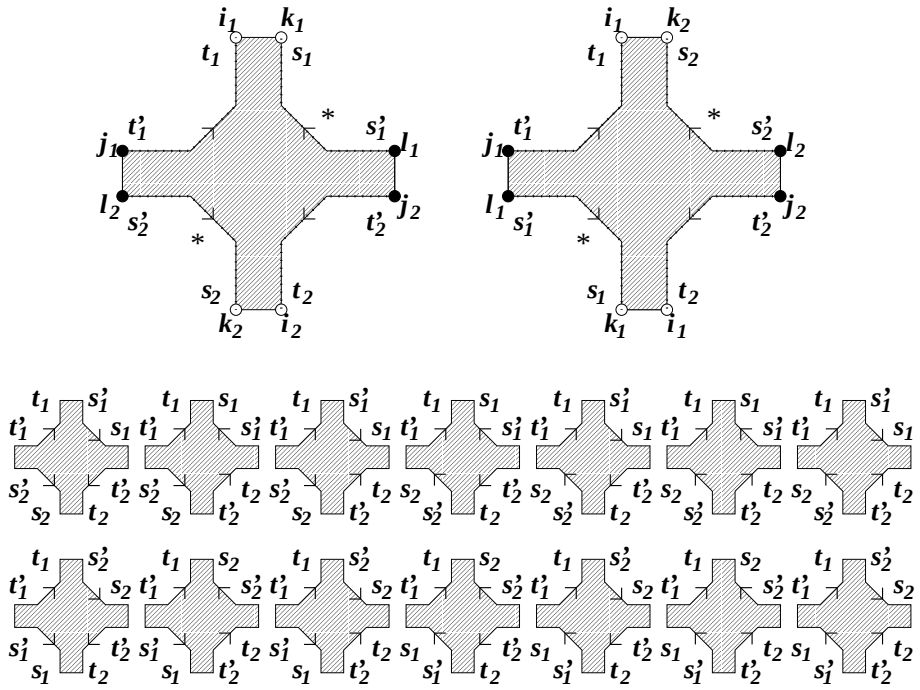

Figure 4.2: Diagrammatic representation of the contributions to the leading non-Gaussian correlator W_2 of equation (4.29), which involves four scattering matrices. The top left diagram has weight $\mathcal{F}(t_1, t_1';\ t_2, t_2';\ s_1, s_1';\ s_2, s_2')$, cf. equation (4.32). The top right diagram is obtained by interchange of two scattering matrices and has weight $\mathcal{F}(t_1, t_1';\ t_2, t_2';\ s_2, s_2';\ s_1, s_1')$. These two diagrams give all contributions to the cumulant W_2 in the absence of time-reversal symmetry. In the presence of time-reversal symmetry, the fourteen lower diagrams, corresponding to the reversal of one or more directions of the vertices, contribute as well.

and $\eta = \mathrm{sign}\,(\tau - \sigma)$, $\eta' = \mathrm{sign}\,(\tau' - \sigma')$. The first term in equation (4.30) is the analogue of the diffuson from standard diagrammatic perturbation theory, while the second term corresponds to the cooperon. For notational convenience, both terms are denoted by the same symbol $\mathcal{D}$. (Note that the order of the time arguments s and s' is reversed in the second term of equation (4.30).) The leading non-Gaussian corrections are given by the cumulant W_2 for which we find

$$\begin{aligned} &W_2^{i_1 j_1, i_2 j_2; k_1 l_1, k_2 l_2}(t_1, t_1'; t_2, t_2'; s_1, s_1'; s_2, s_2') = \mathcal{F}(t_1, t_1'; t_2, t_2'; s_1, s_1'; s_2, s_2') \\ &\times \theta(t_1 - t_1')\theta(t_2 - t_2')\theta(s_1 - s_1')\theta(s_2 - s_2')\delta(t_1 - t_1' + t_2 - t_2' - s_1 + s_1' - s_2 + s_2') \\ &\times \delta_{i_1 k_1}\delta_{j_1 l_2}\delta_{i_2 k_2}\delta_{j_2 l_1} + \text{permutations}. \end{aligned} \tag{4.32}$$

The "permutations" in equation (4.32) refer to one term corresponding to the permutation $(s_1, s_1', k_1, l_1) \leftrightarrow (s_2, s_2', k_2, l_2)$ of the third and fourth arguments of W_2 and fourteen more terms corresponding to the interchange of incoming and outgoing channel and time arguments within the second, third, and fourth argument of W_2. A diagrammatic representation of the cumulant (4.32) and the relevant perturbations is shown in figure 4.2. The kernel $\mathcal{F}$ reads

$$\begin{aligned} \mathcal{F}(\tau_1, \sigma_1; \tau_2, \sigma_2; \tau_1', \sigma_1'; \tau_2', \sigma_2') = \int d\xi\, &\mathcal{D}(\sigma_1 + \eta_1\xi, \sigma_1; \sigma_1' + \eta_1'\xi, \sigma_1') \\ &\times \mathcal{D}(\tau_2 - \tau_1' + \sigma_1' + \eta_2\xi, \sigma_2; \tau_2' - \tau_1 + \sigma_1 + \eta_2'\xi, \sigma_2') \\ &\times \mathcal{D}(\tau_1, \sigma_1 + \eta_1\xi; \tau_2', \tau_2' - \tau_1 + \sigma_1 + \eta_2'\xi) \\ &\times \mathcal{D}(\tau_2, \tau_2 - \tau_1' + \sigma_1' + \eta_2\xi; \tau_1', \sigma_1' + \eta_1'\xi) \\ &\times \Big\{ N + 4\sum_m [x_m(\sigma_1 + \eta_1\xi) - x_m(\tau_2' - \tau_1 + \sigma_1 + \eta_2'\xi)] \\ &\times [x_m(\sigma_1' + \eta_1'\xi) - x_m(\tau_2 - \tau_1' + \sigma_1' + \eta_2\xi)] - \delta(\xi - |\tau_1 - \sigma_1|) \\ &- \delta(\xi - |\tau_1' - \sigma_1'|) + 2[\eta_1\alpha(\sigma_1 + \eta_1\xi) - \eta_2'\alpha(\tau_2' - \tau_1 - \sigma_1 + \eta_2'\xi)] \\ &\times [\eta_1'\alpha(\sigma_1' + \eta_1'\xi) - \eta_2\alpha(\tau_2 - \tau_1' + \sigma_1' + \eta_2\xi)] \Big\}, \end{aligned} \tag{4.33}$$

where we abbreviated $\eta_1 = \mathrm{sign}\,(\tau_1 - \sigma_1)$, $\eta_2 = \mathrm{sign}\,(\tau_2 - \sigma_2)$, $\eta_1' = \mathrm{sign}\,(\tau_1' - \sigma_1')$, and $\eta_2' = \mathrm{sign}\,(\tau_2' - \sigma_2')$. Note that equations (4.30)–(4.33) cover both the cases with and without time-reversal symmetry through the explicit dependence on the magnetic flux α. If time-reversal symmetry is fully broken, all permutations in equation (4.32) that involve the interchange of incoming and outgoing channels, corresponding to the fourteen lower diagrams in figure 4.2, vanish, and only the first two diagrams in figure 4.2 remain. Partial integration of the intermediate time ξ allows one to rewrite terms between brackets $\{\ldots\}$ in equation (4.33), see Appendix C.3 for details. Finally, one verifies that the result (4.20) is recovered for $\alpha = 0$ and $\alpha \gg 1$, corresponding to presence and absence of time-reversal symmetry, when the parameters x_j and α do not depend on time.

4.4 Applications

In order to illustrate the use of equations (4.30)–(4.33), we return to the example of section 4.2 and consider transport through a chaotic quantum dot coupled to two electrons reservoirs by means of ballistic point contacts with N_1 and N_2 channels, respectively. The scattering matrix of the quantum dot has dimension $N = N_1 + N_2$. The current through the dot is defined as a linear combination of the of the currents through the two point contacts,

$$\mathbf{I}(t) \;=\; e \sum_{i,j=1}^{N} \left(\mathbf{a}_i^\dagger(t) \Lambda_{ij} \mathbf{a}_j(t) - \mathbf{b}_i^\dagger(t) \Lambda_{ij} \mathbf{b}_j(t) \right), \tag{4.34}$$

where the $N \times N$ matrix Λ was defined in equation (4.7) and the operators $\mathbf{a}_i(t)$ and $\mathbf{b}_i(t)$ are annihilation operators for incoming and outgoing states in channel $i = 1, \ldots, N$ in the leads, respectively, see section 4.3. The advantage of the definition (4.34) for the current through the quantum dot, instead of a definition where the

current through one of the contacts is used, is that it simplifies the ensemble average taken below. Both definitions of the current give the same result for the quantity of interest, the integral of $\mathbf{I}(t)$ over a large time interval $t_{\rm i} < t < t_{\rm f}$.

The electron distribution function for the electrons entering the quantum dot from the leads is given by the Fourier transform $f(t)$ of the Fermi function in the corresponding electron reservoir [57, 58, 59],

$$\begin{aligned} \overline{\mathbf{a}_j^\dagger(t')\mathbf{a}_i(t)} &= f_{ij}(t'-t), \\ \overline{\mathbf{a}_j(t')\mathbf{a}_i^\dagger(t)} &= \tilde{f}_{ij}(t-t'), \end{aligned} \tag{4.35}$$

where we defined

$$\begin{aligned} f_{ij}(t) &= \delta_{ij}\int \frac{d\varepsilon}{2\pi\hbar}\frac{{\rm e}^{{\rm i}\varepsilon t/\hbar}}{{\rm e}^{(\varepsilon-\mu_i)/kT}+1} \\ &= \delta_{ij}\frac{ikT{\rm e}^{{\rm i}\mu_i t/\hbar}}{2\hbar\sinh(\pi kTt/\hbar)}, \\ \tilde{f}_{ij}(t) &= \delta_{ij}\delta(t) - f_{ij}(t). \end{aligned} \tag{4.36}$$

Here μ_i is the chemical potential of reservoir 1 for $1 \le i \le N_1$ and the chemical potential of reservoir 2 for $N_1 < i \le N$.

Substitution of equations (4.35) and (4.13) into equation (4.34) allows us to calculate the time-averaged expectation value of the current through the quantum dot for a time interval $t_{\rm i} < t < t_{\rm f}$,

$$I = \frac{2e}{t_{\rm f}-t_{\rm i}}\int_{t_{\rm i}}^{t_{\rm f}} dt \int dt_1 dt_2 f(t_1-t_2){\rm tr}\left[\delta(t-t_1)\Lambda\delta(t-t_2) - \mathcal{S}^\dagger(t_1,t)\Lambda\mathcal{S}(t,t_2)\right]. \tag{4.37}$$

(A factor two has been added to account for spin degeneracy. The time interval $t_{\rm i} < t < t_{\rm f}$ during which charge is measured is taken to be the largest time scale in the problem.)

In the absence of a source-drain voltage, equation (4.37) describes the current

that is "pumped" by the time-dependent potential in the dot,

$$I_{\rm pump} = -\frac{2e}{t_{\rm f}-t_{\rm i}}\int_{t_{\rm i}}^{t_{\rm f}} dt \int dt_1 dt_2 {\rm tr}\, \mathcal{S}^\dagger(t_1,t)\Lambda\mathcal{S}(t,t_2) f_{\rm eq}(t_1-t_2), \qquad (4.38)$$

where $f_{\rm eq}$ is the Fourier transform of the Fermi function. Equation (4.38) was first derived in reference [35]; it reduces to the current formulae of references [53] and [54] in the adiabatic limit, where the time dependence of the potential of the quantum dot is slow compared to the dwell time in the quantum dot. At small bias voltage, there is a current proportional to the bias, $I = GV$, where G is the (time-averaged) conductance of the dot. The conductance G can be calculated from equation (4.37) by setting $\mu_i = \Lambda_{ii} eV$ and then linearizing in V [22],

$$\begin{aligned} G &= \frac{2e^2}{h}\left[\frac{N_1 N_2}{N} - \frac{2\pi{\rm i}}{t_{\rm f}-t_{\rm i}}\int_{t_{\rm i}}^{t_{\rm f}} dt \int dt_1 dt_2 (t_1-t_2)\right. \\ &\quad \left. \times\, {\rm tr}\,\Lambda\mathcal{S}(t,t_1)\Lambda\mathcal{S}^\dagger(t_2,t) f_{\rm eq}(t_1-t_2)\right]. \end{aligned} \qquad (4.39)$$

Here $f_{\rm eq}$ is the Fermi function in the absence of the external bias. For time-independent transport, equation (4.39) is equal to the Landauer formula (4.6).

Conductance. The ensemble average and the variance of the conductance G for a quantum dot with a shape depending on a single time-dependent parameter x was calculated by Vavilov and Aleiner using the Hamiltonian approach [22]. Using the scattering matrix correlator (4.28), their result for $\langle G\rangle$ is easily reproduced and generalized to arbitrary values of the (time-independent) magnetic field,

$$\langle G\rangle = \frac{2e^2 N_1 N_2}{hN} + \delta G, \qquad (4.40)$$

$$\begin{aligned} \delta G &= -\frac{2e^2 N_1 N_2}{hN(t_{\rm f}-t_{\rm i})}\int_{t_{\rm i}}^{t_{\rm f}} dt \int_0^\infty d\tau \\ &\quad \times \exp\left[-(N+4\alpha^2)\tau - 2\int_0^\tau d\tau_1 (x(t-\tau+\tau_1)-x(t-\tau_1))^2\right]. \end{aligned} \qquad (4.41)$$

The correction term δG of equation (4.41) is the weak localization correction; it results from the constructive interference of time-reversed trajectories. The presence of

a time-dependent potential breaks time-reversal symmetry and suppresses the weak localization correction. Vavilov and Aleiner investigated the case $x(t) = \delta x \cos(\omega t)$ of a harmonic time dependence for the parameter x in detail. In that case, the suppression of weak localization increases with increasing frequencies and saturates at a value

$$\delta G = -\frac{2e^2 N_1 N_2}{N^2 h} \times \begin{cases} \left[1 - \frac{2(\delta x)^2}{N+4\alpha^2}\right] & \text{if } (\delta x)^2 \ll N + 4\alpha^2, \\ \sqrt{\frac{N+4\alpha^2}{4(\delta x)^2}} & \text{if } (\delta x)^2 \gg N + 4\alpha^2, \end{cases} \tag{4.42}$$

for frequencies $\hbar\omega \sim N\Delta$ [22]. (Applicability of random matrix theory requires that $\omega \ll 1/\tau_{\rm erg}$, where $\tau_{\rm erg}$ is the time for ergodic exploration of the quantum dot.) If the fluctuations of the parameter x are fast and random on the scale $2\pi\hbar/N\Delta$ of the delay time in the dot, they may be considered Gaussian white noise,

$$\langle x(t)x(t')\rangle = \frac{1}{4}\gamma\delta(t-t'). \tag{4.43}$$

In that case, the exponent in equation (4.41) can be averaged separately, and one finds the result

$$\delta G = -\frac{2e^2 N_1 N_2}{hN(N + 4\alpha^2 + \gamma)}. \tag{4.44}$$

The same suppression of weak localization was obtained previously to describe the decohering effect of the coupling to an external bath [60, 61, 62]. Note that the strong-perturbation asymptote for white noise is different from the strong-perturbation asymptote for fast harmonic variations of the dot's shape. The cause for this difference is the existence of small time windows in which time-reversal symmetry is not violated near times t with $\cos(\omega t) = \pm 1$ for harmonic variations $\propto \cos(\omega t)$, while for a random time dependence of $x(t)$ no such special times around which time-reversal symmetry is preserved exist [25, 26].

Similarly the variance of the conductance can also be expressed in terms of the correlator (4.28). (As in the time-independent case, the non-Gaussian correlator

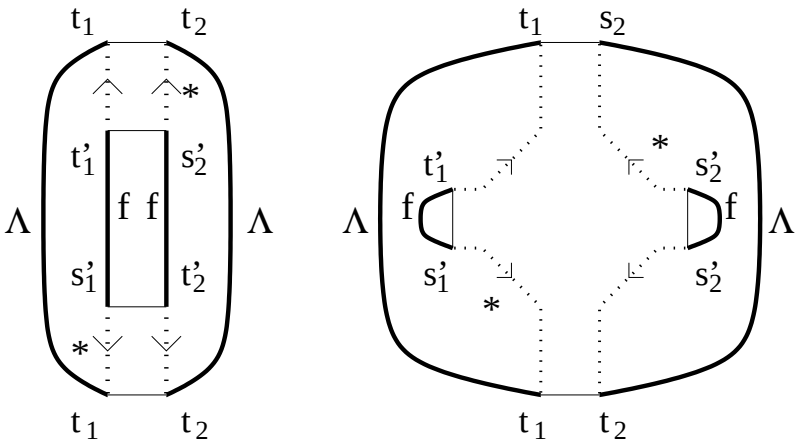

Figure 4.3: Diagrams representing the two contributions to the variance of the pumped current. Following the notation of reference [36], dotted lines correspond to the scattering matrix $\mathcal{S}$, thick solid lines correspond to the fixed matrices Λ and f, and thin solid lines correspond to the Kronecker delta's in the average over the ensemble of scattering matrices.

(4.32) does not contribute to the variance of the conductance.) We refer to reference [23] for the detailed expression for $\operatorname{var} G$ and an analysis of the effect of a harmonic time dependence of the shape function $x(t)$. Conductance fluctuations for the case when $x(t)$ is a sum of two harmonics with different frequencies were considered by Kravtsov and Wang [25].

Pumped current. To first order in the pumping frequency ω, the current in the absence of a source-drain voltage is nonzero only if two or more parameters x_j that determine the dot's shape are varied independently. Even then, the ensemble average of the pumped current is zero, and the first nonzero moment is $\langle I^2\rangle$. The ensemble average $\langle I^2\rangle$ was calculated in reference [53] for small pumping amplitudes $x_1(t) = \delta x_1 \sin(\omega t)$, $x_2 = \delta x_2 \sin(\omega t + \phi)$,

$$\langle I^2\rangle^{1/2} = \frac{e\omega\delta x_1 \delta x_2}{2\pi N}\sin\phi, \tag{4.45}$$

independent of the presence or absence of a magnetic field. The case of pumping amplitudes of arbitrary strength was considered in reference [34].

Beyond the adiabatic regime, one time-dependent parameter is sufficient to generate a finite current through the dot [63, 52]. The second moment $\langle I^2 \rangle$ in that most general case was first calculated in reference [35], using the random Hamiltonian approach. The second moment, which involves an average over four scattering matrix elements, can also be obtained in the random scattering matrix approach, using equations (4.30)–(4.33) of the previous section. We then find that there are two contributions to $\langle I^2_{\rm pump} \rangle$: one contribution with two Gaussian contractions of scattering matrices (giving a factor W_1^2) and one contribution which involves a correlator of four scattering matrices (giving a factor W_2). Diagrams representing these two contributions are shown in figure 4.3. Adding both contributions, we find

$$\begin{aligned}
\langle I^2_{\rm pump} \rangle \;=\; & \frac{8e^2 N_1 N_2}{N(t_{\rm f}-t_{\rm i})^2} \int_{t_{\rm i}}^{t_{\rm f}} dt dt' \int_0^\infty d\tau d\xi d\xi' \int_{-\tau}^{\tau} d\tau' f_{\rm eq}(2\tau') f_{\rm eq}(-2\tau') \\
& \times \mathcal{D}(t, t-\tau-\tau'; t', t'-\tau-\tau') \mathcal{D}(t', t'-\tau+\tau'; t, t-\tau+\tau') \\
& \times \mathcal{D}(t-\tau-\tau', t-\tau-\tau'-\xi; t-\tau+\tau', t-\tau+\tau'-\xi) \\
& \times \mathcal{D}(t'-\tau+\tau', t'-\tau+\tau'-\xi'; t'-\tau-\tau', t'-\tau-\tau'-\xi') \\
& \times \Bigg[(\delta(\xi)-N)(\delta(\xi')-N) + 4 \sum_m (x_m(t'-\tau+\tau') - x_m(t'-\tau-\tau')) \\
& \quad \times (x_m(t-\tau+\tau') - x_m(t-\tau-\tau')) \Bigg], \qquad (4.46)
\end{aligned}$$

independent of the value of the magnetic field. Using equation (C.10) of Appendix C.3 to express the delta functions in terms of the functions $x_m(t)$ and a total derivative of $\mathcal{D}$, performing partial integrations, and shifting $t \to t-\tau$, $t' \to t'-\tau$, this can be rewritten as

$$\begin{aligned}
\langle I^2_{\rm pump} \rangle = & \frac{32e^2 N_1 N_2}{N(t_{\rm f}-t_{\rm i})^2} \int_0^\infty d\tau d\xi d\xi' \int_{-\tau}^{\tau} d\tau' \int_{t_{\rm i}-\tau}^{t_{\rm f}-\tau} dt dt' f_{\rm eq}(2\tau') f_{\rm eq}(-2\tau') \\
& \times \mathcal{D}(t+\tau, t-\tau'; t'+\tau, t'-\tau') \mathcal{D}(t-\tau', t-\tau'-\xi; t+\tau', t+\tau'-\xi)
\end{aligned}$$

$$\times \mathcal{D}(t'+\tau,t'+\tau';t+\tau,t+\tau')\mathcal{D}(t'+\tau',t'+\tau'-\xi';t'-\tau',t'-\tau'-\xi') \times \left[\sum_{m,n}\left(\sum_{\pm}\pm x_m(t\pm\tau'-\xi)\right)^2\left(\sum_{\pm}\pm x_n(t\pm\tau'-\xi')\right)^2 + \sum_{m}\left(\sum_{\pm}\pm x_m(t'-\tau\pm\tau')\right)\left(\sum_{\pm}\pm x_m(t-\tau\pm\tau')\right)\right]. \quad (4.47)$$

This expression agrees with the result found by Vavilov, Ambegaokar, and Aleiner [35]. We refer to reference [35] for a detailed analysis of equation (4.47) for the limiting cases of adiabatic pumping and high-frequency pumping with one and two time-dependent parameters.

Noise. The current noise is defined as the variance of the charge transmitted through the quantum dot in the time interval $t_\mathrm{i} < t < t_\mathrm{f}$

$$S = \frac{1}{t_\mathrm{f}-t_\mathrm{i}}\int dtdt' \left(\overline{\mathbf{I}(t)\mathbf{I}(t')} - \overline{\mathbf{I}(t)}\,\overline{\mathbf{I}(t')}\right). \quad (4.48)$$

As in equation (4.35), $\overline{\cdots}$ denotes a quantum-mechanical or thermal average, not an ensemble average. Performing the quantum-mechanical and thermal average over the incoming states [57, 58, 59], the noise power S can be calculated as

$$S = \frac{2e^2}{t_\mathrm{f}-t_\mathrm{i}}\int_{t_\mathrm{i}}^{t_\mathrm{f}} dtdt' \int dt_1dt_2dt_1'dt_2' \mathrm{tr}\left[\left(\mathcal{S}^\dagger(t_1,t)\Lambda\mathcal{S}(t,t_2) - \delta(t_1-t)\Lambda\delta(t-t_2)\right) \times \tilde{f}(t_1'-t_2)\left(\mathcal{S}^\dagger(t_1',t')\Lambda\mathcal{S}(t',t_2') - \delta(t_1'-t')\Lambda\delta(t'-t_2')\right) f(t_1-t_2')\right]. \quad (4.49)$$

(A factor two has been added to account for spin degeneracy.) In the absence of a time-dependent potential, Equation (4.49) represents the sum of Nyquist noise and shot noise [64]. With time-dependence, it contains an extra contribution to the noise that is caused by the time dependence of the potential in the quantum dot, see Refs. [65, 66, 67, 68, 69] and Chapter 3.

Averaging equation (4.49) for an ensemble of chaotic quantum dots, we find

$$\langle S\rangle = S^N + S^S + S^P,$$

$$
\begin{aligned}
S^N &= 2kTh\langle G\rangle, \\
S^S &= eVh\langle G\rangle \frac{N_1N_2}{2\pi N^2}\left(\coth\frac{eV}{2kT}-\frac{2kT}{eV}\right), \\
S^P &= \frac{e^2N_1N_2(kT/\hbar)^2}{2N(t_\mathrm{f}-t_\mathrm{i})}\int_{t_\mathrm{i}}^{t_\mathrm{f}} dtdt'\left(\frac{1}{N^2}-\left[\int_0^\infty \mathcal{D}(t,t-\xi;t',t'-\xi)d\xi\right]^2\right) \\
&\quad\times\frac{N^2-2(N_1^2+N_2^2)\sin^2[eV(t-t')/2\hbar]}{\sinh^2[\pi kT(t-t')/\hbar]},
\end{aligned}
\tag{4.50}
$$

where $\langle G\rangle$ is the average (time-dependent) conductance, see equation (4.40), and $V=(\mu_1-\mu_2)/e$ the bias voltage. The above ensemble averages for the Nyquist noise and shot noise are the same as the noise power found in the absence of a time-dependent potential [70], up to an eventual weak localization correction. The extra noise generated by the time-dependence of the dot shape is fully described by the term S^P. In the adiabatic regime $\hbar\omega \ll N\Delta$, the pumping noise can be written as

$$
\begin{aligned}
S^P = \frac{e^2N_1N_2(kT/\hbar)^2}{2N(t_\mathrm{f}-t_\mathrm{i})}\int_{t_\mathrm{i}}^{t_\mathrm{f}} dt'dt\left[\frac{1}{N^2}-\left(\frac{1}{N+2\sum_m(x_m(t)-x_m(t'))^2}\right)^2\right] \\
\times\frac{N^2-2(N_1^2+N_2^2)\sin^2[eV(t-t')/2\hbar]}{\sinh^2[\pi kT(t-t')/\hbar]},
\end{aligned}
\tag{4.51}
$$

In the absence of a bias voltage, $eV=0$, Equation (4.51) has been analyzed in detail in Chapter 3. For one time-dependent parameter $x(t)=\delta x\cos(\omega t)$ it is found that

$$
S^P=\frac{\omega e^2N_1N_2}{\pi^2N^2}\begin{cases} 2\pi(\delta x)^2\left(\coth\frac{\hbar\omega}{2kT}-\frac{2kT}{\hbar\omega}\right), & (\delta x)^2\ll N\max(1,k^2T^2/\hbar^2\omega^2), \\ 3|\delta x|N^{1/2}, & (\delta x)^2\gg N\max(1,k^2T^2/\hbar^2\omega^2). \end{cases}
$$

An applied bias voltage has an effect on the pumping noise S^P only if $eV\sim\max(\hbar\omega,kT,\hbar\omega|\delta x|/N^{1/2})$. And even then, the effect of the applied bias is limited to a reduction of S^P by a numerical factor $2N_1N_2/N^2$. In this respect, the effect of an external bias on the pumping noise is much weaker than that of temperature, which tends to suppress S^P as soon as $kT\sim\hbar\omega\max(1,|\delta x|/N^{1/2})$, see Chapter 3.

In summary, we have extended the scattering approach of the random-matrix theory of quantum transport to the case of scattering from a chaotic quantum dot with a time-dependent potential. We addressed the limit that the number of channels N coupling the dot to the electron reservoirs is large. In this limit, the elements of the scattering matrix have a distribution that is almost Gaussian, with non-Gaussian corrections that are small as N becomes large. We calculated the second moment, which defines the Gaussian part of the distribution, and the fourth cumulant, which characterizes the leading non-Gaussian corrections.

The advantage of the scattering matrix approach is that, once the scattering matrix distribution is calculated, the computation of transport properties is a matter of mere quadrature. As an example, we calculated the conductance of a quantum dot with a time-dependent potential or the current pumped through the dot in the absence of an external bias, and found agreement with previous calculations of Vavilov *et al.* that were based on the Hamiltonian approach [22, 23, 35]. The results derived here were used for the calculation of the current noise generated by the time-dependence of the potential in the quantum dot in Chapter 3 The current noise in the presence of both a time-dependent potential in the dot and a bias voltage was studied here.

Whereas the first four moments of the scattering matrix distribution that we calculated here are sufficient for the calculation of most transport properties — most transport properties are quadratic or quartic in the scattering matrix —, we need to point out that there are observables that cannot be calculated with the results presented here. First, in the presence of one or more superconducting contacts, (averaged) transport properties may still depend on higher cumulants of the distribution, despite the fact that these are small by additional factors of $1/N$ [11].

Second, the results presented here fail to quantitatively describe transport properties for very small N, which can have strongly non-Gaussian distributions. Further research in these directions is necessary.

Bibliography

[1] M. L. Mehta, *Random Matrices*, (Academic, New York, 1991).

[2] P. A. Mello in *Mesoscopic Quantum Physics*, edited by E. Akkermans, G. Montambaux, J.-L. Pichard, and J. Zinn-Justin (North-Holland, Amsterdam, 1995).

[3] T. Guhr, A. Müller-Groeling, and H. A. Weidenmüller, Phys. Rep. **299**, 189 (1998).

[4] C. E. Porter, *Statistical Theories of Spectra: Fluctuations* (Academic, New York, 1965).

[5] T. A. Brody *et al.*, Rev. Mod. Phys. **53**, 385 (1981).

[6] O. Bohigas, M.-J. Giannoni, and C. Schmit, Phys. Rev. Lett. **52**, 1 (1984).

[7] O. Bohigas in *Chaos and Quantum Physics*, edited by M.-J. Giannoni, A. Voros, and J. Zinn-Justin (North-Holland, Amsterdam, 1991).

[8] L. P. Kouwenhoven *et al.*, in *Mesoscopic Electron Transport*, NATO ASI Series E **345**, edited by L. L. Sohn, L. P. Kouwenhoven, and G. Schön (Kluwer, Dordrecht, 1997).

[9] Y. Alhassid, Rev. Mod. Phys. **72**, 895 (2000).

[10] K.B. Efetov, Adv. Phys. **32**, 53 (1983); *Supersymmetry in Disorder and Chaos* (Cambridge University Press, New-York, 1997).

[11] C. W. J. Beenakker, Rev. Mod. Phys. **69**, 731 (1997).

[12] J. J. M. Verbaarschot, H. A. Weidenmüller, and M. R. Zirnbauer, Phys. Rep. **129**, 367 (1985).

[13] C. H. Lewenkopf and H. A. Weidenmüller, Ann. Phys. **212**, 53 (1991).

[14] R. Blümel and U. Smilansky, Phys. Rev. Lett. **60**, 477 (1988).

[15] R. Blümel and U. Smilansky, Phys. Rev. Lett. **64**, 241 (1990).

[16] U. Smilansky, in *Chaos and Quantum Physics*, edited by M.-J. Giannoni, A. Voros, and J. Zinn-Justin (North-Holland, Amsterdam, 1991).

[17] H. U. Baranger and P. A. Mello, Phys. Rev. Lett. **73**, 142 (1994).

[18] R. A. Jalabert, J.-L. Pichard, and C. W. J. Beenakker, Europhys. Lett. **27**, 255 (1994).

[19] P. A. Mello, P. Pereyra, and T. H. Seligman, Ann. Phys. **161**, 254 (1985).

[20] P. W. Brouwer, Phys. Rev. B **51**, 16878 (1995).

[21] M. Switkes *et al.*, Science **283**, 1905 (1999).

[22] M. G. Vavilov and I. L. Aleiner, Phys. Rev. B **60**, R16311 (1999).

[23] M. G. Vavilov and I. L. Aleiner, Phys. Rev. B **64**, 085115 (2001).

[24] A. G. Huibers *et al.*, Phys. Rev. Lett. **83**, 5090 (1999).

[25] X.-B. Wang and V. E. Kravtsov, Phys. Rev. B **64**, 033313 (2001).

[26] V. E. Kravtsov, cond-mat/0106241

[27] V. I. Yudson, E. Kanzieper, and V. E. Kravtsov, Phys. Rev. B **64**, 045310 (2001).

[28] F. J. Dyson and M. L. Mehta, J. Math. Phys. **4**, 701 (1963).

[29] M. Büttiker, A. Prêtre, and H. Thomas, Phys. Rev. Lett. **70**, 4114 (1993).

[30] M. Büttiker, J. Phys. Condens. Matter **5**, 9361 (1993).

[31] M. Büttiker, H. Thomas, and A. Prêtre, Z. Phys. B **94**, 133 (1994).

[32] M. Büttiker and T. Christen, in *Quantum Transport in Semiconductor Submicron Structures*, B. Kramer ed., NATO ASI Ser. E, Vol. 326 (Kluwer, Dordrecht, 1996).

[33] M. Büttiker, J. of Low Temp. Phys. **118**, 519 (2000).

[34] T. A. Shutenko, I. L. Aleiner, and B. L. Altshuler Phys. Rev. B **61**, 10366 (2000).

[35] M. G. Vavilov, V. Ambegaokar, and I. L. Aleiner, Phys. Rev. B **63**, 195313 (2001).

[36] P. W. Brouwer and C. W. J. Beenakker, J. Math. Phys **37**, 4904 (1996).

[37] M. L. Polianski, M. G. Vavilov, and P. W.Brouwer, Phys. Rev. B **65**, 245314 (2002).

[38] R. A. Jalabert, H. U. Baranger, and A. D. Stone, Phys. Rev. Lett. **65**, 2442 (1990).

[39] A. D. Stone in *Mesoscopic Quantum Physics*, edited by E. Akkermans, G. Montambaux, J.-L. Pichard and J. Zinn-Justin (North-Holland, Amsterdam, 1995).

[40] S. Samuel, J. Math. Phys. **21**, 2695 (1980).

[41] P. A. Mello, J. Phys. A **23**, 4061 (1990).

[42] N. Argaman, Phys. Rev. Lett. **75**, 2750 (1995).

[43] R. O. Vallejos and C. H. Lewenkopf,J. Phys. A **34**, 2713 (2001).

[44] K.B. Efetov, Phys. Rev. Lett. **74**, 2299 (1995).

[45] K. M. Frahm, Europhys. Lett **30**, 457 (1995).

[46] P. W. Brouwer and M. Büttiker, Europhys. Lett. **37**, 441 (1997).

[47] I. L. Aleiner, P. W. Brouwer, and L. I. Glazman, Phys. Rep. **358**, 309 (2002).

[48] P. W. Brouwer and C. W. J. Beenakker, Phys. Rev. B **54**, 12705 (1996).

[49] P. W. Brouwer, K. M. Frahm, and C. W. J. Beenakker, *Waves in Random Media* **9**, 91 (1999).

[50] T. Kottos and U. Smilansky, Phys. Rev. Lett. **79**, 4794 (1997).

[51] P. W. Brouwer, J. N. H. J. Cremers, and B. I. Halperin, Phys. Rev. B **65**, 081302 (2002).

[52] B. Spivak B, F. Zhou, and M. T. Beal Monod, Phys. Rev. B **51** 13226 (1995).

[53] P. W. Brouwer, Phys. Rev. B **58**, 10135 (1998).

[54] F. Zhou, B. Spivak, and B. Altshuler, Phys. Rev. Lett. **82**, 608 (1999).

[55] K. Frahm and J.-L. Pichard, J. Phys. (France) I **5**, 847 (1995).

[56] S. Adam *et al.*, Phys. Rev. B **66**, 195412 (2002).

[57] M. Büttiker, Phys. Rev. Lett, **65**, 2901 (1990).

[58] M. Büttiker, Phys. Rev. B **45**, 3807 (1992).

[59] M. Büttiker, Phys. Rev. B **46**, 12485 (1992).

[60] H. U. Baranger and P. A. Mello, Phys. Rev. B **51**, 4703 (1995).

[61] I. L. Aleiner and A. I. Larkin, Phys. Rev. B **54**, 14423 (1996).

[62] P. W. Brouwer and C. W. J. Beenakker, Phys. Rev. B **55**, 4695 (1997).

[63] V. I. Fal'ko and D. Khmelnitskii, Zh. Eksp. Teor. Fiz **95**, 328 (1989) [Sov. Phys. JETP **68**, 186 (1989)].

[64] Y. M. Blanter and M. Büttiker, Phys. Rep. **336**, 1 (2001).

[65] A. V. Andreev and A. Kamenev, Phys. Rev. Lett. **85**, 1294 (2000).

[66] L. S. Levitov, cond-mat/0103617 (2001).

[67] A. V. Andreev and E. G. Mishchenko, Phys. Rev. B **64**, 233316 (2001).

[68] Yu. Makhlin and A. D. Mirlin, Phys. Rev. Lett. **87**, 276803 (2001).

[69] M. Moskalets and M. Büttiker, Phys. Rev. B **66**, 035306 (2002).

[70] Yu. V. Nazarov in *Quantum Dynamics of Submicron Structures*, H. A. Cerdeira, B. Kramer and G. Schön ed., NATO ASI Ser, Vol. 291 (Dordrecht: Kluwer, 1995).

[71] W. A. Friedman and P. A. Mello, Ann. Phys. **161**, 276 (1985).

Chapter 5

Current-induced transverse spin wave instability in a thin nanomagnet

Ferromagnets serve as spin filters for an electrical current passing through the magnet: the spin of the electrons that are transmitted through a ferromagnet becomes partially polarized parallel or antiparallel to the direction of the magnetization whereas spin current perpendicular to the magnetization direction is absorbed. Spin filtering is the root cause for the "spin-transfer torque", the phenomenon that a polarized current impinging on a ferromagnet affects its magnetization direction [1, 2, 3]. The source of the spin polarized current can either be a different ferromagnet, or, for a thick magnet, a region of the same ferromagnet upstream or downstream in the current flow. The "spin-transfer torque" gives rise to magnetization reversal in ferromagnet–normal-metal–ferromagnet trilayers [1, 2], which has been observed experimentally by several groups [4, 5, 9, 10, 6, 7, 8]. Dynamic manifestations of the spin-transfer torque include domain wall motion in bulk ferromagnets

[11, 12, 13, 14] and the excitation of spin waves by polarized currents in ferromagnetic multilayers or wires [2, 3, 4, 5, 6, 7, 8, 17, 15, 16]. In all these manifestations, the current-induced spin torque can be distinguished from effects arising from the current induced magnetic field, the main difference being that spin-transfer torque effects depend on the current direction, whereas magnetic field induced effects do not.

In this letter, we show that an unpolarized current can also exert a spin-transfer torque on a ferromagnet, even if the magnet is so thin that its magnetization direction does not change along the current flow: Although an unpolarized current cannot exert a spin-transfer torque that changes the over-all magnetization direction, it can create a transverse spin wave instability for sufficiently high current densities if the source and drain contacts to the ferromagnet are not symmetric. This spin wave instability can be identified unambiguously as a spin-torque effect because of its dependence on current direction: the spin-wave instability is present for one current direction and absent for the other. The spin-wave instability should lead to a non-hysteretic feature in the current-voltage characteristic of the ferromagnetic film that exists for one current direction only. In thick ferromagnets, such features have been observed in recent experiments [4, 17]. The necessary criterion for the spin-wave instability, asymmetric contacts to source and drain, is generically fulfilled in experiments on nanoscale magnets [5].

The issue of current-induced spin-wave excitation has significant practical relevance for devices based on the spin-torque effect in ferromagnetic multilayers. Whereas, experimentally, the presence of dynamical phenomena in these systems is well established, the precise nature of the excitations is not well known. A theoretical understanding of current-induced spin wave excitation in multilayer structures

will shed light on the possibly useful application of the current-induced dynamical excitations, *e.g.*, as GHz resonators, as well as on ways to avoid spin-wave excitation in devices that are designed to exhibit magnetization reversal only. For ferromagnet–normal-metal–ferromagnet trilayers, a comparison between theory and experiment is obstructed by the interplay of spin wave excitations and static magnetization reversal. Our finding that dynamical phenomena exist already in a single ferromagnetic layer allows for a study of spin-wave excitations in a much simpler geometry in which dynamical and static phenomena are well separated.

The geometry of the system under consideration is shown in Fig. 2.1: a nanomagnet of thickness d, small enough to be considered as single domain, is connected to source and drain reservoirs via diffusive normal-metal leads of lengths L_- and L_+, respectively. The leads and the ferromagnet have width $W \gg d$. In the absence of an electrical current through the system, the ferromagnet has a uniform magnetization, with a direction determined by anisotropies and an external magnetic field. A current j flows perpendicular to the ferromagnet. (Note that the electrical current j points opposite to the electron flow.)

For a qualitative explanation of the mechanism of the spin-wave instability, we note that the passage of an electric current through a single ferromagnetic layer creates spin accumulations of opposite signs on both sides of the ferromagnet, see Fig. 2.1, where the sign of the spin accumulation depends on the current direction and on the spin-filtering properties of the ferromagnet. To first order in the spin-wave amplitude, the spin accumulation in the normal metal leads is not affected by the possible presence of spin waves in the ferromagnet, as long as their wavelengths are much smaller than the spin diffusion length in the normal metal. Each spin accumulation exerts a spin-transfer torque on the magnetization; the direction of

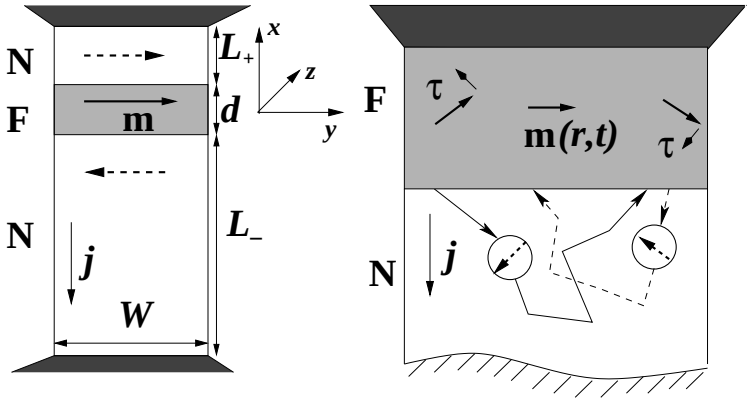

Figure 5.1: Left: Schematic picture of a thin ferromagnetic layer (F) in a "nanopillar" geometry. The ferromagnet is connected to source and drain reservoirs through normal metal leads (N). Current flow through the ferromagnet leads to a spin accumulation in the normal leads, as shown by the dotted arrows. Right: Cartoon of spin wave generation. Spin diffusion of reflected electrons (diffusion paths shown full and dashed) results in a spin torque on the ferromagnet's magnetization that enhances the spin wave amplitude; the transmitted electrons (not shown) damp the spin wave.

the torque is to align the magnetization in the ferromagnet with the direction of the accumulated spins in the leads. Depending on the sign of the spin accumulation, such a torque either damps or enhances non-uniform spin wave excitations in the ferromagnet. The magnitudes of the spin accumulations on each side of the ferromagnet are, generically, different, since they depend on the spin diffusion length, scattering properties of normal-metal–ferromagnet interface, distance to reservoirs, etc. Therefore, an unpolarized current results, generically, in a net torque that either suppresses or enhances non-uniform spin waves in the ferromagnet, depending on current direction. The instability occurs when the current-induced enhancement of a spin wave amplitude overcomes the intrinsic spin-wave damping.

For a quantitative description of the spin-wave instability, we choose the x axis along the leads, with the origin such that the normal-metal–ferromagnet interfaces are at $x = \pm d/2$, see Fig. 2.1. We assume that the ferromagnet is so thin that its magnetization direction varies with respect to the transverse coordinates y and z only, but not with respect to x. In the diffusive normal-metal leads, the electron distribution is described by potentials $\mu_e(\mathbf{r}, t)$ for the electron density and $\boldsymbol{\mu}_s(\mathbf{r}, t)$ for the electron spin [18, 19, 20]. The current is separated into the charge current density j_α, $\alpha = x, y, z$, and the spin current density $\mathbf{j}_{s\alpha}$. Since electrons adjust to the changing magnetization on a time scale much faster than that of the magnetization dynamics, current and potential are related by means of the time-independent diffusion equation in the normal metal leads,

$$\begin{aligned} &\nabla^2 \mu_e = 0, \quad j_\alpha = (\sigma/e)\nabla_\alpha \mu_e, \quad \alpha = x, y, z, \\ &l_{\rm sf}^2 \nabla^2 \boldsymbol{\mu}_s = \boldsymbol{\mu}_s, \quad \mathbf{j}_{s\alpha} = -(\hbar\sigma/2e^2)\nabla_\alpha \boldsymbol{\mu}_s, \end{aligned} \tag{5.1}$$

supplemented by boundary conditions for the source and drain reservoirs $\mu_e(-L_-) = -eV$, $\mu_e(L_+) = 0$, $\boldsymbol{\mu}_s(\pm L_\pm) = \mathbf{0}$. Here σ is the conductivity of the normal metal

leads and $l_{\rm sf}$ the spin-diffusion length. At the normal-metal–ferromagnet interfaces, the charge and spin current j_x and $\mathbf{j}_{sx}$ in the normal metal perpendicular to the interface are related to the potential drop $\Delta\mu$ over the interface as [19, 21]

$$\begin{aligned}
(\mathbf{j}_{sx})_\perp &= (\hbar/2e^2)\mathrm{Re}\, g_{\uparrow\downarrow}\,(2\Delta\boldsymbol{\mu}_s \times \mathbf{m} \pm \hbar\partial_t \mathbf{m}) \times \mathbf{m} \\
&\quad + (\hbar/2e^2)\mathrm{Im}\, g_{\uparrow\downarrow}\,(2\Delta\boldsymbol{\mu}_s \times \mathbf{m} \pm \hbar\partial_t \mathbf{m})\,, \\
(\mathbf{j}_{sx})_\parallel &= -(g_{\uparrow\uparrow}+g_{\downarrow\downarrow})(\hbar/2e^2)\mathbf{m}\cdot\Delta\boldsymbol{\mu}_s - (g_{\uparrow\uparrow}-g_{\downarrow\downarrow})(\hbar/2e^2)\Delta\mu_e, \qquad (5.2) \\
j_x &= (g_{\uparrow\uparrow}+g_{\downarrow\downarrow})(\Delta\mu_e/e) + (g_{\uparrow\uparrow}-g_{\downarrow\downarrow})\mathbf{m}\cdot(\Delta\boldsymbol{\mu}_s/e).
\end{aligned}$$

Here $\mathbf{m}(\mathbf{r},t)$ is the unit vector pointing in the direction of the magnetization of the ferromagnet, $(\mathbf{j}_{sx})_\perp$ and $(\mathbf{j}_{sx})_\parallel$ are the x-components of the spin current perpendicular and parallel to $\mathbf{m}$, respectively, $g_{\uparrow\uparrow}$ and $g_{\downarrow\downarrow}$ are interface conductivities for spins aligned parallel and antiparallel to $\mathbf{m}$, whereas $g_{\uparrow\downarrow}$ is the "mixing conductivity" [19, 21], $\Delta\mu = \mu(\pm d/2+0) - \mu(\pm d/2-0)$ is the potential drop over the interface. (We assume identical conductivities and spin-flip lengths in the leads, and identical scattering properties of the ferromagnet–normal-metal interfaces, although our results are readily generalized to unequal values of σ, $l_{\rm sf}$ and $g_{\alpha\beta}$.) At the normal-metal–ferromagnet interface, $(\mathbf{j}_{sx})_\parallel$ and j_x are continuous, whereas $(\mathbf{j}_{sx})_\perp = 0$ in the ferromagnet. We assume that the ferromagnet is so thin that all potential drops occur at the interfaces, so that we can neglect the x-dependence of the potentials in the ferromagnet. Then Eqs. (5.1) and (5.2) fully determine the potentials and currents in the normal metal and the ferromagnet, as a function of $\mathbf{m}$.

For a thin ferromagnet, variations of the magnetization direction $\mathbf{m}$ along the x axis will have a large energy cost and, hence, a large threshold for excitation. Therefore, we consider transverse modulation of $\mathbf{m}$ only and take $\mathbf{m}$ independent of x. The dynamics of $\mathbf{m}(y,z,t)$ is determined by the Landau-Lifschitz-Gilbert

equation (without an applied magnetic field [1]) [2, 13],

$$\begin{aligned}\partial_t \mathbf{m} &= \alpha \mathbf{m} \times \partial_t \mathbf{m} + J\gamma M \nabla^2 \mathbf{m} \times \mathbf{m} - (\gamma/M)(K_1 m_1 \hat{e}_1 + K_2 m_2 \hat{e}_2) \times \mathbf{m} \\ &\quad + (\gamma/Md)[\mathbf{j}_{sx}(-d/2 - 0) - \mathbf{j}_{sx}(d/2 + 0)], \end{aligned} \tag{5.3}$$

where α and J are the bulk Gilbert damping coefficient and spin stiffness (exchange constant) respectively, $\gamma = \mu_B g/\hbar$ is the gyromagnetic ratio, M is the magnetization per unit volume, and K_1 and K_2 are anisotropy constants along principal directions $\hat{e}_1$ and $\hat{e}_2$, respectively, obtained by expanding the magnet's free energy around a preferred axis $\hat{e}_3$. The magnetization satisfies the boundary condition $(\hat{n} \cdot \vec{\nabla})\mathbf{m} = 0$, where $\hat{n}$ is the normal to the ferromagnet's surface. We neglect the effect of the current-induced magnetic field on the magnetization dynamics, which is allowed if the width W is sufficiently small, $\ll 1$ μm for typical experimental parameters. The parameters in the Landau-Lifschitz-Gilbert equation define a length scale $1/q_{\rm f}$ and current scale $j_{\rm f}$,

$$q_{\rm f}^2 = \frac{K_1 + K_2}{2JM^2}, \quad j_{\rm f}^2 = \left(\frac{2e}{\hbar}\right)^2 JM^2 \frac{K_1 + K_2}{2}. \tag{5.4}$$

The quantities $1/q_{\rm f}$ and $\hbar j_{\rm f}/e$ are proportional to the width and energy of a domain wall, respectively. Order-of-magnitude estimates of the various parameters involved here are $d \sim 10$ nm, $W \sim 10^2$ nm, $l_{\rm sf}$(Cu)$\sim 10^2$ nm [5, 22]; $\mathrm{Im}\, g_{\uparrow\downarrow} \ll \mathrm{Re}\, g_{\uparrow\downarrow} \sim g_{\uparrow\uparrow} \sim g_{\downarrow\downarrow} \sim 10^{14}$ Ω^{-1}m^{-2} [23, 24] for Co/Cu and Fe/Cr interfaces; $\sigma/l_{\rm sf}$(Cu)$\sim 10^{15}$ Ω^{-1}m^{-2}, and typically $q_{\rm f} \sim 10^{-1}$ nm^{-1}, $j_{\rm f} \sim 10^8$ A/cm^2 for Co, Fe or Ni [2].

[1] The effect of a magnetic field is mathematically equivalent to a change of the equilibrium magnetization direction $\hat{e}_3$ and the anisotropy constants K_1 and K_2. A magnetic field parallel (antiparallel) to the easy axis increases (decreases) K_1 and K_2 and, hence, shifts the spin-wave instability to higher (lower) current densities.

[2] See E. P. Wohlfahrt in E. P. Wohlfahrt, Ed., *Ferromagnetic Materials*, Vol. 1 (North-Holland, 1980) for material constants. For a thin magnet the shape anisotropy dominates over the bulk easy axis anisotropy, $K_1 \approx 4\pi M \gg K_2$.

We first solve these equations for a uniform magnetization, $\mathbf{m}$ independent of the transverse coordinates y and z. The spin accumulation $\boldsymbol{\mu}_s$ in the normal metal leads close to the normal-metal–ferromagnet interface is

$$\boldsymbol{\mu}_s(\pm d/2) \;=\; \mp(ej_x/g_m)\tanh(L_\pm/l_{\rm sf})\mathbf{m}, \tag{5.5}$$

where j_x is the charge current density and

$$g_m \;=\; \frac{(\sigma/l_{\rm sf})(g_{\uparrow\uparrow}+g_{\downarrow\downarrow})+2g_{\uparrow\uparrow}g_{\downarrow\downarrow}\sum_\pm \tanh(L_\pm/l_{\rm sf})}{g_{\uparrow\uparrow}-g_{\downarrow\downarrow}}.$$

The spin accumulation is shown schematically in Fig. 2.1.

In the case of uniform magnetization, the spin accumulation $\boldsymbol{\mu}_s$ is always parallel to $\mathbf{m}$, and no current-induced torque is applied to the magnetization. The situation changes if $\mathbf{m}$ varies in the transverse direction. In this case, transverse diffusion of spin in the normal-metal leads gives rise to an angle between $\boldsymbol{\mu}_s$ and $\mathbf{m}$, and, hence, to a current-induced torque. In order to study this scenario in detail, we analyze Eqs. (5.1)–(5.3) for a small deviation of $\mathbf{m}$ from the equilibrium direction $\hat{e}_3$. The result can be represented in terms of an equation of motion for $\delta\mathbf{m} = \mathbf{m} - \hat{e}_3$. We assume a rectangular cross section of dimensions W_y and W_z in the y and z directions and perform a Fourier transform with respect to the transverse coordinates y and z. The allowed wavevectors are $q_y = \pi n_y/W_y$, $q_z = \pi n_z/W_z$, where n_y and n_z are non-negative integers. Representing $\delta\mathbf{m}$ through $m_\pm(\mathbf{q}) = \delta m_1(\mathbf{q}) \pm i\delta m_2(\mathbf{q})$, one finds that, to first order in $m_\pm$, the equations of motion of different Fourier modes separate,

$$\left(\frac{\tilde{\alpha}}{\gamma} \pm \frac{i}{\tilde{\gamma}}\right) M\partial_t m_\pm \;=\; \frac{K_2-K_1}{2}m_\mp - \frac{\hbar j_{\rm f}(q^2+q_{\rm f}^2)}{2eq_{\rm f}}m_\pm - \frac{\hbar j_x(S_2 \mp iS_1)}{2ed}m_\pm, \tag{5.6}$$

Here $\tilde{\alpha}$ and $\tilde{\gamma}$ are renormalized Gilbert damping parameter and gyromagnetic ratio,

$$\frac{1}{\tilde{\gamma}} \;=\; \frac{1}{\gamma} + \frac{\hbar^2}{2Mde^2}{\rm Im}\sum_\pm \frac{g_{\uparrow\downarrow}G_\pm(q)}{G_\pm(q)+g_{\uparrow\downarrow}}, \tag{5.7}$$

$$\tilde{\alpha} = \alpha + \frac{\gamma\hbar^2}{2Mde^2}\mathrm{Re}\sum_{\pm}\frac{g_{\uparrow\downarrow}G_{\pm}(q)}{G_{\pm}(q)+g_{\uparrow\downarrow}}, \tag{5.8}$$

whereas the dimensionless numbers S_1 and S_2 set the magnitude of the current-induced torque,

$$S_1 = \frac{\sigma}{g_m l_{\mathrm{sf}}}\mathrm{Re}\sum_{\pm}\frac{\pm g_{\uparrow\downarrow}}{G_{\pm}(0)}\frac{G_{\pm}(0)-G_{\pm}(q)}{g_{\uparrow\downarrow}+G_{\pm}(q)}, \tag{5.9}$$

$$S_2 = \frac{\sigma}{g_m l_{\mathrm{sf}}}\mathrm{Im}\sum_{\pm}\frac{\pm g_{\uparrow\downarrow}}{G_{\pm}(0)}\frac{G_{\pm}(0)-G_{\pm}(q)}{g_{\uparrow\downarrow}+G_{\pm}(q)}, \tag{5.10}$$

where g_m was defined below Eq. (5.5) and

$$G_{\pm}(q) = \frac{\sigma}{2}\sqrt{l_{\mathrm{sf}}^{-2}+q^2}\coth\left(L_{\pm}\sqrt{l_{\mathrm{sf}}^{-2}+q^2}\right).$$

In the limit $q \to 0$, Eqs. (5.7, 5.8) coincide with the enhanced Gilbert damping and gyromagnetic ratio reported by Tserkovnyak *et al.* [21].

In the absence of a current, any spatial modulation of the magnetization is damped. It is the existence of the source terms S_1 and S_2 in Eq. (5.6) that leads to a spin-wave instability at sufficiently large current density j. Note that the source terms exist only if the normal leads are asymmetric (different lengths, or different conductivities, spin-flip lengths or interface conductivities), and if the ferromagnet is a spin filter, $g_{\uparrow\uparrow} \neq g_{\downarrow\downarrow}$. The source term S_2 gives rise to a small change of the ferromagnetic resonance frequency, whereas S_1 increases or decreases the amplitude of the spin wave, depending on the current direction. An instability occurs if the current-induced enhancement of the spin-wave amplitude overcomes the damping, i.e., if

$$\left(\frac{\gamma S_1}{\tilde{\alpha}\tilde{\gamma}} - S_2\right)(-j) > \frac{(q^2+q_{\mathrm{f}}^2)d}{q_{\mathrm{f}}}j_{\mathrm{f}}. \tag{5.11}$$

Using the order-of-magnitude estimates listed below Eq. (5.4), the instability criterion simplifies considerably if we set $\mathrm{Im}\, g_{\uparrow\downarrow} = 0$, take the limits $d \to 0$ and

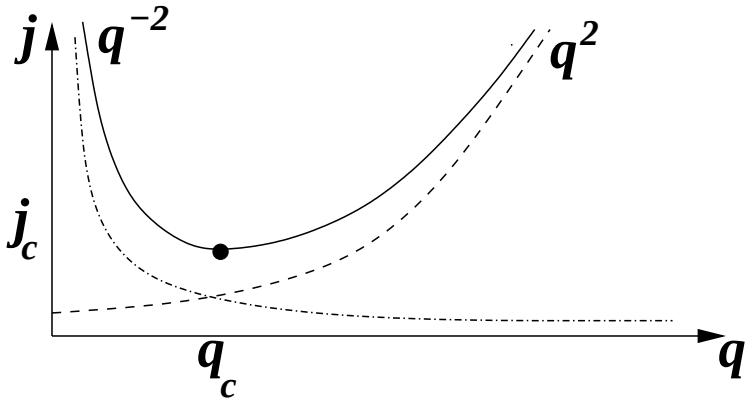

Figure 5.2: Schematic picture of the current density j_e required to excite a spin-wave at wavevector $\mathbf{q}$. The spin-wave instability occurs at the wavevector $\mathbf{q}$ for which j is minimal.

$\sigma/l_{\rm sf} \gg \mathrm{Re}\, g_{\uparrow\downarrow}$, and consider the case $L_- \gg l_{\rm sf} \gg L_+$ of maximally asymmetric contacts,

$$\frac{-j}{j_{\rm f}} \;>\; \frac{\hbar^2 \gamma g_m}{M q_{\rm f} e^2} \frac{q_{\rm f}^2 + q^2}{1-(1+q^2 l_{\rm sf}^2)^{-1/2}}. \tag{5.12}$$

The r.h.s. of Eq. (5.12) is shown schematically in Fig. 2.2. For large $q \gg 1/l_{\rm sf}$, the spin-wave instability is dominated by the stiffness of the spin wave, which leads to a critical current density $\propto q^2$. For small $q \ll 1/l_{\rm sf}$, the magnetization accumulation in the normal metal leads tends to remain locally parallel to the magnetization, so that the current-induced torque is strongly reduced and the critical current density for excitations at small q is increased $\propto q^{-2}$. For a thick ferromagnet, the effect of bulk Gilbert damping becomes dominant, causing the critical current density to increase linearly with the thickness d.

The wave-vector q which minimizes the r.h.s. of Eq. (5.12) corresponds to the onset of a spin-wave instability. In the experimentally relevant parameter regime

$1/q_{\rm f} \ll l_{\rm sf} \ll \sigma/{\rm Re}\, g_{\uparrow\downarrow}$, the critical current density is

$$j_{\rm c} \;=\; \frac{\hbar^2 \gamma g_m q_{\rm f}}{Me^2} j_{\rm f}, \quad q_{\rm c} = \left(q_{\rm f}^2/2l_{\rm sf}\right)^{1/3}. \tag{5.13}$$

For a Cu/Co/Cu geometry, we estimate $\tilde{\alpha} \sim (0.1{\rm nm})/d$ and $\hbar^2 \gamma g_m q_{\rm f}/Me^2 \sim 0.2$, as long as $dq_{\rm f} < 1$. We then find $j_{\rm c} \sim 10^7$ A/cm^2, which is of the same order of magnitude as the critical current for magnetization reversal in a ferromagnet–normal-metal–ferromagnet trilayer[5]. The estimate (5.13) is valid as long as the width $W \gg 1/q_{\rm c}$. For small W, the instability occurs at the lowest possible wavenumber, $q_{\rm c} = \pi/W$.

In conclusion, we have shown that an unpolarized electric current passing through a thin ferromagnetic layer can create a spin wave instability with wavevector transverse to the current. The instability occurs at one current direction only and depends on the asymmetry of normal metal contacts. The mechanism for the instability is the same as the one believed to cause magnetization reversal in ferromagnetic multilayers, *i.e.,* a spin-transfer torque arising from spin accumulation in the normal metal contacts perpendicular to the magnetization direction $\mathbf{m}$ and spin-filtering at the normal-metal–ferromagnet interfaces [1, 2, 13].

Current-induced excitations that occur for one current direction only have been observed in single ferromagnetic layers [4, 16, 17]. For ferromagnets much thicker than the inverse wavevector $q_c^{-1} \sim 3 \times 10^1$nm for transverse spin waves, cf. Eq. (5.13), spin wave excitations with wavevector along the current flow may have a lower threshold current than transverse excitations [13, 16]. Such thick ferromagnetic layers are common in the point-contact geometry [4, 6, 16]. It is for the thin layers used in the nanopillar geometry [5, 7, 8, 9, 22] that we believe the transverse instability considered here is most significant.

Bibliography

[1] J. Slonczewski, J. Magn. Magn. Mater. **159**, L1 (1996).

[2] J. Slonczewski, J. Magn. Magn. Mater. **195**, L261 (1999)

[3] L. Berger, Phys. Rev. B **54**, 9353 (1996).

[4] E. B. Myers *et al.*, Science **285**, 867 (1999).

[5] J. A. Katine *et al.*, Phys. Rev. Lett. **84**, 3149 (2000).

[6] W. H. Rippard, M. R. Pufall, and T. J. Silva, Appl. Phys. Lett. **82**, 1260 (2003).

[7] J. Z. Sun *et al.*, Appl. Phys. Lett. **81**, 2202 (2002).

[8] S. Urazhdin *et al.*, Phys. Rev. Lett. **91**, 146803 (2003).

[9] J. Grollier *et al.*, Appl. Phys. Lett. **78**, 3663 (2001).

[10] J.-E. Wegrowe *et al.*, Appl. Phys. Lett. **80**, 3775 (2002).

[11] L. Berger, Phys. Lett. A **46A**, 3 (1973).

[12] P. P. Freitas and L. Berger, J. Appl. Phys. **57**, 1266 (1985); C.-Y. Hung and L. Berger, J. Appl. Phys. **63**, 4276 (1988).

[13] Ya. B. Bazaliy, B. A. Jones, and S.- C. Zhang, Phys. Rev. B **57**, R3213 (1998).

[14] X. Waintal and M. Viret, Europhys. Lett. **65** , 427 (2004).

[15] M. Tsoi *et al.*, Nature **406**, 46 (2000).

[16] Y. Ji, C. L. Chien, and M. D. Stiles, Phys. Rev. Lett. **90**, 106601 (2003).

[17] W. H. Rippard, M. R. Pufall, and T. J. Silva , Appl. Phys. Lett. **83**, 323 (2003).

[18] T. Valet and A. Fert, Phys. Rev. B **48**, 7099 (1993).

[19] A. Brataas, Yu. V. Nazarov, and G. E. W. Bauer, Phys. Rev. Lett. **84**, 2481 (2000).

[20] D. Huertas-Hernando *et al.*, Phys. Rev. B **62**, 5700 (2000).

[21] Ya. Tserkovnyak, A. Brataas, and G. E. W. Bauer, Phys. Rev. Lett. **88**, 117601 (2002); Phys. Rev. B **66**, 224403 (2002).

[22] F. J. Albert *et al.*, Phys. Rev. Lett. **89**, 226802 (2002).

[23] M. D. Stiles, J. Appl. Phys. **79**, 5805 (1996); Phys. Rev. B. **54**, 14679 (1996).

[24] K. Xia *et al.*, Phys. Rev. B **65**, 220401 (2002).

Appendix A

Results for mesoscopic distributions in the single-channel limit

Below we present results for the "intermediate" distributions of the normalized current $\bar{i}$, voltage $\bar{v}$, and of the difference $\bar{d} = \bar{v}g - \bar{i}$ after integration over the matrices Q_1 and Q_2 at fixed S and Q, but before integration over S and Q, for the case of a chaotic quantum dot with two single-channel point contacts. For that case, the distribution of $\bar{d}$ is given by

$$P(\bar{d}) \;=\; \left\langle \frac{1}{2\sigma_d} e^{-|\bar{d}|/\sigma_d} \right\rangle_{S,Q}, \tag{A.1}$$

where the brackets $\langle \ldots \rangle_{S,Q}$ denote the remaining average over the scattering matrix S and the symmetrized time-delay matrix Q. The distributions for $\bar{i}$, $\bar{v}$ have the same form with σ_d replaced by σ_i and σ_v, respectively. However, we should note that, unlike for the difference $\bar{d}$, the form (A.1) does not hold for the distributions of $\bar{i}$ and $\bar{v}$ when $N > 1$.

Below we list (statistical) expressions for σ_d, σ_i and σ_v for $N = 1$ for the case $C\Delta \ll e^2$. We introduce the eigenvalues τ_1, τ_2 of the normalized time-delay matrix R. Their distribution can be found in Ref. [1]. Further, we introduce two independent random variables t (uniformly distributed between 0 and 1) and ϕ (uniformly distributed between 0 and 2π) that arise from the randomly distributed eigenvectors of R and the phases of the scattering matrix S. Finally, the equations for σ_d, σ_i, and σ_v contain the dimensionless conductance $g \in [0, 1]$, which has distribution $P(g) = (\beta/2)g^{-1+\beta/2}$. We then find

$$
\begin{aligned}
\sigma^2_{d,\beta=1} &= 256\frac{(\tau_1\tau_2)^3}{(\tau_1+\tau_2)^2}\frac{(1-g)^2}{g}, \\
\sigma^2_{i,\beta=1} &= 256\frac{(\tau_1\tau_2)^3}{(\tau_1+\tau_2)^2}g, \\
\sigma^2_{v,\beta=1} &= 256\frac{(\tau_1\tau_2)^3}{(\tau_1+\tau_2)^2}\frac{1}{g^3}, \\
\sigma^2_{d,\beta=2} &= \frac{1-g}{g}\left(\frac{8\tau_1\tau_2}{\tau_1+\tau_2}\right)^2\left(\tau_1\tau_2 + t(1-t)(\tau_1-\tau_2)^2\sin^2\phi\right), \\
\sigma^2_{i,\beta=2} &= (4\tau_1\tau_2)^2\left(1 - 4t(1-t)\left(\frac{\tau_1-\tau_2}{\tau_1+\tau_2}\right)^2\right), \\
\sigma^2_{v,\beta=2} &= \frac{1}{g^3}\left(\frac{8\tau_1\tau_2}{\tau_1+\tau_2}\right)^2\left[\tau_1\tau_2 + (\tau_1-\tau_2)^2\left(2\sqrt{(1-g)t(1-t)}\sin\phi + (1-2t)\sqrt{g}\right)^2\right].
\end{aligned}
$$

Appendix B

Integration over the matrices $\mathcal{R}$.

For the integration over the matrices $\mathcal{R}_1$ and $\mathcal{R}_2$ we make use of the fact that they can be parameterized as [1]

$$\mathcal{R}_j = -i\frac{\Delta}{2\pi\hbar} U\hat{\tau}^{1/2} H_j \hat{\tau}^{1/2} U^\dagger \otimes \mathbf{1}_2, \quad j = 1, 2, \tag{B.1}$$

where U is an $N \times N$ unitary matrix, $\hat{\tau}$ is a diagonal $N \times N$ matrix containing the eigenvalues τ_m, $m = 1, \ldots, N$, of the Wigner-Smith time-delay matrix on the diagonal [2], H_j is an $N \times N$ hermitian (real symmetric) matrix is time-reversal symmetry is broken (present), and $\mathbf{1}_2$ is the 2×2 unit matrix in spin grading.

For a chaotic quantum dot, the distributions of the hermitian matrices H_1 and H_2, the unitary matrix U, and the diagonal matrix $\hat{\tau}$ are all independent. The matrices H_j, $j = 1, 2$, have a Gaussian distribution,

$$P(H) \propto \exp(-\beta \mathrm{tr}\, H^2/8), \tag{B.2}$$

where $\beta = 1$ if time-reversal symmetry is present and $\beta = 2$ if time-reversal symmetry is broken by a magnetic field. The matrix U is uniformly distributed in the unitary group, and the eigenvalues τ_m, $m = 1, \ldots, N$ of the time-delay matrix have

distribution

$$P \propto \left(1+\frac{e^2}{\pi\hbar C}\sum_{m=1}^{N}\tau_m\right)\prod_{m=1}^{N}\prod_{m<n}^{N}|\tau_m-\tau_n|^{\beta}\Theta(\tau_m)\tau_m^{-3\beta N/2+\beta-2}e^{-\beta\pi\hbar/\Delta\tau_m}. \quad \text{(B.3)}$$

Knowing these distributions, finding the distribution for small N becomes a matter of mere quadrature. We have obtained the plots of the distributions of S^P and I/S^P by numerically generating 10^7–10^8 matrices $\mathcal{R}_j$ distributed according to the above distribution. We refer to Ref. [3] for the details of implementation of this procedure. Moments of the noise and the current can be found by performing the Gaussian integrations over H and the integrations over the unitary group with the help of the technique of Ref. [4]. For small N, the remaining integration over the τ_m can be done explicitly. For large N, it is sufficient to know the density and two-point correlator of the τ_m in order to find the first two moments of I or S^P. The density of time-delays is [1]

$$\begin{aligned}\rho(\tau) &= \sum_{m=1}^{N}\langle\delta(\tau_m-\tau)\rangle = \frac{N}{2\pi\tau^2}\sqrt{(\tau_+-\tau)(\tau-\tau_-)},\\ \tau_\pm &= 2\pi\hbar(3\pm\sqrt{8})/N\Delta\end{aligned}$$

The pair correlation function $K_2(\tau_1,\tau_2)$ is a universal function of the arguments τ_1 and τ_2 and the "spectrum edges" τ_- and τ_+ [5, 6]. With the help of the pair correlation function [6] we find that, up to corrections of order $1/N^4$,

$$\left\langle\left(\sum_{m=1}^{N}\tau_m\right)^q\right\rangle = \left(\frac{2\pi\hbar}{\Delta}\right)^q\left(1+q(q-1)\frac{2}{\beta N^2}\right).$$

Appendix C

Scattering matrix results

C.1 Nonideal contacts

Nonideal contacts are characterized by channels that have a transmission coefficient Γ_j smaller than unity, $j = 1, \ldots, N$. The imperfect transmission of the contacts is characterized by an $N \times N$ reflection matrix $r_c(t, t')$, for which we take the simple form

$$r_c(t, t') = (1 - \Gamma)^{1/2} \delta(t - t'), \tag{C.1}$$

where Γ is an $N \times N$ diagonal matrix containing the transmission coefficients Γ_j on the diagonal. The direct backscattering from the contacts is fast compared to the scattering that involves ergodic exploration of the dot, hence the delta function $\delta(t - t')$ in equation (C.1). In order to describe time dependent scattering with nonideal leads, we use a modification of the stub model of equation (4.22) [7, 8],

$$\mathcal{S} = r_c + \Gamma^{1/2} S^{\mathrm{fl}} \Gamma^{1/2}, \quad S^{\mathrm{fl}} = P\mathcal{U}(1 - R\mathcal{U})^{-1} P^\dagger, \tag{C.2}$$

$$R = Q^\dagger \mathrm{e}^{-2\pi \mathrm{i} H/M\Delta} Q - P^\dagger r_c P. \tag{C.3}$$

The first term in equation (C.2) takes into account the direct backscattering at the contact for electrons coming in from the reservoirs, whereas the extra term in equation (C.3) describes backscattering at the contact for electrons coming from the dot. The additional factors $\Gamma^{1/2}$ in the second term of equation (C.2) account for the decreased transmission probability for entering or exiting the quantum dot. With the inclusion of reflection in the contacts as in equation (C.2), the scattering matrix approach for time-independent scattering was proven to be fully equivalent to the Hamiltonian approach with arbitrary coupling to the leads [8]. The corresponding distribution of the scattering matrix $\mathcal{S}$ for time-independent scattering is known as the Poisson kernel [9].

Like in the case of ideal leads, the distribution of the elements of the scattering matrix $\mathcal{S}$ for a quantum dot with nonideal leads is almost Gaussian, with non-Gaussian corrections that are small if $N \gg 1$. The main difference with the case of an ideal contact is that, as a result of the direct reflection from the contact, the average of $\mathcal{S}$ is nonzero for a nonideal contact. The fluctuations of $\mathcal{S}$ around the average are described by $\mathcal{S}^{\mathrm{fl}}$, cf. equation (C.2). In order to find the distribution of $\mathcal{S}^{\mathrm{fl}}$, we note that the expression (C.2) for $\mathcal{S}^{\mathrm{fl}}$ is formally equivalent to the stub model equation (4.22) used to describe time-dependent scattering from a quantum dot with ideal contacts. Hence we conclude that the moments of $\mathcal{S}^{\mathrm{fl}}$ can be obtained directly from the results for the case of ideal contacts, see section 4.3 and appendix C, provided we substitute equation (C.3) for the matrix R. This amounts to the replacement $\mathcal{S} \to \mathcal{S}^{\mathrm{fl}}$ in the final results (4.30)–(4.33), $N \to \sum_j \Gamma_j$ in equation (4.31), and $N \to \sum_j \Gamma_j^2$ in equation (4.33).

C.2 Correlators for time-independent scattering

The scattering matrix correlators for time-independent scattering serve as input for the calculation of the correlators for time-dependent scattering. They can be calculated using the Hamiltonian approach (see references [10, 11, 12]), or, alternatively, in the scattering matrix approach, using a time-independent version of the "stub model" of section 4.3. Following the latter method, the scattering matrix $\mathcal{S}$ is written as [13]

$$\mathcal{S}(\varepsilon) = P\mathcal{U}(1 - R\mathcal{U})^{-1}P^{\dagger}, \quad R = Q^{\dagger}\mathrm{e}^{2\pi\mathrm{i}\varepsilon/M\Delta}Q. \tag{C.4}$$

Here the matrices P and Q are as in equation (4.22), whereas $\mathcal{U}$ is an $M \times M$ unitary matrix taken from the circular orthogonal ensemble or circular unitary ensemble of random matrix theory, depending on the presence or absence of time-reversal symmetry. The picture underlying equation (C.4) is that a stub with $M - N$ scattering channels is attached to the chaotic quantum dot as in figure 4.1, such that the dwell time in the stub is much larger than the dwell time in the dot, but much smaller than the total dwell time in the combined dot-stub system. The first condition implies that the $M \times M$ scattering matrix of the chaotic dot (without stub) may be taken energy independent, and distributed according to the appropriate circular ensemble from random matrix theory. The total scattering matrix $\mathcal{S}$ then acquires its energy dependence through the energy dependence of the $(M - N) \times (M - N)$ reflection matrix R of the stub. The second condition, which requires $M \gg N$, ensures that the dot plus stub system is explored ergodically before an electron escapes into the lead, so that the spatial separation of the energy dependence (stub) and chaotic scattering (dot)) does not affect the correlators of the scattering matrix $\mathcal{S}$.[1]

[1]Note that this version of the "stub model" is different from that used in the main text. In time representation, the matrix $\mathcal{U}$ of equation (C.4) is proportional to a delta function $\delta(t - t')$, whereas

Using the diagrammatic technique of reference [4] to average over the random unitary matrix $\mathcal{U}$, we find that the second moment W_1 is given by

$$W_1^{ij;kl}(\varepsilon;\varepsilon') \;=\; \frac{1}{M-\operatorname{tr} R(\varepsilon)R^\dagger(\varepsilon')} \times \begin{cases} (\delta_{ik}\delta_{jl}+\delta_{il}\delta_{jk}) & \text{with TRS,} \\ \delta_{ik}\delta_{jl} & \text{without TRS.} \end{cases} \tag{C.5}$$

Substitution of equation (C.4) for R gives equation (4.10) of section 4.3. Note that equation (4.10) is valid in the semiclassical limit of large N only. Within the diagrammatic technique this follows from the observation that for large N the only contributions to W_1 are the "ladder" and "maximally crossed" diagrams, whereas for small N more contributions exist and a non-perturbative calculation is needed to calculate the scattering matrix correlator [4]. The correlator $W_1(\varepsilon,\varepsilon')$ was calculated by Verbaarschot *et al.* in reference [10] for arbitrary N using the Hamiltonian approach and the supersymmetry technique.

For the cumulant W_2 we find in the absence of time-reversal symmetry

$$\begin{aligned} W_2^{i_1j_1,i_2j_2;k_1l_1,k_2l_2}(\varepsilon_1,\varepsilon_2;\varepsilon_1',\varepsilon_2') = &-(\delta_{i_1k_1}\delta_{j_1l_2}\delta_{i_2k_2}\delta_{j_2l_1}+\delta_{i_1k_1}\delta_{j_1l_2}\delta_{i_2k_2}\delta_{j_2l_1}) \\ &\times [M-\operatorname{tr} R(\varepsilon_1)R(\varepsilon_2)R^\dagger(\varepsilon_1')R^\dagger(\varepsilon_2')][M-\operatorname{tr} R(\varepsilon_1)R(\varepsilon_1')]^{-1} \\ \times [M-\operatorname{tr} R(\varepsilon_2)R(\varepsilon_1')]^{-1}&[M-\operatorname{tr} R(\varepsilon_1)R(\varepsilon_2')]^{-1}[M-\operatorname{tr} R(\varepsilon_2)R(\varepsilon_2')]^{-1}. \end{aligned} \tag{C.6}$$

In the presence of time-reversal symmetry, fourteen terms corresponding to the permutations $i_2 \leftrightarrow j_2$, $k_1 \leftrightarrow l_1$, and $k_2 \leftrightarrow l_2$ have to be added. Equation (4.11) is recovered upon substitution of equation (C.4) for R.

---

the matrix R involves a time delay with time $t-t' = 2\pi\hbar/M\Delta$. For the model of section 4.3 of the main text, the time delay is described by $\mathcal{U}$, whereas scattering from the stub is instantaneous. Both versions of the "stub model" are equivalent to the Hamiltonian approach. Which one to use is a matter of convenience.

C.3 Correlators for time-dependent scattering

In this appendix we present the derivations of equations (4.30)–(4.33).

We first calculate the second moment W_1 of the scattering matrix distribution, equations (4.30) and (4.31). To find W_1 we use equation (4.22) to expand $\mathcal{S}$ in powers of $\mathcal{U}$ and R and then average over $\mathcal{U}$. In the limit of large M and large N, that average can be done using the cumulants (4.18) and (4.20) and the diagrammatic rules of reference [4]. This calculation is similar to the standard diagrammatic perturbation theory: the matrices $\mathcal{U}, \mathcal{U}^\dagger$, and $R(t)$ play the role of the unperturbed retarded and advanced Green functions and the random potential, respectively.

Performing the average over $\mathcal{U}$ this way, we find that, to leading order in M^{-1} and N^{-1}, the cumulant W_1 is dominated by two leading contributions: the "ladder diagram" of figure C.1 and the "maximally crossed diagram" of figure C.2. Since every factor in these two diagrams involves equal time differences for $\mathcal{S}$ and $\mathcal{S}^*$, we conclude that this contribution to W_1 is nonzero only if $t - t' = s - s'$, cf. equation (4.18). Further, we conclude that the ladder diagram gives a nonzero contribution only if $i = k$ and $j = l$, while the maximally crossed diagram contributes when $i = l$ and $j = k$.

We first consider the contribution of the ladder diagram, which we write as

$$\delta_{ik}\delta_{jl}\delta(t - t' - s + s')D(t, t'; s, s'), \tag{C.7}$$

where the kernel D is the equivalent of the "diffuson" from standard diagrammatic perturbation theory. Note that, in view of the delta function in equation (C.7), the kernel D depends on three arguments, not on four. For notational convenience, we prefer, however, to continue to use the two initial times t' and s' and the two final times t and s to denote the time-arguments of D.

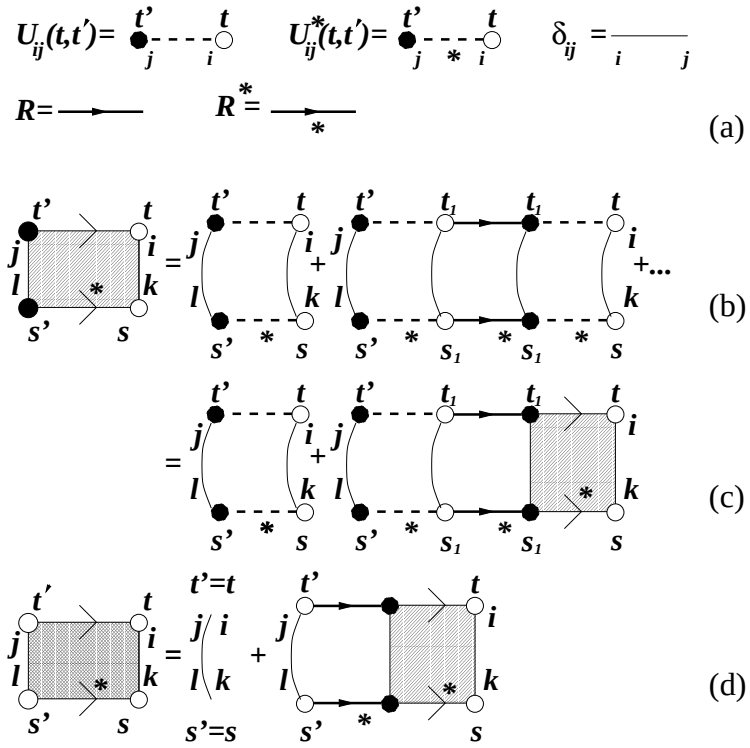

Figure C.1: (a) Notations, following reference [36]. (b) Calculation of the kernel $D(t,t';s,s')$. (c) Diagrammatic representation of the Dyson equation (C.8) for $D(t,t-\tau;s,s-\tau)$, with $t'=t-\tau$, $t_1=t-\tau_1$, $s'=s-\tau$, and $s_1=s-\tau_1$. (d) Diagrammatic representation of the differential equation (C.10) for $D(t,t-\tau;s,s-\tau)$. Left hand side: $(M+\partial_\tau)D(t,t-\tau;s,s-\tau)$; Right hand side:
$\delta(\tau)+\mathrm{tr}\,R(t-\tau)R^\dagger(s-\tau)D(t,t-\tau;s,s-\tau)$.

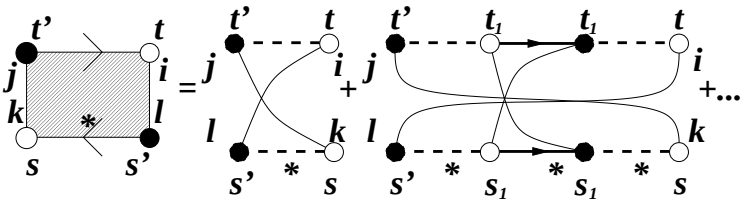

Figure C.2: Diagram representing the kernel $C(t,t';s,s')$ of equation (C.12).

Considering the ladder diagrams to all orders, the diffuson D is found to obey the Dyson equation

$$D(t,t-\tau;s,s-\tau) = \theta(\tau)\mathrm{e}^{-M\tau} + \theta(\tau)\int_0^\tau d\tau_1 D(t,t-\tau_1;s,s-\tau_1) \times \mathrm{tr}\, R(t-\tau_1)R^\dagger(s-\tau_1)\mathrm{e}^{-M(\tau-\tau_1)}. \qquad \text{(C.8)}$$

The solution of equation (C.8) is

$$D(t'+\tau,t';s'+\tau,s') \;=\; \theta(\tau)\mathrm{e}^{-\int_0^\tau d\tau_1\left(M-\mathrm{tr}\, R(t'+\tau_1)R^\dagger(s'+\tau_1)\right)}, \qquad \text{(C.9)}$$

where we used that $D=0$ if $\tau<0$. Substitution of $R=\exp(2\pi H/\Delta)$ reproduces the first term in the result (4.30). For future use, we note that the function D of equation (C.9) obeys the differential equations

$$\left(\frac{\partial}{\partial\tau} + M - \mathrm{tr}\, R(t-\tau)R^\dagger(s-\tau)\right) D(t,t-\tau;s,s-\tau) = \delta(\tau), \qquad \text{(C.10)}$$
$$\left(\frac{\partial}{\partial\tau} + M - \mathrm{tr}\, R(t'+\tau)R^\dagger(s'+\tau)\right) D(t'+\tau,t';s'+\tau,s') = \delta(\tau).$$

Calculation of the contribution of the maximally crossed diagram proceeds in an analogous way. This contribution reads

$$\delta(t-t'-s+s')\delta_{il}\delta_{jk}C(t,t';s,s'), \qquad \text{(C.11)}$$

where the analogue of the Cooperon is given by

$$C(t'+\tau,t';s'+\tau,s') \;=\; \theta(\tau)\mathrm{e}^{\int_0^\tau d\tau_1\left(M-\mathrm{tr}\, R(t'+\tau_1)R^\dagger(s'+\tau-\tau_1)\right)}. \qquad \text{(C.12)}$$

Substitution of $R = \exp(2\pi H/\Delta)$ gives the second term of equation (4.30).

We now turn to the four scattering-matrix correlator (4.29), which is the equivalent of the Hikami box in standard diagrammatic perturbation theory. We first calculate the first term of equation (4.32). It is represented diagrammatically in figure C.3. There are two contributions: One contribution involving Gaussian contractions with the cumulant (4.18) only, which is depicted as the first term on the r.h.s. of figure C.3, and one contribution that involves the non-Gaussian contraction of equation (4.20) once and otherwise Gaussian contractions, see the second term on the r.h.s. of figure C.3. Adding those two contributions, the function $\mathcal{F}$ is found to be

$$\begin{aligned}
&\mathcal{F}(t_1, t_1'; t_2, t_2'; s_1, s_1'; s_2, s_2') = \\
&\int d\tau D(t_1' + \tau, t_1'; s_1' + \tau, s_1') D(t_2 - s_1 + s_1' + \tau, t_2'; s_2 - t_1 + t_1' + \tau, s_2') \\
&\times D(t_1, t_1' + \tau; s_2, s_2 - t_1 + t_1' + \tau) D(t_2, t_2 - s_1 + s_1' + \tau; s_1, s_1' + \tau) \\
&\times \operatorname{tr} R(t_1' + \tau) R^\dagger(s_2 - t_1 + t_1' + \tau) R(t_2 - s_1 + s_1' + \tau) R^\dagger(s_1' + \tau) \\
&- \int d\tau_1 d\tau_2 d\tau_3 d\tau_4 (M + \partial_{\tau_1}) D(t_1' + \tau_1, t_1'; s_1' + \tau_1, s_1') \\
&\times (M + \partial_{\tau_2}) D(t_1, t_1 - \tau_2; s_2, s_2 - \tau_2) (M + \partial_{\tau_3}) D(t_2' + \tau_3, t_2'; s_2' + \tau_3, s_2') \\
&\times (M + \partial_{\tau_4}) D(t_2, t_2 - \tau_4; s_1, s_1 - \tau_4) \theta(t_1 - t_1' - \tau_1 - \tau_2) \theta(t_2 - t_2' - \tau_3 - \tau_4) \\
&\times \theta(s_1 - s_1' - \tau_1 - \tau_4) \theta(s_2 - s_2' - \tau_2 - \tau_3) \mathcal{F}^0(t_1 - t_1' - \tau_1 - \tau_2; \\
&t_2 - t_2' - \tau_3 - \tau_4; s_1 - s_1' - \tau_1 - \tau_4; s_2 - s_2' - \tau_2 - \tau_3). \qquad \text{(C.13)}
\end{aligned}$$

Here we used equation (C.11) to express the four legs of the diagrams of figure C.3b in terms of the diffuson D and its derivative. The second term in equation (C.13) can be simplified noting that the time integration is dominated by all four arguments of $\mathcal{F}^0$ being of order $1/M$. Using the smallness of these time arguments, the diffusons can be expanded around $t_1 - t_1' - \tau_1 - \tau_2 = t_2 - t_2' - \tau_3 - \tau_4 = s_1 - s_1' - \tau_1 - \tau_4 =$

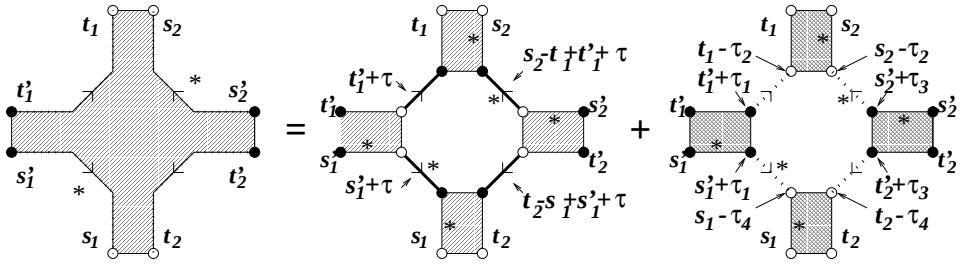

Figure C.3: Diagrams representing the two contributions to the correlator $\mathcal{F}(t_1, t_1'; t_2, t_2'; s_1, s_1'; s_2, s_2')$ (l.h.s.). The first diagram on the r.h.s. contains Gaussian contractions only; the shaded blocks in denote the kernel D. The second diagram on the r.h.s. contains one non-Gaussian contraction, which is in the center of the diagram; the shaded blocks represent factors of the form $(M + \partial_\tau)D$, see equation (C.13) and figure C.1d.

$s_2 - s_2' - \tau_2 - \tau_3 = 0$ and three of four time integrations can be done. The result is

$$\begin{aligned}\mathcal{F}(t_1, t_1'; t_2, t_2'; s_1, s_1'; s_2, s_2') &= \int d\tau D(t_2 - s_1 + s_1' + \tau, t_2'; s_2 - t_1 + t_1' + \tau, s_2') \\ &\times D(t_1' + \tau, t_1'; s_1' + \tau, s_1') D(t_1, t_1' + \tau; s_2, s_2 - t_1 + t_1' + \tau) \\ &\times D(t_2, t_2 - s_1 + s_1' + \tau; , s_1, s_1' + \tau) \mathbf{\Gamma}(t_1, t_1'; t_2, t_2'; s_1, s_1'; s_2, s_2'; \tau), \end{aligned} \tag{C.14}$$

where we abbreviated

$$\begin{aligned}\mathbf{\Gamma} &= M - \operatorname{tr} R(t_1' + \tau) R^\dagger(s_2 - t_1 + t_1' + \tau) - \operatorname{tr} R(t_2 - s_1 + s_1' + \tau) R^\dagger(s_1' + \tau) \\ &\quad + \operatorname{tr} R(t_1' + \tau) R^\dagger(s_2 - t_1 + t_1' + \tau) R(t_2 - s_1 + s_1' + \tau) R^\dagger(s_1' + \tau) \\ &\quad - \delta(t_1 - t_1' - \tau) - \delta(s_1 - s_1' - \tau). \end{aligned} \tag{C.15}$$

We used equations (C.11) and (C.10) to calculate time derivatives of the diffusons. Alternatively, using a partial integration, the function $\mathcal{F}$ can be expressed by equation (C.14) with

$$\mathbf{\Gamma} = M - \operatorname{tr} R(t_1' + \tau) R^\dagger(s_1' + \tau) - \operatorname{tr} R(t_2 - s_1 + s_1' + \tau) R^\dagger(s_2 - t_1 + t_1' + \tau)$$

$$+ \operatorname{tr} R(t_1' + \tau) R^\dagger(s_2 - t_1 + t_1' + \tau) R(t_2 - s_1 + s_1' + \tau) R^\dagger(s_1' + \tau)$$
$$- \delta(\tau) - \delta(\tau - t_1 + t_1' + s_2 - s_2'). \tag{C.16}$$

or with $\mathbf{\Gamma}$ given by a convenient linear combination of equations (C.15) and (C.16) with coefficients C_1, C_2 satisfying the condition $C_1 + C_2 = 1$.

Finally, using equation (4.22) for R, the first term of equation (4.32) is obtained. The other contributions to equation (4.32) can be found after permutation of the channel indices and time-variables as indicated in figure 4.2.

Bibliography

[1] P. W. Brouwer, K. M. Frahm, and C. W. J. Beenakker, Phys. Rev. Lett. **78**, 4737 (1997); *Waves in Random Media* **9**, 91 (1999).

[2] E. P. Wigner, Phys. Rev. **98**, 145 (1955), and F. T. Smith, Phys. Rev. **118**, 349 (1960).

[3] J. N. H. J. Cremers and P. W. Brouwer, Phys. Rev. B **65** , 115333 (2002).

[4] P. W. Brouwer and C. W. J. Beenakker, J. Math. Phys **37**, 4904 (1996).

[5] E. Brézin and A. Zee, Nucl. Phys. B **402**, 613 (1993).

[6] C. W. J. Beenakker, Nucl. Phys. B **422**, 515 (1994).

[7] W. A. Friedman and P. A. Mello, Ann. Phys. **161**, 276 (1985).

[8] P. W. Brouwer, Phys. Rev. B **51**, 16878 (1995).

[9] P. A. Mello, P. Pereyra, and T. H. Seligman, Ann. Phys. **161**, 254 (1985).

[10] J. J. M. Verbaarschot, H. A. Weidenmüller, and M. R. Zirnbauer, Phys. Rep. **129**, 367 (1985).

[11] K.B. Efetov, Phys. Rev. Lett. **74**, 2299 (1995).

[12] K. M. Frahm, Europhys. Lett **30**, 457 (1995).

[13] P. W. Brouwer and M. Büttiker, Europhys. Lett. **37**, 441 (1997).